MOLECULAR FACTORS CONTROLLING PLANT ORGANELLE MOVEMENT AND POSITIONING

Chiara Perico

A dissertation submitted to the University of Bristol in accordance with the requirements for award of the degree of Doctor of Philosophy (PhD) in the Faculty of Life Sciences.

School of Biological Sciences

September 2019

Word count: 35178

Abstract

Plant cell organelles are highly motile and their positioning plays key roles in plant growth and development and responses to changing environmental conditions. Movement of organelles relies on the actin cytoskeleton and on myosins, the associated motor proteins. Myosins are suggested to bind to receptors and adaptors on organelle membranes allowing them to move on actin filaments in a step-wise manner. Despite controlling the dynamics of several organelles, the myosins and myosin receptors identified so far in *Arabidopsis thaliana* generally do not localise to the organelles whose movement they control, raising the issue of how specificity is determined. Our group have isolated a family of potential myosin receptors (MyoB). Here I show that unlike other members from the same family, the myosin receptor *At*MRF7 specifically localises to Golgi due to the targeting information contained within its C-terminal region. MRF7 causes the class XI myosins known to affect Golgi movement, XI-K and MYA1, to relocate to the Golgi, linking these myosins for the first time to a specific compartment. MRF7 doesn't affect the localisation of a myosin not linked to Golgi dynamics. Furthermore, FRET-FLIM confirmed the *in vivo* interaction between MRF7 and the myosin XI-K globular tail, showing this interaction takes place *via* the MRF7 N-terminal predicted myosin binding domain, DUF593. I also show that the full-length and truncated constructs of MRF7 affect, to different extents, Golgi and peroxisome dynamics. This study provides evidence that myosins from class XI can localise to organelles whose movement they control. I present a model for Golgi dynamics driven by a heterogeneous myosin population regulated through adaptor/receptor complexes.

Acknowledgements

Many wonderful people have contributed directly and indirectly to the realisation of this project. I would like to thank my supervisor Dr. Imogen Sparkes for giving me this opportunity and for her constant encouragement and support. Thank you also to my other supervisors: Prof. Stan Botchway, for the great discussions and his wizard skills with the FLIM system, and Prof. Alistair Hetherington for the support and useful discussions on the project.

Thanks to mum, dad, Bea, Michi and Giuli for their constant cheering and understanding, even if a few countries were separating us most of the time. Thanks to all the past and present members of the Sparkes lab: Hongbo, Ian, Rhi and Alice, and to the good friends I met and that shared part of this journey with me, particularly Diana, Gi, Zoe, Chiara and Ashley. Thank you also to my friends back in Italy, Sara, Ale, Marco, Luca and Dario, whom I've always felt very close despite the distance.

Thanks to the Gatsby Charitable Foundation for funding the project and for the constant support and training throughout these past four years.

Author's declaration

I declare that the work in this dissertation was carried out in accordance with the requirements of the University's Regulations and Code of Practice for Research Degree Programmes and that it has not been submitted for any other academic award. Except where indicated by specific reference in the text, the work is the candidate's own work. Work done in collaboration with, or with the assistance of, others, is indicated as such. Any views expressed in the dissertation are those of the author.

SIGNED: ..... DATE: .....

Contents

Abstract iii

Acknowledgements v

Author's Declaration vii

List of figures xv

List of tables xix

Abbreviations xxi

1 General Introduction 1

1.1 Compartimentalisation and specialisation of the plant cell environment 3

1.2 Observations on organelle movement in plant cells 3

1.3 Myosin motors and effects on organelle motility 4

1.3.1 Structure and organisation of plant myosin families . 4

1.3.2 Role of myosin motors on organelle dynamics and plant growth 7

1.4 Biological relevance of organelle movement 10

1.5 Myosin recruitment 12

1.6 Role of microtubules and associated motor proteins 14

1.7 Contribution of organelle tethering to the movement 15

1.8 Aim of the project 16

2 Materials and Methods 19

2.1 Plant material and growth conditions 21

2.1.1 *Arabidopsis thaliana* 21
2.1.2 *Nicotiana tabacum* 21
2.1.3 Seed surface sterilisation 21
2.1.4 Soil medium 21
2.1.5 Agar medium 22
2.2 Molecular biology methods 22
2.2.1 Phenol:chloroform gDNA extraction from *Arabidopsis thaliana* leaves 22
2.2.2 Plasmid DNA extraction from *Escherichia coli* cells 22
2.2.3 Cloning of Gateway® compatible expression plasmids 23
2.2.4 DNA amplification by Polymerase Chain Reaction . 24
2.2.5 Agarose gel electrophoresis 24
2.2.6 Heat-shock transformation of *Escherichia coli* cells . 26
2.2.7 Heat-shock transformation of *Agrobacterium tumefaciens* 26
2.3 Transient and stable expression of fusion proteins 27
2.3.1 Transient expression in *Nicotiana tabacum* leaf epidermal cells 27
2.3.2 Transformation of *Arabidopsis thaliana* 27
2.3.3 Crossing of *Arabidopsis thaliana* plants 28
2.4 Drug treatments 28
2.4.1 Latrunculin B treatment for actin depolymerisation 28
2.5 Microscopy 29
2.5.1 Confocal microscopy 29
2.5.2 FRET-FLIM 30
2.6 Quantification of organelle dynamics 33
2.7 Protein methods 35
2.7.1 Protein extraction and quantification from *A.thaliana* seedlings 35
2.7.2 Immunoprecipitation with GFP-Trap ®_A beads . . 35
2.7.3 SDS-PAGE and Western Blot 36
2.8 Statistical analysis 36
2.9 Bioinformatic tools 37

2.9.1 Multiple alignment of DNA and protein sequences . 37
2.9.2 Gene expression 37

3 Localisation of myosin receptors 39

3.1 Introduction 41
3.1.1 Domain architectures of MyoB receptors 41
3.1.2 Localisation of MyoB myosin receptors 41
3.1.3 Aims 45
3.2 Results 47
3.2.1 Cloning of wild-type and truncated MRF7 fluorescent fusions for subcellular localisation studies 47
3.2.2 Over-expression of wild-type GFP-MRF7 reveals a dual "beads-on-a-string" and Golgi membrane localisation 49
3.2.3 The DUF593 domain is not responsible for MRF7 Golgi localisation 50
3.2.4 Localisation of MRF7 fusions in *A.thaliana* transgenic plants 55
3.2.5 The Golgi targeting information is contained within the C-terminus of MRF7 56
3.2.6 Effects of actin depolymerisation on GFP-MRF7, GFP-MRF7S and GFP-ΔMRF7 localisation 59
3.3 Discussion 67
3.3.1 MRF7 puncta move at high speeds on the actin cytoskeleton 67
3.3.2 Role of the C-terminus of MRF7 on Golgi targeting 69
3.3.3 Regulation of MRF7 localisation 71
3.3.4 Effects of actin cytoskeleton depolymerisation on MRF7 subcellular localisation 73

4 Control of organelle dynamics 75

4.1 Introduction 77
4.1.1 Effects of dominant negative mutants *At*MyoB receptors on organelle movement 77

4.1.2 Effects of full-length MyoB receptors on organelle movement . . . 78
4.1.3 Effects of myosin receptors on organelle dynamics in yeast and mammals . . . 80
4.1.4 Aims . . . 81
4.2 Results . . . 83
4.2.1 Triple expression system as a tool to study the effects of MRF7 fusions on multiple compartments . . . 83
4.2.2 GFP-MRF7 does not influence Golgi and peroxisome speed in *N.tabacum* . . . 85
4.2.3 GFP-MRF7S increases Golgi and peroxisome movement in *N.tabacum* and *A.thaliana* . . . 85
4.2.4 GFP-ΔMRF7 increases Golgi and peroxisome movement in *N.tabacum* . . . 91
4.2.5 Summary of movement analyses . . . 94
4.3 Discussion . . . 99
4.3.1 Partial or complete deletion of DUF593 increases Golgi and peroxisome speed . . . 99
4.3.2 Effects of GFP-MRF7S on Golgi dynamics are consistent in *N.tabacum* and *A.thaliana* . . . 103
4.3.3 Comment on the relationship between MRF7 localisation and function . . . 105

5 Myosin recruitment **107**
5.1 Introduction . . . 109
5.1.1 Myosin class XI localisation in higher plants . . . 109
5.1.2 Myosin recruitment in plants . . . 111
5.1.3 Myosin recruitment in non-plant systems . . . 115
5.1.4 Expression profiles of MyoB receptors and class VIII and XI myosins . . . 119
5.1.5 Aims . . . 119
5.2 Results . . . 121
5.2.1 Identification of MRF7 interactors . . . 121

5.2.2 Assessment of the effects of MRF7 and ΔMRF7 expression on myosin XI-K localisation 122
5.2.3 Validation of *in vivo* interaction between MRF7 and XIK tail by FRET-FLIM 125
5.2.4 Effects of MRF7 expression on MYA1 and XI-A tail subcellular localisation 132
5.3 Discussion 137
5.3.1 Myosin XI-K tail collocates to Golgi in presence of full-length MRF7 137
5.3.2 The DUF593 domain mediates the interaction between MRF7 and XI-K tail 139
5.3.3 Effects of MRF7 on other myosin XI tails localisation 141

6 General discussion 143
6.1 General discussion 145
6.1.1 Summary 145
6.1.2 Proposed model for the effects of MRF7 on organelle movement 146
6.1.3 Origin and role of the MRF7 puncta 149
6.1.4 Interaction with myosin motors 151
6.2 Future directions 154
6.2.1 Golgi localisation and targeting information 154
6.2.2 Effects of variations of Golgi movement on its subcellular activity 155
6.2.3 Effects of organelle movement on plant growth and development 155
6.2.4 Myosin recruitment 156

Appendix A 159
A.1 Accession numbers 161
A.2 List of Primers 162
A.3 List of Plasmids 163
A.4 Sequences of full-length and truncated MRF7 constructs . . 164
A.4.1 DNA sequence of the *A.thaliana* MRF7 gene 164

A.4.2 Amino acidic sequences of full-length and truncated MRF7 constructs 165
A.5 Constructs diagram 167
A.6 Mass spectrometry results 168

Bibliography **171**

List of Figures

1.1 Example of Golgi movement in and out of the cytoplasmic streaming 5
1.2 Myosin motors domain composition 8
1.3 Lever arm swing model for myosin movement on the actin cytoskeleton 9

2.1 Schematic representation of the main concepts of FRET . . 32
2.2 Comparison between displacement and full-length of a track 34

3.1 Architectures of the *A.thaliana* MyoB myosin receptors . . 42
3.2 Amino acid conservation of the DUF593 domain containing proteins in *A.thaliana* 43
3.3 Schematic representation of the domain composition of wild-type and truncated MRF7 constructs. 48
3.4 GFP-MRF7 moves on discrete puncta along the actin cytoskeleton. 51
3.5 Subcellular localisation of GFP-MRF7, GFP-MRF7S and GFP-ΔMRF7 in *N. tabacum* leaf epidermal cells. 53
3.6 Quantification of Golgi localisation of wild-type and N-terminal truncations of GFP-MRF7 in tobacco cells. . . . 54
3.7 Localisation of MRF7, MRF7S and ΔMRF7 in *A.thaliana* plants 14 days after germination. 57
3.8 Quantification of GFP-MRF7S localisation in *A.thaliana* and *N. tabacum* leaf epidermal cells 58
3.9 Cytoplasmic localisation of GFP-DUF593 domain, MRF7S-GFP and ΔMRF7-GFP. 60

3.10 C-terminal truncations of GFP-MRF7S and GFP-ΔMRF7 localise to the cytoplasm in tobacco leaf epidermal cells . . 61
3.11 Effects of 25 µM Latrunculin B on GFP-MRF7 localisation 64
3.12 Effects of 25 µM Latrunculin B on GFP-MRF7S and GFP-ΔMRF7 localisation. 65

4.1 Suggested model for the generation of cytoplasmic streaming and organelle movement in plant cells 79
4.2 Representative image of triple expression of Golgi and peroxisome markers and MRF7 GFP-tagged fusions 84
4.3 Effects of GFP-MRF7 expression on Golgi dynamics 86
4.4 Effects of GFP-MRF7 expression on peroxisomes dynamics 87
4.5 Effects of GFP-MRF7S expression on Golgi dynamics . . . 89
4.6 Effects of GFP-MRF7S on peroxisome dynamics 90
4.7 Effects of GFP-MRF7S on Golgi dynamics in *A.thaliana* . . 92
4.8 Effects of GFP-ΔMRF7 on Golgi dynamics 96
4.9 Effects of GFP-ΔMRF7 on peroxisomes dynamics 97
4.10 Suggested model for MRF7 role on Golgi movement 101
4.11 Model for MRF7 role on peroxisome movement 104

5.1 Schematic representation of interaction network of myosin and myosin receptors from *A.thaliana* 116
5.2 Examples of myosin V/Myo2p recruitment complexes from yeast and mammalian cells 118
5.3 Expression profile of *At*MyoB receptors and myosins from class VIII and XI 120
5.4 Expression of GFP-MRF7, GFP-MRF7S and GFP-ΔMRF7 in crude extracts and antibody-purified samples from *A.thaliana* transgenic plants 123
5.5 Qualitative observations of myosin XI-K tail localisation following co-expression with GFP-MRF7 and GFP-ΔMRF7 126
5.6 GFP-MRF7 and RFP-XIK tail co-localisation study in transiently transfected tobacco leaf epidermal cells 127

5.7 Representative confocal images and FRET-FLIM analysis for the GFP-MRF7 and RFP-XIK tail co-expression 129
5.8 FRET-FLIM analysis of RFP-XIK tail interaction with full-length and truncated MRF7 131
5.9 Co-localisation study of GFP-MRF7, RFP-MYA1 tail and RFP-XIA tail in transiently transfected tobacco leaf epidermis 134

6.1 Role of MRF7 and ΔMRF7 on Golgi movement 150
6.2 Schematic of the possible roles of the MyoB/MadA-B compartment on organelle movement 152

A.1 N- and C-terminally GFP-tagged fusions used in this study 167
A.2 Pie chart subdivisions of the mass spectrometry top hits for GFP-MRF7, GFP-MRF7S and GFP-ΔMRF7 169

List of Tables

2.1 Antibiotics and working concentrations used for selective bacterial growth. 23

2.2 DNA Polymerases, reaction mixes and amplification conditions 25

2.3 Primary and secondary antibodies used for detection of GFP fusion proteins. 36

3.1 25 µM Latrunculin B effects on GFP-MRF7 Golgi localisation 64

4.1 Effects of expression of GFP-MRF7 on Golgi dynamics, absolute values 86

4.2 Effects of expression of GFP-MRF7 on peroxisome dynamics, absolute values 87

4.3 Effects of GFP-MRF7S on Golgi dynamics, absolute values 89

4.4 Effects of GFP-MRF7S on peroxisome dynamics 90

4.5 Golgi movement 10 and 14 days after-germination, absolute values 93

4.6 Golgi movement 10 and 14 days after-germination, relative values 93

4.7 Summary of GFP-MRF7, GFP-MRF7S and GFP-ΔMRF7 effect on Golgi and peroxisomes, relative mean values 95

4.8 Effects of GFP-ΔMRF7 on Golgi dynamics 96

4.9 Effects of GFP-ΔMRF7 on peroxisomes dynamics 97

5.1 Subcellular localisation of full-length and truncated *A.thaliana* myosins from class XI 112

5.2 FRET efficiencies and intermolecular distances determined by FLIM 130
5.3 Percentage of MRF7 localisation to the Golgi in the presence and absence of myosin XI-K, MYA1 and XI-A 135
5.4 Percentage of myosin XI-K, MYA1 and XI-A Golgi localisation in the presence and absence of MRF7 135

6.1 Summary of localisation, effects on Golgi dynamics and interaction with myosins of the MRF7 constructs used in this study 150

A.1 TAIR accession numbers 161
A.2 List of primers for cloning PCR 162
A.3 List of plasmids for Gateway cloning 163

Abbreviations

At	*Arabidopsis thaliana*
AU	Arbitrary units
CC	Coiled-coil
co-IP	co-ImmunoPrecipitation
CFP	Cyan Fluorescent Protein
DAG	Days after germination
dNTP	deoxyribonucleotide triphosphate
DUF	Domain of Unknown Function
FLIM	Fluorescence Lifetime Imaging
FRET	Förster Resonance Energy Transfer
GFP	Green Fluorescent Protein
LatB	Latrunculin B
MI	Meandering index
MRF7	Myosin Recruitment Factor 7
Nb	*Nicotiana benthamiana*
Nt	*Nicotiana tabacum*
Px	Peroxisome
PM	Plasma membrane
PCR	Polymerase Chain Reaction
RFP	Red Fluorescent Protein
TGN	Trans-Golgi Network
TM	Trans-membrane
TMD	Trans-membrane domain
YFP	Yellow Fluorescent Protein
Zm	*Zea mays*

Chapter 1

General Introduction

1.1 Compartimentalisation and specialisation of the plant cell environment

Eukaryotic cells are subdivided into defined compartments in the form of membrane-bounded organelles. Each organelle has a characteristic structure, which can be more or less dynamic, and carries out specific functions within the cell. Quite often, biochemical pathways can span multiple organelles, requiring the reposition of the organelles involved to allow docking and exchange of molecules.

Unlike in mammalian cells, where organelles occupy very defined positions with respect to the central nucleus, plant cell organelles are highly motile. Their movement is suggested to play a key role in redistribution of solutes and metabolites within the cell, as well as allowing communication and docking between different organelle classes. The following sections focus on the basic movement characteristics of plant cell organelles and the effects of movement on plant development and response to external and internal cues.

1.2 Observations on organelle movement in plant cells

A striking feature of plant cells is cytoplasmic streaming, the bulk flow movement of cytoplasm. Cytoplasmic streaming is an actin-dependent phenomenon (Boevink et al., 1998; Nebenführ et al., 1999; Mathur et al., 2002; Van Gestel et al., 2002; Sparkes et al., 2008; Avisar et al., 2009) and although it is common to other organisms, it reaches its highest speeds (70 µm/s) in the algae *Chara* and *Nitella* (Kamiya and Kuroda, 1956; Nothnagel and Webb, 1982; Shimmen, 2007; Tominaga and Ito, 2015). In higher plants, the streaming velocity is of about an order of magnitude lower than in algae (Tominaga et al., 2013).

Streaming events in tip-growing cells such as root hairs and pollen tubes are ordered towards a specific direction to perhaps encourage anisotropic growth (Hepler et al., 2001); in other cell types, cytoplasmic

streaming is still present but shows more heterogeneous patterns. The exact nature and function of cytoplasmic streaming is not clear; it is suggested that remixing of the cytoplasmic content could be important for polarised growth (Hepler et al., 2001), distribution of solutes and metabolites within the cell (Goldstein et al., 2008) and cell expansion (Tominaga et al., 2013).

It was initially suggested that organelles can move primarily in a passive way within cytoplasmic streams. However, further observations of organelle movement characteristics (Boevink et al., 1998; Nebenführ et al., 1999; Mathur et al., 2002; Van Gestel et al., 2002) raised the possibility that they can in fact move actively within the cytoplasm, occasionally entering or exiting the stream. Movement within the stream is very directional (Fig.1.1a-d), with the organelles following the direction of the stream and moving at relatively high speeds ($\sim$ 8 µm/s) (Boevink et al., 1998; Nebenführ et al., 1999; Van Gestel et al., 2002; Stefano et al., 2014). Movements outside of the stream are less ordered and more heterogeneous, with organelles following a certain trajectory, pausing and then changing direction to follow another trajectory (Fig.1.1e-h).

The possible relationship between organelle movement and cytoplasmic streaming is so far still largely unclear. Mathematical models have shown that actin cytoskeleton dynamics alone are not able to generate the necessary drag force to create the stream (Nothnagel and Webb, 1982). The movement of a membranous structure such as the endoplasmic reticulum (ER) could play a fundamental role in generating a flow (Nothnagel and Webb, 1982; Ueda et al., 2010; Stefano et al., 2014).

1.3 Myosin motors and effects on organelle motility

1.3.1 Structure and organisation of plant myosin families

Organelle relocation in plant cells is an actin-dependent phenomenon (Boevink et al., 1998; Nebenführ et al., 1999; Mathur et al., 2002; Van Gestel et al., 2002; Sparkes et al., 2008; Avisar et al., 2009). G-actin

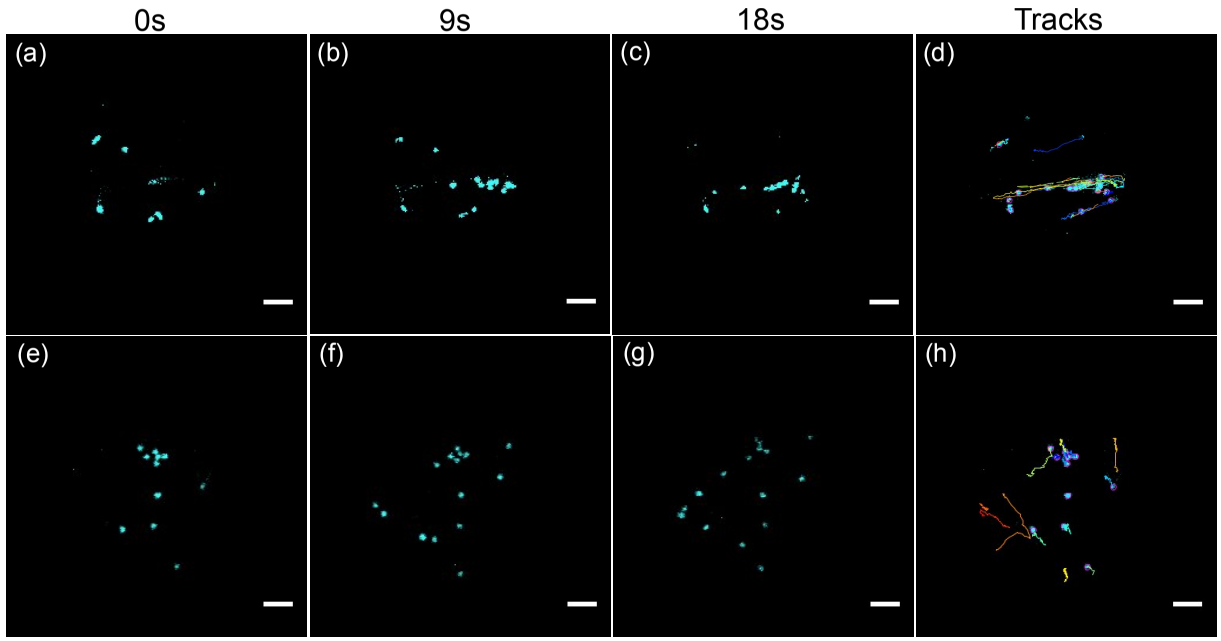

Figure 1.1: Example of Golgi movement in and out of cytoplasmic streaming. Movement of Golgi bodies in transiently infiltrated leaf epidermal cells of *N.tabacum* plants. Imaging was carried out on a confocal microscope; Golgi bodies are labelled by the ST-CFP Golgi marker. Panels (a-d) show movement of Golgi when in a stream; Panels (e-h) represent the movement of Golgi out of the stream. Golgi bodies were tracked over a period of 18s and three stills for each movie are shown (a-c and e-g). Panels (d) and (h) show the final results of individual Golgi bodies tracking carried out with the ImageJ plugin TrackMate. Tracks belonging to different Golgi bodies are colour coded.
Scale bars = 5 µm.

monomers polymerise to form actin filaments (F-actin) to consistute the tracks over which myosins, the associated motor proteins, move (Fig.1.2b). Actin filaments show a polarity, in that they can depolymerise (collapse) faster at one extremity, labelled as the minus-end.

Myosins are the motor proteins associated to the actin cytoskeleton and they provide the driving force to relocate organelles within the cytoplasm. Despite slight differences between families, myosins have overall a very similar domain composition (Fig.1.2a-b): an N-terminal actin-binding motor domain, a neck region with multiple calmodulin-binding IQ repeats and a coiled-coil region for dimerisation, and a C-terminal globular tail. The globular tail domain is responsible for myosin receptor recognition on organelle membranes (Fig.1.2). Myosins move in an ATP-dependent manner from the minus to the plus-end of the actin filaments. Studies on the *N.tabacum* 175 kDa myosin XI revealed that two myosin monomers dimerise through their coiled-coil regions and proceed on the actin cytoskeleton with a hand-over-hand movement, at 35 nm-long steps (Tominaga et al., 2003) in what has been described as a level arm swing model (Tominaga and Nakano, 2012; Hammer and Sellers, 2012). A myosin dimer is attached through both its leading and trailing ADP-bound heads to the actin cytoskeleton (Fig.1.3, step 1). The trailing head then releases ADP and binds to ATP (Fig.1.3, step 2). The ATP-bound trailing head swings forward, becoming the new leading head and hydrolysing ATP to ADP + Pi (Fig.1.3, step 3). The new leading head binds to the actin, releasing Pi (Fig.1.3, step 4).

Myosins are classified into different families based on domain composition and on the similarities between their motor domains (Odronitz and Kollmar, 2007; Kollmar and Mühlhausen, 2017). The *A.thaliana* genome encodes for 17 myosins, four from class VIII and 13 from class XI (Reddy and Day, 2001; Foth et al., 2006; Peremyslov et al., 2011). Myosins from class VIII are generally smaller and slower than myosins from class XI and were suggested to act more as tensors for the actin network than as movers of organelles (Ryan and Nebenführ, 2018). Myosins from class VIII localise to plasmodesmata (Golomb et al., 2008),

the cell plate (Van Damme et al., 2004) and the phragmoplast microtubules (Wu and Bezanilla, 2014). Localisation of myosins from class XI is discussed in Chapter 5.

Class XI myosins constitute the major contributors to organelle movement (Peremyslov et al., 2008; Prokhnevsky et al., 2008; Sparkes et al., 2008; Avisar et al., 2009; Peremyslov et al., 2010a; Ueda et al., 2010). Myosin XIs are structurally and functionally similar to myosins from family V of mammals and yeast (Kinkema and Schiefelbein, 1994; Reddy and Day, 2001): they have a similar length neck region and a "dilute" (DIL) and PAL domains within the globular tail, suggested to be responsible for cargo binding (Sattarzadeh et al., 2011; Sattarzadeh et al., 2013) (Fig.1.2a). Dimerisation of myosin monomers appears to stabilise the binding to the target cargoes (Li and Nebenführ, 2007).

1.3.2 Role of myosin motors on organelle dynamics and plant growth

Multiple techniques have been employed to reconcile the localisation of plant myosins with their role on organelle movement and plant development, from expression of dominant negative mutants, immunolocalisation, RNAi and knockout of myosin genes. Localisation experiments and effects of dominant negative mutants on organelle movement are extensively described in Chapter 5; so far these works suggest that plant myosins do not specifically localise to organelle membranes and that they mostly have overlapping effects on organelle dynamics (Li and Nebenführ, 2007; Avisar et al., 2009; Sattarzadeh et al., 2011; Sattarzadeh et al., 2013). Movement data indicated that one myosin can affect movement of multiple organelles, and movement of an organelle can be affected by several myosins (Avisar et al., 2009; Peremyslov et al., 2008).

Redundancy within the *A.thaliana* plant myosin families appears to be confirmed by knock-out experiments. Single knock-outs of myosin genes did not display a noticeable phenotype, with the exception of *xi-k* and *xi-2* knock-out plants, which had shorter root hair and in which

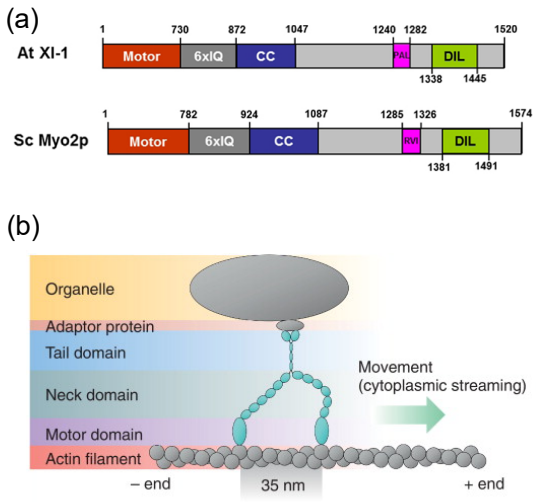

Figure 1.2: Myosin domain composition; adapted from (Tominaga et al., 2013; Sattarzadeh et al., 2013). (a) Domain composition and similarities between the *A.thaliana* class XI myosin XI-1 (MYA-1) and *S.cerevisiae* class V myosin Myo2p. Both classes present a motor domain responsible for ATP-dependent movement on actin, a neck region containing IQ-repeats and a coiled-coil motif for dimerisation, and lastly a globular tail domain for receptor binding. Note the presence of the PAL and DIL domain within the tail region (Sattarzadeh et al., 2011; Sattarzadeh et al., 2013). (b) Class XI myosin dimer moves an organelle along the actin cytoskeleton in a hand-over-hand manner, with a step size of 35 nm (Tominaga et al., 2013), from the minus to the plus-end of the actin cytoskeleton.

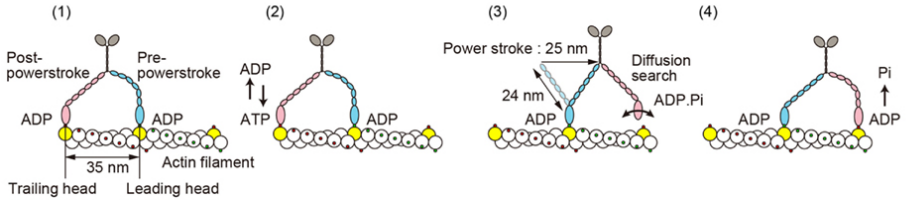

Figure 1.3: Lever arm swing model for myosin movement on the actin cytoskeleton (Tominaga and Nakano, 2012). 1) ADP-bound myosin trailing and leading heads are strongly associated to the actin tracks, 35 nm apart. 2) The trailing head releases ADP and binds to ATP; this represents the limiting step of the myosin movement cycle. 3) Power stroke step: the ATP-bound trailing head detaches from the actin and swings forward (24 nm) due to the strain in the neck region of the myosin. ATP is hydrolysed to ADP + Pi. 4) The new leading head binds to actin and releases Pi, stabilising the interaction with the cytoskeleton.

Golgi, peroxisome and mitochondria movement was affected (Peremyslov et al., 2008). Severe developmental defects were only observed following multiple myosin genes knock-out (Prokhnevsky et al., 2008; Peremyslov et al., 2010a), thus confirming that the plant myosin system is redundant and perhaps tightly regulated.

Expression of motor-less dominant negative tails and IQ-tails of *A.thaliana* myosins led to a significant decrease in the movement of multiple organelles such as Golgi, peroxisomes and mitochondria (Sparkes et al., 2008; Avisar et al., 2009). Despite such effects on organelle dynamics, one of the main challenges consists in reconciling these effects with the myosins localisation. So far, only myosin XI-I was specifically localised on the nuclear envelope (Avisar et al., 2009) and shown to regulate its movements in response to dark, whereas other myosin tails localise to so far unidentified puncta in the cytoplasm.

Myosin XIs have also been shown to play a role in gravity induced bending of inflorescence stems (Talts et al., 2016), development of pavement cells and trichomes (Ojangu et al., 2012), auxin response and senescence induced cell death (Ojangu et al., 2018), root organogenesis (Abu-Abied et al., 2018) and response to fungal pathogens (Yang et al., 2014). No defects were observed for *A.thaliana* plants lacking all four myosin VIII genes (Talts et al., 2016). It is still unclear what role the movement of single organelles plays in these processes.

1.4 Biological relevance of organelle movement

Organelle movement plays a role in plant response to biotic and abiotic stimuli and in directing cell growth and development. Nevertheless, the role of movement of specific classes of organelles on these processes is not yet fully understood.

Increase and decrease in cytoplasmic streaming speed was correlated with variations in cell size and plant growth (Tominaga et al., 2013). The study was conducted on *A.thaliana* plants expressing respectively: wild-type myosin MYA2 (7.2 µm/s); a high-speed (16 µm/s) chimeric MYA2,

where the motor domain of MYA2 is replaced by that of *C.corallina* myosin XI; a low-speed (0.19 µm/s) chimeric MYA2, where the motor domain is replaced by that of myosin Vb of *H.sapiens* (Tominaga et al., 2013). Plants expressing the high-speed chimeric construct displayed higher cytoplasmic streaming speed and increased plant and cell size than plants expressing wild-type MYA2 (Tominaga et al., 2013). *Viceversa*, plants expressing the low-speed chimeric construct displayed slower cytoplasmic streaming velocities and a decrease in plant and cell size compared to plants expressing wild-type MYA2 (Tominaga et al., 2013).

Chloroplasts and nuclei relocate within the cell in response to variations in light intensities. Chloroplasts reposition from periclinal to anticlinal walls of mesophyll cells (avoidance response) in conditions of high blue light intensities to avoid photodamage (Kasahara et al., 2002). Interestingly, nuclei react similarly to the same light conditions (Iwabuchi et al., 2010) and one of the proteins involved in this response, phototropin2 (phot2), also directs the avoidance response of chloroplasts (Kagawa et al., 2001). It was later observed that the nucleus is generally sorrounded by plastids and that its light-induced movement relies entirely on the ability of chloroplasts to reposition within the cell (Higa et al., 2014). Interestingly, this work highlights that movement of one specific organelle class is not only important in response to an external stimuli, but also in affecting the movement of organelles that are physically attached or in close proximity.

In growing root hair, nuclei have been observed to move forward towards the growing end, but maintaining the same distance from the tip (Ketelaar et al., 2002). Impairment of nuclear movement by actin depolymerisation or optical trapping suggested that correct positioning of the nucleus is important for root hair growth (Ketelaar et al., 2002).

Peroxisomes are organelles involved in a variety of processes such as β-oxidation, phytohormone metabolism, photorespiration and control of reactive oxigen (ROS) and nitrogen (RNS) species metabolism (Sandalio and Romero-Puertas, 2015). Treatments of *A.thaliana* leaves with cadmium (Cd), a heavy metal that induces ROS accumulation and

oxidative stress in multiple plant species (Sandalio et al., 2012), indicates that ROS can affect peroxisome dynamics (Rodríguez-Serrano et al., 2016). Dynamic membrane extensions called peroxules start forming minutes after Cd treatment and peroxisome elongation and division followed after two hours (Rodríguez-Serrano et al., 2016). Speed was also shown to increase upon cadmium treatment. Peroxisome proliferation and increase in speed upon heavy metal treatments could thus represent the mechanism through which the cell responds to ROS accumulation.

Organelle relocation was also observed in response to pathogen invasion. Following activation of the plant immune response, chloroplasts produce multiple defensive signals, including calcium bursts, ROS and phytohormones (Zabala et al., 2015; Park et al., 2017). Chloroplasts were observed to cluster around the nucleus upon infection of *N.benthamiana* leaves with viruses and bacteria (Ding et al., 2019). Exogenous application of pro-defense molecules such as H_2O_2 or salicylic acid (SA) in *N.benthamiana* leaves elicits a similar response (Caplan et al., 2015). Upon application of such molecules, chloroplasts surrounding the nucleus produce dynamic membrane extensions called stromules, which surround the nucleus and are suggested to allow the transport of pro-defense molecules from chloroplasts to the nucleus (Caplan et al., 2015).

Whilst the role of certain organelles in response to external and internal cues has been partially elucidated, understanding the functional role of relocation of specific organelles on overall plant growth and development still represents a challenge.

1.5 Myosin recruitment

The large number of myosin proteins present in *A.thaliana* and their simultaneous effects on multiple organelles suggest that myosin recruitment requires a higher level of regulation. Research has therefore begun to focus on the interface between myosins and organelles, to identify the molecular players involved in myosin recruitment. Studies from mammals and yeast indicated that the myosin recruitment process is

generally mediated by a scaffold of proteins which assemble in a step-wise manner to recruit a myosin motor (Fagarasanu et al., 2006; Tang et al., 2003; Yan et al., 2005; Hume et al., 2007).

Perhaps the best studied interaction between a receptor and a myosin localising to the same compartment is the complex constituted by XI-I/WIT1/WIT2 on the *A.thaliana* nuclear envelope (Tamura et al., 2013). Myosin XI-I tail was previously identified on the nuclear membrane (Avisar et al., 2009) and was shown to interact with the WIT1 and WIT2 proteins on the outer nuclear envelope (Tamura et al., 2013). Although myosin XI-I was observed to regulate other compartments movement (Avisar et al., 2009), its interaction with the WIT1/WIT2 complex specifically mediates dark-induced nuclear relocation (Tamura et al., 2013).

Recent works in *A.thaliana* have identified two families of potential myosin-interacting proteins: the MyoB family (16 members) and MadA-B families (four members each) (Peremyslov et al., 2013; Peremyslov et al., 2015; Kurth et al., 2017). Despite slightly different architectures, all the MyoB proteins share a predicted myosin binding Domain of Unknown Function 593 (DUF593) and are present in all land plants (Holding et al., 2007; Peremyslov et al., 2013; Stephan et al., 2014). Interpretation of the MyoB and Mad receptors role on specific organelles dynamics has so far proven elusive; with the exception of MadA1, they do not localise to defined subcellular structures but rather on unidentified membrane-bounded puncta moving in straight trajectories (Peremyslov et al., 2013; Kurth et al., 2017).

A pairwise yeast-2-hybrid screen highlighted the redundant nature of the network of interactions of MyoB and Mad proteins with myosins from class XI (Kurth et al., 2017). The movement of the MyoB and Mad puncta is myosin-specific (Peremyslov et al., 2013; Kurth et al., 2017) and binding of MyoB receptors to myosins is mediated by the DUF593 domain (Peremyslov et al., 2013). Transient over-expression of *Nb*MyoB1 and *Nb*MyoB2 DUF593 domains led to a generalised decrease in organelle movement, much like that observed upon expression of dominant negative

myosin tails (Avisar et al., 2009; Peremyslov et al., 2015).

Single knock-out *madb1* plants showed reduced root hair length, as previously described for *xi-k* and *xi-2* knock-outs (Peremyslov et al., 2008; Kurth et al., 2017). Single knock-outs for *myob 1-4* genes did not lead to any noticeable phenotype, but multiple knock-outs showed reduced height and a delay in flowering time. Interestingly, quintuple *xi-k/xi-2/myob1/myob2/myob3* knock-out plants showed exhacerbated developmental defects compared to either the *xi-k/xi-2* or the *myob1/myob2/myob3* knock-out plants (Peremyslov et al., 2015), which appears to suggest that myosins and myosin receptors work synergistically.

Recent advances in myosin research have highlighted that myosin expression could be subject to circadian rhythm, tissue specificity and developmetal stage of the plant (Peremyslov et al., 2011; Haraguchi et al., 2018). It is possible that the MyoB and Mad receptors are subject to a similar spatial and temporal regulation, and this could provide an additional layer of regulation for organelle relocation in plants.

1.6 Role of microtubules and associated motor proteins

Microtubules are the second type of cytoskeletal structure found in plant cells. Microtubules are hollow tubes constituted of 13 "protofilaments", formed by head-to-tail polymerisation of α- and β-tubulin dimers (Ledbetter and Porter, 1963; Ledbetter and Porter, 1964; Mohri, 1968). Like actin, microtubules have a polarity, with the α-tubulin side on the minus end and the β-tubulin side on the plus end of the polymer.

Microtubules constitute the tracks for two types of motor proteins: dyneins, which are minus-end directed motors, and kinesins, traditionally considered plus-end directed motors. Although not a prerogative of all land plants (King, 2002), *A.thaliana* appears to lack genes encoding for dyneins (Lawrence et al., 2001). Interestingly, perhaps to suffice to the absence of predicted dynein genes, the *A.thaliana* genome encodes for a

total of 61 kinesins, 21 of which are predicted to be minus end-directed (Reddy and Day, 2001). Like myosins, kinesins are subdivided into multiple subfamilies and are composed of a motor domain, a stalk and a tail (Lawrence et al., 2004).

Whilst in mammalian and fungi microtubules and the associated motor proteins play an important role in long range movement of organelles, it appears that in plants they could rather be responsible for fine tuning of organelle positioning (Van Gestel et al., 2002; Crowell et al., 2009; Idilli et al., 2013). Golgi bodies have been shown to pause at specific sites at cortical microtubules of *A.thaliana* hypocotyl cells; this mechanism is suggested to allow the correct delivery of cellulose synthase complexes (CSCs) towards the plasma membrane (Crowell et al., 2009). Microtubules also play a role in endo- and exocytosis of TGN derived vesicles (Renna et al., 2018), endosomal movement in pollen tubes of tobacco (Idilli et al., 2013) and ER tubule extension in *A.thaliana* (Hamada et al., 2014).

Recent works provided important evidence for a structural and functional coordination between the actin and microtubular networks (Sampathkumar et al., 2011; López et al., 2014; Wu and Bezanilla, 2018). For example, drug-induced depolymerisation and stabilisation of both cytoskeletal structures revealed that organisation and assembly of the actin cytoskeleton is guided by microtubules (Sampathkumar et al., 2011). Furthermore, it was observed that certain formins, proteins generally associated with actin dynamics regulation, were also able to bind microtubules (Deeks et al., 2010; Wang et al., 2013; Sun et al., 2017). Future works will help shed light on the molecular players and mechanisms coordinating the two cytoskeletal structures.

1.7 Contribution of organelle tethering to the movement

Multiple biochemical pathways in plants are partitioned between various organelles; examples are protein production and glycosylation between the

ER and Golgi, photorespiration between chloroplasts, mitochondria and peroxisomes, production of jasmonic acid (JA) between chloroplasts and peroxisomes.

Evidences for a physical interaction between some of these compartments were provided by optical tweezers studies, such as the association between Golgi and ER (Sparkes et al., 2009; Osterrieder et al., 2017) and between chloroplasts and peroxisomes (Gao et al., 2016). It is possible that the physical interaction between organelles could favour the exchange of important signal molecules, metabolites and enzymes. Despite proof of physical association, the molecular components at plant membrane contact sites (MCS), the interface region between interacting organelles, are yet to be discovered.

Physical interaction between organelles could influence the effects of the motor-driven movement. As mentioned in 1.4, movement derived from the avoidance response of chloroplasts triggers the simultaneous relocation of the nucleus, which is normally sorrounded by chloroplasts (Higa et al., 2014). In a similar fashion, movement of laser trapped Golgi bodies induces the rapid elongation of the attached ER tubules and remodelling of the local ER configuration (Sparkes et al., 2009).

Given these evidences, it is important to consider that movement of a certain organelle could certainly be the result of the effects of motor proteins and receptors acting on it, but also of the interactions that the organelle in object establishes with other organelles.

1.8 Aim of the project

Organelle movement correlates with plant growth and development and is involved in response to biotic and abiotic stimuli. Nevertheless it is still unclear what role organelle relocation plays in these processes and how movement of a specific class of organelles can affect certain responses. This project aims to identify the molecular factors involved in plant organelle movement and positioning, and in particular to generate the molecular tools necessary to specifically influence the dynamics of one organelle class.

All the work was carried out on a potential myosin receptor from the MyoB family, here named Myosin Recruitment Factor 7 (MRF7). Similarly to other MyoB receptors, MRF7 is localised to punctate structures moving in straight trajectories but, unlike any other MyoB protein, MRF7 also localises to the Golgi (Hongbo Gao *et al.*, unpublished data). Given its interesting localisation on a specific compartment, MRF7 is here used as case study to define the molecular components involved in myosin recruitment to organelle membranes. In particular, the work described in this dissertation aims to untangle the factors that trigger the localisation of MRF7 to the Golgi (Chapter 3), determine if MRF7 affects Golgi movement (Chapter 4) and whether myosin interaction and recruitment to the Golgi is involved (Chapter 5). Detailed backgrounds on myosin and MyoB localisation (Chapter 3), effects of the MyoB family on organelle dynamics (Chapter 4) and myosin recruitment (Chapter 5) are provided in the introductions to each respective results chapter.

Chapter 2

Materials and Methods

2.1 Plant material and growth conditions

2.1.1 *Arabidopsis thaliana*

All wild-type and transgenic *Arabidopsis thaliana* plants used for this project are in Columbia-0 (Col-0) background. They were germinated and grown in a growth chamber (Sanyo) at 20°C on a 16 h light, 8 h dark cycle, with a light intensity of 110 µmol photons · m^{-2} · s^{-1} and 60% humidity.
Plants were used at different ages and stages of growth, specified case-by-case.

2.1.2 *Nicotiana tabacum*

All *Nicotiana tabacum* plants used for this project are wild-type *cv.* Petit Havana SR1. Transient transfection of leaf epidermal cells was performed on 5-week-old plants. Plants were germinated and grown in a controlled environment chamber at 20°C on a 16h light, 8 h dark cycle. Following infiltration, they were placed in a growth chamber (Sanyo) at 21 °C on a 14 h light, 10 h dark cycle, with a light intensity of 45 µmol photons · m^{-2} · s^{-1} and 70% humidity.

2.1.3 Seed surface sterilisation

A.thaliana or *N.tabacum* seeds were suspended in a 20% v/v NaClO solution and shaken by vortexing for 10 minutes. They were then washed 5 times with autoclaved water, tubes wrapped in aluminium foil and seeds stratified in the dark at 4°C for 3 to 7 days. After stratification, seeds were placed on either soil or agar using a pipette, and grown at the appropriate conditions.

2.1.4 Soil medium

A.thaliana plants were grown in 5 cm^2 pots on non-sterile Levington F2 soil (Everris). *N.tabacum* plants were grown in round or square 10 cm pots on either a 1:1 v/v mixture of non-sterile New Horizon

(Westland)/Levington F2 (Everris) at University of Exeter or on non-sterile Sinclair general purpose growing medium at University of Bristol. The following insecticides were added to the soil: 0.4 g/L Exemptor (Everris) for plants grown at University of Bristol or 0.2 g/L Intercept 70 WG for plants grown at University of Exeter (Everris).

2.1.5 Agar medium

Medium suitable for plant sterile cultivation was prepared by autoclaving a 2.15 g/L solution of Murashige and Skoog (Duchefa) (Murashige and Skoog, 1962) Basal Salts and 1% w/v agar (LabM) in distilled water.

2.2 Molecular biology methods

2.2.1 Phenol:chloroform gDNA extraction from *Arabidopsis thaliana* leaves

An *A.thaliana* leaf disk was clipped using the lid of an Eppendorf tube. 100 µL of DNA extraction buffer (0.2 M Tris-HCl (Melford) pH 8.8, 1% w/v SDS (Melford), 0.4 M LiCl (Sigma Aldrich), 25 mM EDTA (Fisher Chemical)) was added and the tissue was homogenised with a micropestle. 100 µL of a 25:24:1 v/v/v solution of phenol:chloroform:isoamyl alcohol (Sigma Aldrich) was added to the homogenised tissue. The mixture was vortexed for 5 s and centrifuged for 5 min at 13,000g at room temperature. The aqueous phase (upper layer) was then transferred to a fresh tube, 100 µL of isopropanol (Sigma Aldrich) was added and centrifuged again for 5 min at 13,000g. The supernatant was discarded and the pellet rinsed with 100 µL 70% v/v EtOH. After one last centrifugation for 3 min at 13,000g the pellet was air dried and re-suspended in 50 µL of sterile water.

2.2.2 Plasmid DNA extraction from *Escherichia coli* cells

Extraction of plasmid DNA from *E.coli* cells was carried out using a suitable miniprep commercial kit (E.Z.N.A. Plasmid DNA Mini Kit I, VWR). *E.coli* cells carrying the vector of interest were grown overnight in 5 mL of liquid LB medium (Luria-Bertani medium, Sigma Aldrich)

supplemented with the appropriate antibiotics (Table 2.1), at 37°C in a shaking incubator. Cells were pelleted by centrifuging the cultures at room temperature for 10 min at 3,000g. The supernatant was discarded and the pellet used for plasmid extraction using the above mentioned kit, following the manufacturer instructions.

Antibiotic	**Manufacturer**	**Cat. No**	**Working concentration**
Kanamycin	Melford	G0124	100 µg/mL
Spectinomycin	Melford	S0188	50 µg/mL
Gentamicin	Melford	G0124	10 µg/mL

Table 2.1: Antibiotics and working concentrations used for selective bacterial growth.

2.2.3 Cloning of Gateway® compatible expression plasmids

The Gateway® technology (Thermo Fisher Scientific) was used to insert genes of interest into vectors suitable for *Agrobacterium tumefaciens*-mediated transient and stable expression in plant cells. The procedure can be summarised as follows:

1. Amplification of the gene of interest from plasmid or gDNA by Polymerase Chain Reaction (PCR, see 2.2.4). Forward and reverse primers used for the amplification were designed to have flanking attB sites.

2. BP reaction to insert the PCR product into pDONR207. The attB sites flanking the PCR product recombine with the attP sites on the empty pDONR207, leading to the formation of an attL entry vector.

3. Transformation of *E.coli* cells (see 2.2.6) with the entry vector and extraction of plasmid DNA.

4. LR reaction to transfer the gene of interest from the entry vector to the destination vector. The attL sites on the entry vector recombine with the attR sites on the empty destination vector, allowing the transfer of the gene sequence and reforming the original attB sites.

5. Transformation of *E.coli* cells (see 2.2.6) with the destination vector and extraction of plasmid DNA.

6. Transformation of *A.tumefaciens* cells (see 2.2.7).

7. Stable or transient expression of the transgene in *A.thaliana* or *N.tabacum* (see 2.3.1 and 2.3.2).

The protocol was performed according to the instructions provided by Thermo Fisher Scientific. Correct insertion and frame of genes in the entry clones and destination vectors were checked by sequencing (MWG Eurofins).
Constructs GFP-MRF7S, MRF7S-GFP, GFP-ΔMRF7 and ΔMRF7-GFP were produced by Dr. Hongbo Gao.

2.2.4 DNA amplification by Polymerase Chain Reaction

Genes of interest to be cloned with the Gateway® strategy (see 2.2.3) were amplified from *A.thaliana* gDNA or plasmid DNA by Polymerase Chain Reaction (PCR). Gene specific forward and reverse primers with attB flanking regions were purchased from MWG Eurofins and amplification was carried out with proof-reading DNA polymerases (see Table 2.2).

2.2.5 Agarose gel electrophoresis

Amplification products obtained as detailed in 2.2.4 were checked by agarose gel electrophoresis. Electrophoresis was carried out on 1% w/v agarose gels (Sigma Aldrich) melted in 1x Tris/Borate EDTA buffer (TBE, 89 mM Tris-HCl pH 7.6 (Melford), 89 mM $B(OH)_3$ (VWR), 2 mM EDTA pH 8 (Fisher Chemical)). MIDORI^{Green} Advance DNA stain (Nippon Genetics) was used as DNA detecting agent and added to the agarose gels according to the manufacturer's instructions. Gels were run in a horizontal tank at 100 V and, when appropriate separtion was obtained, imaged with a UVP GelDoc imaging system (Thermo Fisher Scientific).

Polymerase	**Manufacturer**	**DNA amplified**	**Reaction mix**		**PCR amplification**
Platinum Pfx	Invitrogen	Plasmid DNA	1x Pfx amplification buffer		95°C, 5'
			0.3 mM dNTP mixture		
			1 mM Mg2SO4		95°C, 15"
			0.3 µM forward primer	27x	anneal T, 30"
			0.3 µM reverse primer		68°C, 1' per kb
			1U Platinum Pfx polymerase		
			50-100 ng template DNA		68°C, 5'
			autoclaved H2O up to 50 µL		
					4°C, ∞

Polymerase	**Manufacturer**	**DNA amplified**	**Reaction mix**		**PCR amplification**
GoTaq	Promega	gDNA	1x GoTaq® Green Master Mix		95C, 2'
			1uM forward primer		
			1uM reverse primer		95C, 30"
			50-100 ng template DNA	27x	anneal T, 30"
			autoclaved H2O up to 50 µL		72C, 1' per kb
					72C, 5'
					4C, ∞

Table 2.2: DNA Polymerases, reaction mixes and amplification conditions.

2.2.6 Heat-shock transformation of *Escherichia coli* cells

Gateway®cloning-compatible vectors assembled as described in 2.2.3 were transferred into *E.coli* cells, strain DH5α (Thermo Fisher Scientific), by heat-shock.

An aliquot of frozen cells was thawed for 5 minutes on ice, 50 ng of plasmid DNA added to the cells and incubated on ice for 30 min. Cells were heat-shocked in a water bath at 42 °C for 45 s and returned on ice for 2 min. 800 µL of liquid sterile LB medium (Luria-Bertani medium, Sigma Aldrich) were added and tubes were placed in a shaking incubator for 1 h at 37 °C. Cells were centrifuged at 3,500g for 3 minutes, most of the supernatant (except for 100 µL) removed and the pellet resuspended and plated onto LB agar plates supplemented with the appropriate antibiotics (see Table 2.1). Plates were left at 37°C overnight allowing transformed bacteria to grow.

2.2.7 Heat-shock transformation of *Agrobacterium tumefaciens*

Gateway®cloning-compatible vectors assembled as described in 2.2.3 were transferred into *A.tumefaciens* GV3101::pMP90 cells by heat-shock.
25 ng of DNA were added to 50 µL of frozen cells and allowed to thaw on ice for 15 min. Cells were then flash frozen in liquid nitrogen and heat-shocked in a water bath at 37°C for 5 min. 1 mL of YEB medium (5 g/L beef extract (BD Biosciences), 5 g/L peptone (Sigma Aldrich), 0.5 g/L $MgCl_2 \cdot 6H_2O$ (Sigma Aldrich), 1 g/L yeast extract (OXOID), 5 g/L sucrose (Fisher Chemical)) was added and cells were grown at 28°C in a shaking incubator for 4 hours. Cells were centrifuged at 3,000g for 3 min at room temperature, the supernatant was discarded and the pellet resuspended and plated on YEB agar plates supplemented with the appropriate antibiotics (see Table 2.1). Plates were left for 48 h at 28 °C allowing transformed bacteria to grow.

2.3 Transient and stable expression of fusion proteins

2.3.1 Transient expression in *Nicotiana tabacum* leaf epidermal cells

Transient expression in tobacco leaf epidermis was achieved by *Agrobacterium tumefaciens*-mediated infiltration (Sparkes et al., 2006). Briefly, *A.tumefaciens* cells carrying the destination vector with the gene of interest were inoculated in 5 mL of YEB medium (5 g/L beef extract (BD Biosciences), 5 g/L peptone (Sigma Aldrich), 0.5 g/L $MgCl_2 \cdot 6H_2O$ (Sigma Aldrich), 1 g/L yeast extract (OXOID), 5 g/L sucrose (Fisher Chemical)) supplemented with the appropriate antibiotics (see Table 2.1), and grown for 16-20 hours at 28°C in a shaking incubator.

1 mL of bacterial culture was centrifuged at room temperature at 3,000g for 5 min and resuspended in 1 ml of infiltration medium (5mg/mL glucose (Fisher Chemical), 50 mM MES (VWR Chemicals), 2 mM $Na_3PO_4 \cdot 12H_2O$ (Fisher Chemical), 0.1 mM acetosyringone (Sigma Aldrich)). The last step was repeated once and the optical density (OD) at 600 nm (OD_{600}) was measured with a spectrophotometer. The bacterial suspension was diluted at the appropriate final OD: unless otherwise stated, cells carrying organelle markers were diluted to a final $OD_{600} = 0.04$, while cells carrying other constructs were diluted to a final $OD_{600} = 0.1$. Bacteria suspensions at the appropriate concentrations were infiltrated with a needle-less syringe through the abaxial surface of tobacco leaves. Gene expression was checked on a fluorescence microscope 2 to 4 days post-infiltration.

2.3.2 Transformation of *Arabidopsis thaliana*

Generation of *A.thaliana* plants stably overexpressing genes of interest was achieved by floral dipping (Clough and Bent, 1998). Briefly, developing floral tissues of 4-week-old *A.thaliana* wild-type plants were dipped in a solution containing the appropriate strain of *A.tumefaciens* at a final OD_{600} = 0.8, 5 % w/v of sucrose (Fisher Chemical) and 0.05% v/v of Silwet L-77

(Fisher Scientific). Aerial tissues were dried from excess dipping solution, covered with a plastic bag to maintain humidity and plants were then laid on their sides for 24 h. On the following day, the plastic bags were removed and plants returned to a vertical position.

Seeds collected from the dipped plants were sterilised as in 2.1.3 and sown on agar plates supplemented with the appropriate herbicide to select transformants. In this instance, all transformants were selected on media containing phosphinotricin (glufosinate, Sigma Aldrich) at a final concentration of 15 µg/mL.

2.3.3 Crossing of *Arabidopsis thaliana* plants

A.thaliana plants stably overexpressing GFP-MRF7, GFP-MRF7S or GFP-ΔMRF7 were obtained as described in 2.3.2. Stable lines overexpressing the Golgi marker ST-mRFP were already available in the lab.

A.thaliana transgenic plants overexpressing ST-mRFP were used as paternal plants for crossing with plants overexpressing GFP-MRF7, GFP-MRF7S or GFP-ΔMRF7. Maternal plants were used at a stage where they had developed a few inflorescences. Smaller buds were removed from the maternal plant meristems, leaving only one unopened bud for each meristem. All remaining buds were emasculated with clean tweezers and pollinated with pollen from a mature open flower from the father plant. The pollinated inflorescences were carefully wrapped in cling film and marked with a bit of tape. Seeds were collected when ready and progeny checked on a fluorescence microscope.

2.4 Drug treatments

2.4.1 Latrunculin B treatment for actin depolymerisation

The actin polymerisation inhibitor Latrunculin B (LatB, Sigma Aldrich) was stored at -20°C as a 10 mM stock solution in DMSO. The working solution was made up fresh by diluting the stock in distilled water to a final concentration of 25 µM.

A 0.5x0.5 cm^2 square of leaf was excised from the plant using a blade

and divided into 4 smaller squares which were left floating for 1 h on 500 µL of LatB working solution. Controls were performed by following the same procedure but leaving the leaf squares floating on 500 µL of a 0.25% (v/v) DMSO solution.

2.5 Microscopy

2.5.1 Confocal microscopy

Confocal Laser Scanning Microscopy

At the University of Exeter, confocal laser scanning microscopy data were collected on a Zeiss LSM 510 Meta microscope. Leaf squares of about 5 mm^2 were excised 2 to 4 days post-infiltration and expression was analysed with a 63x oil immersion objective. CFP, GFP and mRFP were excited at 405 nm, 488 nm and 543 nm respectively. Emissions were detected using 470-500, 505-530 and 560-615 band pass filters for CFP, GFP and mRFP respectively. All images were captured with 512x512 pixel resolution, using a 2.8x digital zoom for Golgi and a 1.8x digital zoom for peroxisome, 8x line average. Movies were taken with 256x256 pixel resolution, 1x line average over 19s (100 frames) at 2.8x digital zoom and 150x125 pixel ROI for Golgi, and over 26s (200 frames) at 1.8x digital zoom and 154x86 pixel ROI for peroxisomes. Only the cortical region of leaf epidermal cells was imaged.

At the University of Bristol, confocal laser scanning microscopy data were collected on a Leica SP5-AOBS confocal laser scanning microscope. As for experiments conducted at University of Exeter, leaf squares of about 5 mm^2 were excised 2 to 4 days post-infiltration and expression was analysed with a 63x HCX PL APO lambda blue (NA 1.4) oil immersion objective. CFP, GFP and mRFP were excited at 405 nm, 488 nm and 561 nm respectively. Emissions were detected 460-480 nm, 500-515 nm and 585-595 nm filters for CFP, GFP and mRFP respectively. All images were captured using bidirectional sequential scanning with 512x512 pixel resolution, using a digital zoom of 6x and 8x line average. Movies were taken using sequential bidirectional scanning, with 512x256 pixel

resolution, at a digital zoom of 6x, 1x or 2x line average for 100 frames. Only the cortical region of leaf epidermal cells was imaged.

2.5.2 FRET-FLIM

Principles of fluorescence lifetime imaging

In vivo protein-protein interaction can be investigated by FRET-FLIM. FRET (Förster Resonance Energy Transfer) is a photophysical process in which energy is non-radiatively transferred from an excited donor molecule to a non-excited acceptor molecule (or quencher) within a maximum distance of around 10 nm (Förster, 1948). For FRET to happen, the donor emission and the acceptor absorption spectra must have a certain degree of overlap (Fig.2.1a, light grey); dipole orientation and overlap and a good quantum yield are also required, and therefore appropriate choice of fluorophores is crucial (Bajar et al., 2016).

FRET can be quantified in several ways, one of which is fluorescence lifetime imaging (FLIM). One of the effects of FRET is a reduction of the excited state lifetime (τ) of the donor molecule; in other words, the donor will remain in an excitated state for a shorter period of time if FRET occurs. Thus, by tagging two potentially interacting proteins with a donor and an acceptor fluorophore respectively, and measuring the lifetime of the donor in the presence and absence of the acceptor allows to determine whether or not they might be interacting based on the occurrence of FRET.

Moreover, the energy transfer efficiencies and related molecular distances between donor and acceptor can be estimated by calculating FRET efficiency (Eq.2.1).

$$E_{\mathrm{FRET}} = 1 - \frac{\tau_{\mathrm{DA}}}{\tau_{\mathrm{D}}} \tag{2.1}$$

In Eq.2.1, τ_{DA} indicates the donor lifetime in the presence of the acceptor, while τ_{D} indicates the donor lifetime in the absence of the acceptor. Efficiency decreases with the increase of the distance between fluorophores (Fig.2.1b). FRET efficiency values can be used to calculate an estimated distance (r) between the donor and the acceptor (Eq.2.2).

$$r = R_0 \cdot \sqrt[6]{(\frac{1}{E_{\mathrm{FRET}}} - 1)} \tag{2.2}$$

In Eq.2.2, E_{FRET} is the FRET efficiency as calculated in Eq.2.1, while R_0 represents the Förster radius, the distance at which 50% of FRET occurs. R_0 will vary depending on which donor and acceptor molecules are employed for FRET studies. For the FRET pair used here, R_0 = 5.4 nm (Lam et al., 2012).

Experimental procedure

N.tabacum leaf epidermis samples were excised and treated with Latrunculin B as described in 3.2.6 and FLIM data were collected using a single-photon system at the Central Laser Facility (Research Complex at Harwell). The FLIM platform was assembled and calibrated by the Central Laser Facility Prof Stan Botchway prior to use. The confocal and lifetime set up was assembled as follows.

The system is equipped with a SuperK EXTREME NKT-SC 470-2000 nm supercontinuum laser (NKT Photonics) which generates 80 MHz pulses every 70 ps. The desired wavelengths were selected using a SuperK SELECT 29 multi-line tunable filter (NKT photonics). Prior to FLIM, confocal imaging of GFP, RFP and transmitted light was carried out on a Nikon Ti microscope with a Nikon D-eclipse C1 scan head (EZ-C1 v.3.91 software, Nikon). GFP and RFP were excited at wavelengths of 488 nm and 561 nm, respectively and imaged using a Nikon 60x VC (NA 1.20) with water correction objective, at a field zoom of 50 µm. Fluorescence emissions of GFP and RFP were selected with a Nikon 520±35 and a Comar 633IU filters, respectively.

Following confocal imaging, GFP lifetime was measured with a PMH100 detector and raw FLIM data were generated by single-photon counting SPC-150 v.9.77 software (Becker and Hickl, GmbH). All data presented here were collected in "Scan Sync In" mode, with a 128x128 resolution and a pixel dwell time of 7.92 µs. Raw FLIM images were analysed with

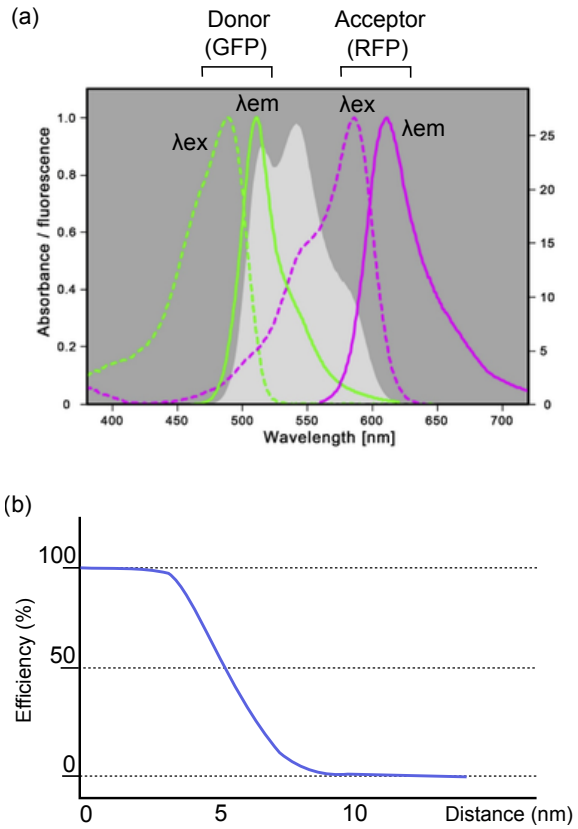

Figure 2.1: Schematic representation of the main concepts of FRET. FRET (Förster Resonance Energy Transfer) is dependent upon two main factors: (a) spectra overlay between the donor emission and the acceptor absorption (Addgene.org); (b) distance between fluorophores. FRET efficiency is an indicator of the distance between donor and acceptor. Adapted from (Willem Borst and Visser, 2010).

the SPCImage software v.6.9 (Becker and Hickl, GmbH); an incomplete multiexponential fit model with a laser repetition time value of 12.5 ns was used for the decay curve fitting. Lifetime values with χ^2 between 0.8 and 1.3 were taken into account. GFP lifetime was measured both on individual Golgi bodies and in the cell cytoplasm.

2.6 Quantification of organelle dynamics

Quantification of organelle dynamics from movies collected as described in 2.5.1 was carried out with the commercial software Imaris (Bitplane) on movies aquired at University of Exeter. The ImageJ (NIH) plugin TrackMate was used to track organelle movement for movies aquired at University of Bristol.

Among the parameters extracted from organelle tracking data, the following were taken into account for further analyses:

- Track duration (s): time length of the track.
- Track displacement (µm): length of the shortest line connecting the initial and final position of the organelle for that particular track (see Figure 2.2).
- Track speed (µm/s): entire length of the track (see Figure 2.2) over time.
- Track displacement rate (µm/s): track displacement over duration. This is the length of the shortest path between the start and end point of the track, over time (Equation 2.3).
- Meandering index (Arbitrary Units, AU): track displacement rate over speed (Equation 2.4). This is an indicator of the directionality of the movement and therefore of the track straightness: organelles with highly directional movement will have a meandering index value closer to 1 AU, while organelles with rather saltatory movement will have a meandering index value closer to 0 AU.

$$Displacement\ Rate\ (\mu m/s) = \frac{Track\ displacement\ (\mu m)}{Track\ duration\ (s)} \tag{2.3}$$

$$Meandering\ Index\ (A.U.) = \frac{Displacement\ rate\ (\mu m/s)}{Speed\ (\mu m/s)} \tag{2.4}$$

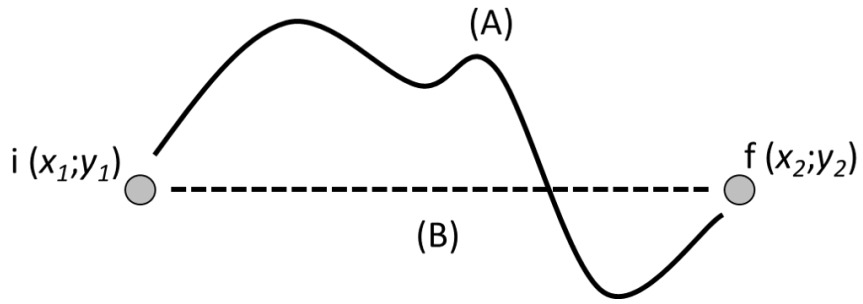

Figure 2.2: Comparison between displacement and full-length of a track. Given i(x_1;y_1) and f(x_2;y_2) as the coordinates of the initial and final positions, the full length of the track (A, bold line) is the length of the entire path followed by an organelle moving from i(x_1;y_1) to f(x_2;y_2). Track displacement (B, dotted line) indicates the length of the shortest path from i(x_1;y_1) to f(x_2;y_2).

2.7 Protein methods

2.7.1 Protein extraction and quantification from *A.thaliana* seedlings

0.5 to 2 grams of leaf tissue from 4-week-old *A.thaliana* plants or 2-week-old whole *A.thaliana* seedlings were harvested and flash frozen in liquid nitrogen. The harvested material was ground in liquid nitrogen and 1µL of GFP-Trap lysis buffer *per* mg (fresh weight) of plant material was added (GFP-Trap® lysis buffer composition: 10 mM Tris-HCl (Melford) pH 7.5, 150 mM NaCl (Fisher Chemical), 0.5 mM EDTA (Fisher Chemical) pH 7.5, 0.5% v/v Triton X-100 (Alfa Aesar), 1x cOmplete™ protease inhibitor cocktail (SigmaAldrich)). Samples were incubated on ice for 30 minutes and centrifuged at 12,000g for 15 min at 4°C. Supernatants were transferred to a fresh tube and the centrifugation step repeated for another 10 min.

Total protein content was quantified by Bradford quantification assay (Bradford, 1976), according to the Bradford reagent manufacturer's protocol (SERVA Electrophoresis GmbH).

2.7.2 Immunoprecipitation with GFP-Trap ®_A beads

Total protein extract obtained as in 2.7.1 was diluted 1:5 v/v in ice cold GFP-Trap® dilution buffer (10 mM Tris-HCl (Melford) pH 7.5, 150 mM NaCl (Fisher Chemical), 0.5 mM EDTA (Fisher Chemical) pH 7.5, 1x cOmplete™ protease inhibitor cocktail). Co-immunoprecipitation was performed according to the GFP-Trap®_A beads manufacturer's protocol (Chromotek).

Briefly, 30 µL of beads for each sample were washed 3 times in 500 µL ice cold dilution buffer. The diluted protein extracts were then added to the beads and incubated at 4°C for 2 hours under constant mixing. Tubes were centrifuged at 2,700g for 2 min at 4°C and the supernatant discarded. Beads were sent to the University of Bristol proteomics facility for Liquid Chromatography-Mass Spectrometry (LC-MS) analysis.

2.7.3 SDS-PAGE and Western Blot

Equal amounts of total protein extracts prepared as in 2.7.1 and purified GFP fusion proteins obtained as in 2.7.2 were separated on a 4-15% gradient acrylamide gel by SDS-PAGE, using Mini-PROTEAN® TGX™ Precast Gels (Bio-Rad).

Proteins were transferred onto a PVDF membrane (Pall Corporation, BioTrace™ PVDF, 0.45 µm) by standard tank blotting. Ponceau S (Fisher Chemicals) staining solution (0.1% w/v Ponceau S, 0.5 % v/v HAc) was used to check the loading. The membrane was destained in distilled water and blocked for 1 h at room temperature in 5% w/v de-fatted milk (Marvel) solution in TBS-T (150 mM Tris-HCl (Melford) pH 7.6, 150 mM NaCl (Fisher Chemical), 0.05% Tween-20 (Sigma Aldrich)). Following blocking, the membrane was incubated over-night at 4°C, under gentle shaking, with the primary antibody. It was then washed 3 times in TBS-T and incubated 1 h with the secondary antibody. Following 3 more washes in TBS-T, the membrane was developed using a chemiluminescent substrate. The substrates used were either the SuperSignal® West Femto or the Pierce® ECL western blotting substrates (both from Thermo Fisher Scientific).

All protocols, solutions and running conditions were as suggested by Bio-Rad, Abcam and Thermo Fisher Scientific. Table 2.3 specifies the type of antibodies used, manufacturers and working concentrations.

Antibody	**Cat. No**	**Manufacturer**	**Dilution**
Rabbit IgG α-GFP	ab290	Abcam	1:2,500
Goat α-rabbit IgG fC- HRP	ab97200	Abcam	1:5,000

Table 2.3: Primary and secondary antibodies used for detection of GFP fusion proteins.

2.8 Statistical analysis

Graphical representations and statistical analysis were generated with Microsoft Office Excel and GraphPad Prism 8. Format of data representation and statistical tests were chosen on a case-to-case basis,

depending on the type of data collected. Specifications on the choice of tests is provided within each section.

2.9 Bioinformatic tools

2.9.1 Multiple alignment of DNA and protein sequences

Clustal Omega (EMBL-EBI) was used for multiple alignments of DNA and protein sequences. Alignments were run with the default parameters provided by the tool. Alignments were run with the default parameters provided by the tool: "Dealign input sequences = no"; "Mbed-like clustering guide-tree = yes"; "Mbed-like clustering iteration = yes"; "Number of combined iterations = default (0)"; "Max guide tree iterations' = defaults"; "Max hmm iterations =defaults"; "Order = aligned".

2.9.2 Gene expression

Gene expression levels were analysed with GENEVESTIGATOR®.

Chapter 3

Localisation of myosin receptors

Unlike other *A.thaliana* MyoB receptors MRF7 localises to a known compartment, the Golgi apparatus. The myosin and myosin receptor families in *A.thaliana* show a certain degree of redundancy, so the ability of MRF7 to specifically localise to Golgi is fundamental in an attempt to decipher which factors determine specific myosin recruitment to an organelle. In this chapter, I aim to define what triggers the Golgi localisation of MRF7, what are the roles of the other domains within the protein and what the role of the DUF593 domain is for MRF7 localisation.

3.1 Introduction

3.1.1 Domain architectures of MyoB receptors

The *Arabidopsis thaliana* Myosin-Recruitment Factor 7 (MRF7) is one of 16 members of the MyoB family of myosin receptors. MyoB proteins are divided into six subfamilies based on their architecture (Holding et al., 2007; Peremyslov et al., 2013). Although their length and domain composition can vary (Fig.3.1), they all harbour a Domain of Unknown Function 593 (DUF593) responsible for myosin binding (Peremyslov et al., 2013; Stephan et al., 2014). DUF593 is conserved in all land plants, from vascular and non-vascular mosses to flowering plants, without any apparent distinction between monocots and dicots (Holding et al., 2007; Peremyslov et al., 2013). DUF593 was shown to mediate the interaction between *At*MyoB2 and *At*XI-K tail (Peremyslov et al., 2013) and between *Nt*RISAP and *Nt*MYOXIpt (Stephan et al., 2014) (see Chapter 5 introduction). Multiple alignment of DUF593 sequences from all the *At*MyoB receptors highlights the presence of eight conserved residues, which appear to be divided into two motifs (Fig.3.2). An ExxxERxA motif nearer to the N-terminus of the domain, and an LxxxKxxxxxExxQ motif (Fig.3.2, yellow).

Arabidopsis thaliana MRF7 is a 324 amino acids protein from subclass IIA of the MyoB receptor family (Peremyslov et al., 2013). MRF7 has a relatively simple architecture (Fig.3.3a), with the DUF593 domain occupying the N-terminus of the amino acidic sequence, and four coiled-coil domains, two of which are situated within DUF593. The ExxxERxA region falls exactly within the first coiled-coil domain. Given the lack of predicted trans-membrane domains (TMDs) and of predicted myristoylation or palmytoilation sequences for membrane association, MRF7 is considered to be a soluble protein.

3.1.2 Localisation of MyoB myosin receptors

*At*MyoB receptors were shown to influence the movement of organelles such as Golgi, mitochondria and peroxisomes (Peremyslov et al., 2015).

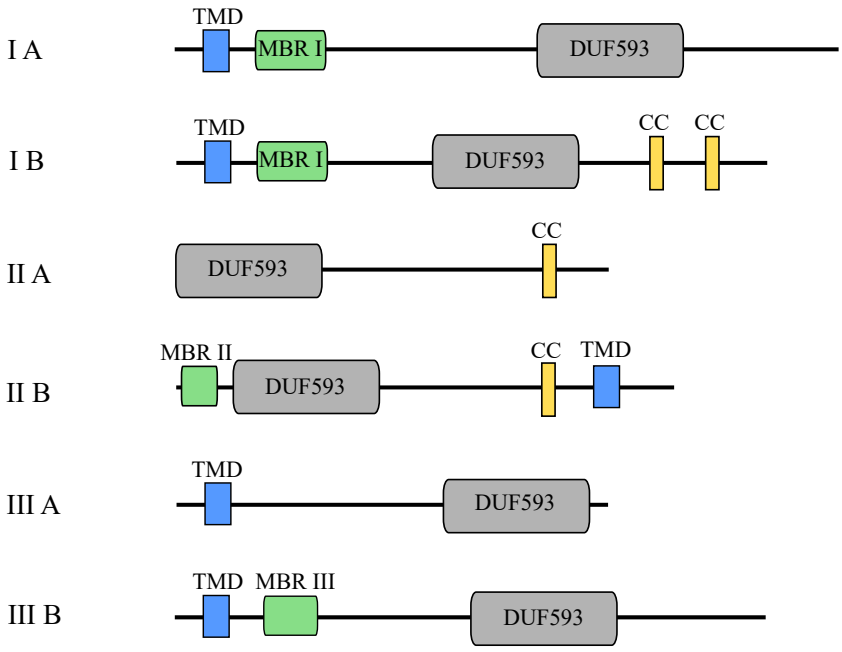

Figure 3.1: Architectures of the *A.thaliana* MyoB myosin receptors. Schematic representation of the six subclasses of MyoB receptors from the model plant *A.thaliana*. Subclasses are indicated on the left hand side and different domains are labelled by different colours. MRF7 belongs to subclass IIA. DUF593 = Domain of Unknown Function 593 (Predicted myosin binding domain), TMD = Trans-Membrane Domain, MBR = Metal-Binding Region, CC = Coiled-Coil. Adapted from (Peremyslov et al., 2013).

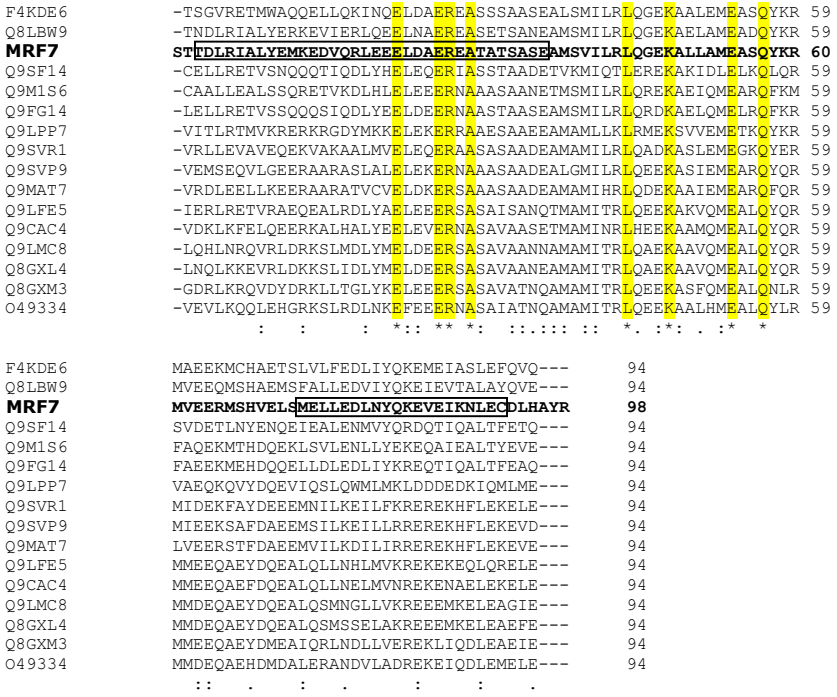

Figure 3.2: Amino acid conservation of the DUF593 domain containing proteins in *A.thaliana*. The figure shows a multiple sequence alignment of the DUF593 domain from all 16 members of the MyoB family. FASTA protein sequences were retrieved from the UniProt database and aligned using the Clustal Omega tool. Conserved amino acids are highlighted in yellow and the position of the two coiled-coil domains within DUF593 of MRF7 are indicated with black rectangular boxes. UniProt accession numbers are displayed on the left hand side and the DUF593 sequence from MRF7 is in bold. The alignment was run on the Clustal Omega default settings.

In particular, expression of the DUF593 domain led to a similar effect to that of the over-expression of dominant negative myosin XI tails or knock-out of certain myosin genes, resulting in a non specific decrease of various organelles movement (Avisar et al., 2009; Peremyslov et al., 2015) and growth and developmental defects (Peremyslov et al., 2010b; Ojangu et al., 2012; Peremyslov et al., 2013; Peremyslov et al., 2015). Despite the effects that MyoBs have on multiple organelles dynamics, attempts to detect them on a specific compartment have so far proven challenging (Peremyslov et al., 2013; Kurth et al., 2017).

MyoBs in *A.thaliana* were shown to localise to punctate structures moving in straight trajectories and with high speeds in the cell cytoplasm, with what has been defined as a "beads-on-a-string" configuration (Peremyslov et al., 2013; Peremyslov et al., 2015; Kurth et al., 2017). Expression of MyoB1-YFP in *xi-k xi-1 xi-2 A.thaliana* background showed that the localisation of such receptor is myosin-dependent (Peremyslov et al., 2013). The triple myosin knock-out exhibits a misarranged actin network (Cai et al., 2014), thus suggesting that the MyoB1-YFP cytoplasmic diffusion could be attributed to an altered cytoskeletal organisation. Furthermore, subcellular fractionation studies from leaf extracts of MyoB1-YFP expressing plants have highlighted that these punctate structures have a membranous nature, and that targeting of MyoB1 (subfamily IA, Fig.3.1) and MyoB2 (subfamily IB, Fig.3.1) to such structures relies on their N-terminal transmembrane domain (Peremyslov et al., 2013). Brefeldin A treatments appear to exclude that MyoB vesicles belong to BFA sensitive compartments (Peremyslov et al., 2013).

The only examples of MyoB receptors localised to specific organelles come from non-*A.thaliana* plant systems. *Zm*Fluory1 (Fl1)(Holding et al., 2007) is a DUF593 containing protein responsible for the correct distribution of 22-kDa α-zein in maize protein bodies; immunolocalisation showed that Fl1 is localised to the ER membrane surrounding protein bodies. Localisation of Fl1 to the ER membrane is suggested to occur through one of the N-terminal trans-membrane domains (Holding et al., 2007).

*Nt*RISAP is a DUF593 protein associated with the Trans-Golgi Network (TGN) (Stephan et al., 2014) and, like MyoB1, belongs to subfamily IA (Fig.3.1). It interacts with a pollen tube specific tobacco myosin (MYOXIpt) through the DUF593 domain (Stephan et al., 2014). Pollen tubes elongate by polar tip growth and requires continuous fusion of Golgi-derived secretory vesicles with the plasma membrane. This process is tightly coordinated and requires precise positioning of organelles and the actin cytoskeleton within the subapical region (Derksen et al., 1995; Hepler et al., 2001). RISAP localisation to the pollen tube TGN and to secretory vesicles is suggested to be the result of the contribution of the N-terminal hydrophobic region and the C-terminal domain, which modulates binding with the ROP GTPase RAC5. Over-expression of both RISAP and pollen tube ROP GTPases (Li et al., 1999; Stephan et al., 2014) severely interferes with tip growth. Localisation of RISAP is also altered upon actin depolymerisation, as it relocates from a strictly apical localisation to more diffuse pattern within the pollen tube cytoplasm (Stephan et al., 2014).

3.1.3 Aims

This chapter explores the molecular mechanisms of MRF7 targeting to the Golgi and the role of other domains within the protein, particularly of the predicted myosin-binding DUF593 domain on MRF7 localisation.

3.2 Results

3.2.1 Cloning of wild-type and truncated MRF7 fluorescent fusions for subcellular localisation studies

The MRF7 wild-type gene sequence was initially amplified from *A.thaliana* gDNA and cloned into Gateway destination vectors harbouring a Green Fluorescent Protein (GFP) tag. N- or C- terminal fusions under CaMV 35S promoter were produced to test for positional effect.

Studies carried out on subdomains of myosin tails, such as the DIL and PAL domains from several myosins XI (Sattarzadeh et al., 2011; Sattarzadeh et al., 2013) and the GT1 and GT2 regions from myosin XI-1 (Li and Nebenführ, 2007), suggest that different domains within the same myosin tail could be responsible for localisation to different organelles. The strategy used to determine critical regions within MRF7 required for subcellular localisation was to generate and compare several truncated MRF7 constructs with full-length MRF7 fusions. Deletions at either the N- or C- terminus, or a combination of both, are depicted in Fig.3.3. In addition, these fusions would narrow down the contribution of single domains required for potential binding to myosins (Chapter 5) and adaptor proteins, and the effect on organelle movement (Chapter 4).

Fig.3.3a represents the wild-type MRF7 protein (324aa). N-terminal deletions of MRF7 involve the progressive shortening of the DUF593 domain: MRF7S (Fig.3.3b) and ΔMRF7 (Fig.3.3d) lack half or all of the myosin binding domain respectively. C-terminal deletions, labelled as "ΔC" following the constructs name (Fig.3.3c, e), consist of a 54 amino acids truncation from the end of the fourth coiled-coil region up to the 324th amino acid. A construct only harbouring the full-length DUF593 domain is reported in Fig.3.3f.

Like their wild-type counterpart, all truncations were tagged with GFP at the N or C terminus and put under the control of the CaMV 35S promoter. The chimeric constructs were then agroinfiltrated into tobacco to obtain a strong transient expression, or transformed into *A.thaliana* plants by floral dipping to obtain stably expressing lines.

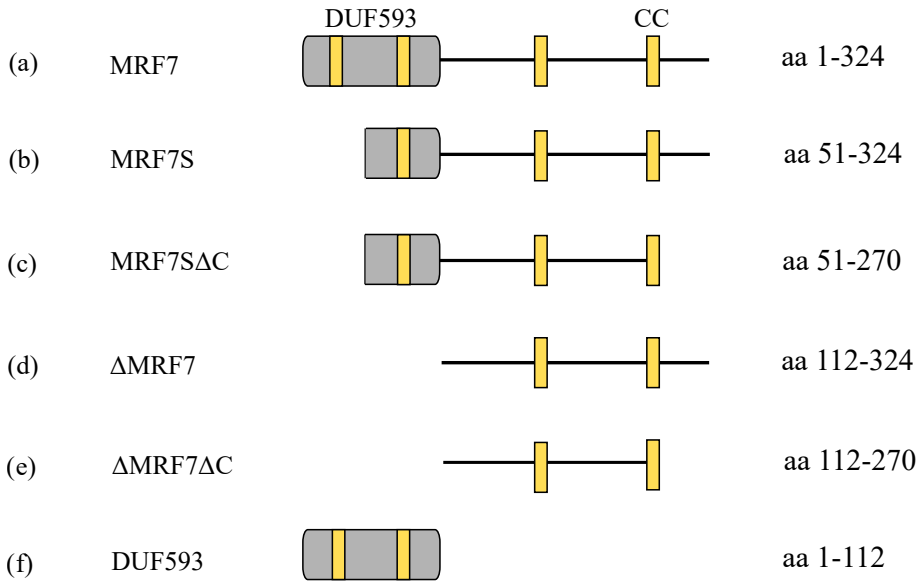

Figure 3.3: Schematic representation of the domain composition of wild-type and truncated MRF7 constructs. The figure summarises all the MRF7 constructs used in this project. The wild-type AtMRF7, 324 amino acids long, is represented in panel (a). Panels (b) to (f) are a series of N- and C-terminal truncations of the protein, or a combination of both. Grey boxes represent the Domain of Unknown Function 593 (DUF593), yellow rectangles represent coiled-coil (CC) domains. Amino acid range of each construct with respect to the wild-type sequence is reported on the right hand-side. GFP was fused to either the N- or C- terminus of these constructs and the chimeras obtained were transiently or stably over-expressed in *N.tabacum* or *A.thaliana* plants respectively.

3.2.2 Over-expression of wild-type GFP-MRF7 reveals a dual "beads-on-a-string" and Golgi membrane localisation

With rare exceptions from tobacco and maize (Stephan et al., 2014; Holding et al., 2007), the MyoB receptors described so far in the literature appear to be localised exclusively on unidentified punctate structures, which move in the cell cytoplasm with straight trajectories (Peremyslov et al., 2013; Peremyslov et al., 2015; Kurth et al., 2017), a configuration referred to as "beads-on-a-string". MyoB1 co-localises with the full-length myosin XI-K in leaves of *Arabidopsis* following the same pattern (Peremyslov et al., 2013), therefore suggesting that MyoB receptors move on existing actin tracks.

Transient over-expression of GFP-MRF7 in tobacco leaf epidermal cells showed consistency with the localisation of other MyoB receptors: MRF7 moves on punctate structures within the cytoplasm (Fig.3.4a). Co-expression with the actin marker LifeAct-mRFP (Fig.3.4b-c) demonstrates that GFP-MRF7 indeed moves along actin tracks. The timelapse in Fig.3.4d-f provides a visual example: cyan, magenta and yellow panels represent successive still images taken at 15 seconds intervals. Panel (g) is the overlay of all timepoints, where white pixels indicate still regions: very few puncta appear to be non-motile, while most of them seem to travel very dynamically in the cell. GFP-MRF7 puncta were tracked with the ImageJ plugin TrackMate, and compared with reported speed values for other MyoBs (Peremyslov et al., 2015). On a first observation it was evident that the MRF7 puncta were moving, on average, faster than organelles. In particular, it was challenging to identify a scan speed fast enough to allow TrackMate not only to follow the GFP-MRF7 puncta movement fully throughout the movie, but to also obtain an adequate resolution for the software to be able to distinguish the puncta from the background fluorescence.

The frequency distributions in Fig.3.4h-i describe the speeds and straightness of the tracks. On average, GFP-MRF7 puncta move at 4

µm/s; the lowest and highest speeds registered span between 1 µm/s and 8 µm/s respectively. The lowest speeds are similar to the average values registered for spheroid organelles such as Golgi (∼1 µm/s) and peroxisomes (∼0.6 µm/s) (Peremyslov et al., 2015; Osterrieder et al., 2017). The highest speeds are comparable with the speed of cytoplasmic streaming and of the organelles moving within the stream (4-10 µm/s) (Nebenführ et al., 1999; Jedd and Chua, 2002; Mathur et al., 2002). Interestingly, the average speed of the puncta (4 µm/s) is consistent with that observed for other MyoB receptors (Peremyslov et al., 2015) and can be compared with the *in vitro* velocities of certain full-length or motor domains from *A.thaliana* myosins (Tominaga et al., 2013; Haraguchi et al., 2018).

Meandering indexes of the tracks, expressed in Arbitrary Units (AU) and reported in Fig.3.4i, indicate that most of the tracked puncta display a very directional movement, as the majority of the values are included between 0.5 and 1 AU. This result supports what is observed in Fig.3.4a-c.

In addition to its punctate localisation and unlike other *A.thaliana* MyoBs, GFP-MRF7 was detected on the Golgi (Fig.3.5a-c). Graphs in Fig.3.6a-b provide a quantification of the Golgi localisation. GFP-MRF7 tended to collocate to a percentage of Golgi within the cell, rather than the whole population of Golgi within the imaged area. To summarise, when infiltrating GFP-MRF7 it is expected that, on average, 10% of the cells analysed will have a certain degree of GFP-MRF7 localisation on Golgi (Fig.3.6a). Moreover, in cells with GFP-MRF7 localisation on Golgi, on average 45% of the Golgi will have GFP-MRF7 on the membrane (Fig.3.6b).

3.2.3 The DUF593 domain is not responsible for MRF7 Golgi localisation

As discussed in 3.2.2, GFP-MRF7 is located to the Golgi in addition to the typical MyoB punctate structures (Fig.3.5a-c). The current literature on *A.thaliana* MyoB receptors lacks evidence for MyoBs collocating to a known oganelle whose movement they affect (Peremyslov et al., 2013;

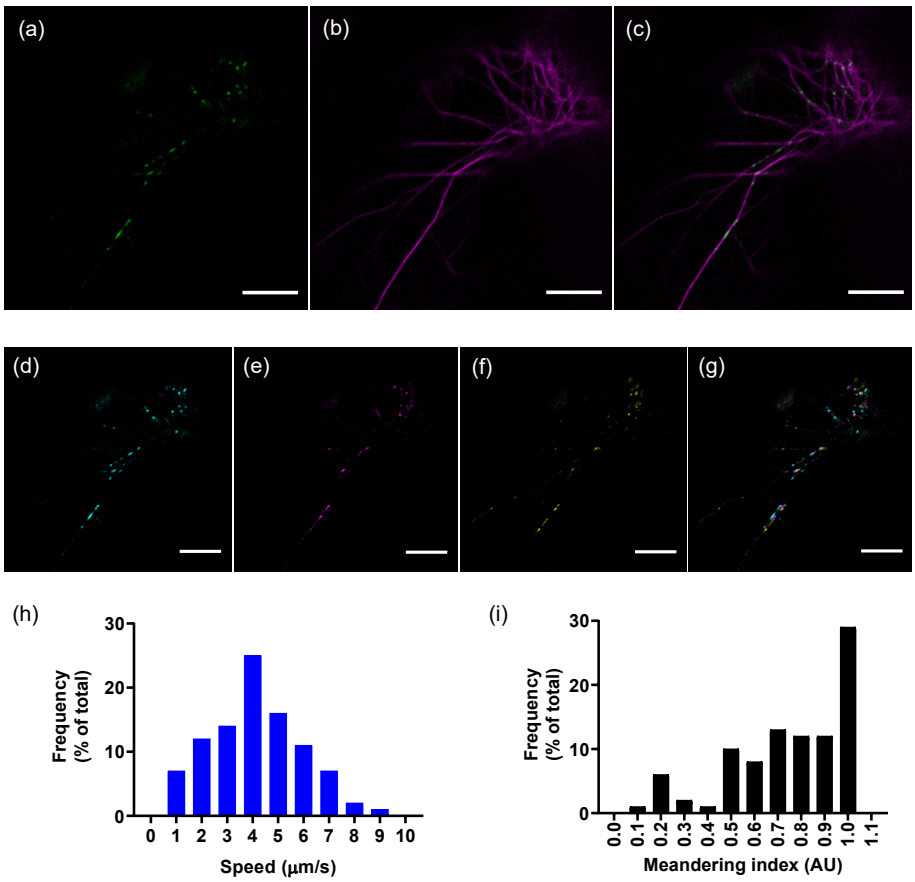

Figure 3.4: GFP-MRF7 moves on discrete puncta along the actin cytoskeleton. GFP-MRF7 localises to discrete puncta in a beads-on-a-string configuration (a). Co-expression with the actin marker LifeAct-RFP (b,c), shows that GFP-MRF7 moves on actin tracks. GFP-MRF7 and LifeAct-RFP were transiently expressed in tobacco leaf epidermal cells and imaged 2 days post-infiltration (DPI) on a confocal microscope. The false-colour timelapse images in panels (d) to (g) highlight the dynamicity of the GFP-MRF7 structures: cyan (d), magenta (e) and yellow (f) panels represent successive still images taken at 15 s intervals. Panel (g) is the overlay of the three timepoints: white pixels depict static regions. Histograms in (h) and (i) describe the movement characteristics of the GFP-MRF7 puncta, specifically the frequency distribution of speeds (h) and straightness of their tracks (i) registered by automated tracking (TrackMate). Puncta were tracked from 13 cells across 2 independent experiments. All images and movies were taken 2 DPI. Scalebars = 10 µm.

Peremyslov et al., 2015; Kurth et al., 2017). Here, the role of DUF593 in MRF7 localisation was investigated, and specifically how the localisation is influenced in constructs with a partially or fully deleted DUF593 domain. For this purpose, MRF7 constructs lacking half (MRF7S, Fig.3.3b) or all of the DUF593 (ΔMRF7, Fig.3.3d) were generated. The two constructs, fused to GFP at their N-termini, were transiently expressed in tobacco leaf epidermal cells with the Golgi marker ST-mRFP and imaged 2 days post-infiltration.

The first noticeable effect of the partial (GFP-MRF7S, Fig.3.5d-f) or complete (GFP-ΔMRF7, Fig.3.5g-i) deletion of DUF593 is the disappearance of the punctate structures characteristic of GFP-MRF7 (Fig.3.5a-c), and of other MyoB receptors in general (Peremyslov et al., 2013; Peremyslov et al., 2015; Kurth et al., 2017). GFP-MRF7S and GFP-ΔMRF7 seem to have lost the ability to localise to/form punctate structures, instead displaying a more cytoplasmic distribution, although the ability to localise to Golgi doesn't appear to be affected in the truncated constructs. As observed for GFP-MRF7, not all the Golgi bodies within a cell display GFP-MRF7S and GFP-ΔMRF7 encircling the Golgi membrane marker, ST-mRFP. It appears that GFP-MRF7S and GFP-ΔMRF7 expression leads to a higher percentage of cells with Golgi localisation when compared to GFP-MRF7 ($P<0.05$, Fig.3.6a), whereas there seems to be no substantial difference between the two truncations ($P=0.95$, Fig.3.6a). In addition, there is no significant difference in the percentage of Golgi localisation in those cells ($P>0.05$, Fig.3.6b). These results indicate that Golgi targeting of GFP-MRF7 is independent of the potential myosin-binding domain (DUF593). In addition, MRF7 DUF593 truncations are more reliably present on Golgi, inferring that DUF593 may have a regulating but not essential role in Golgi localisation. Interestingly, the same relative subpopulation of Golgi within a cell display MRF7 (∼45%).

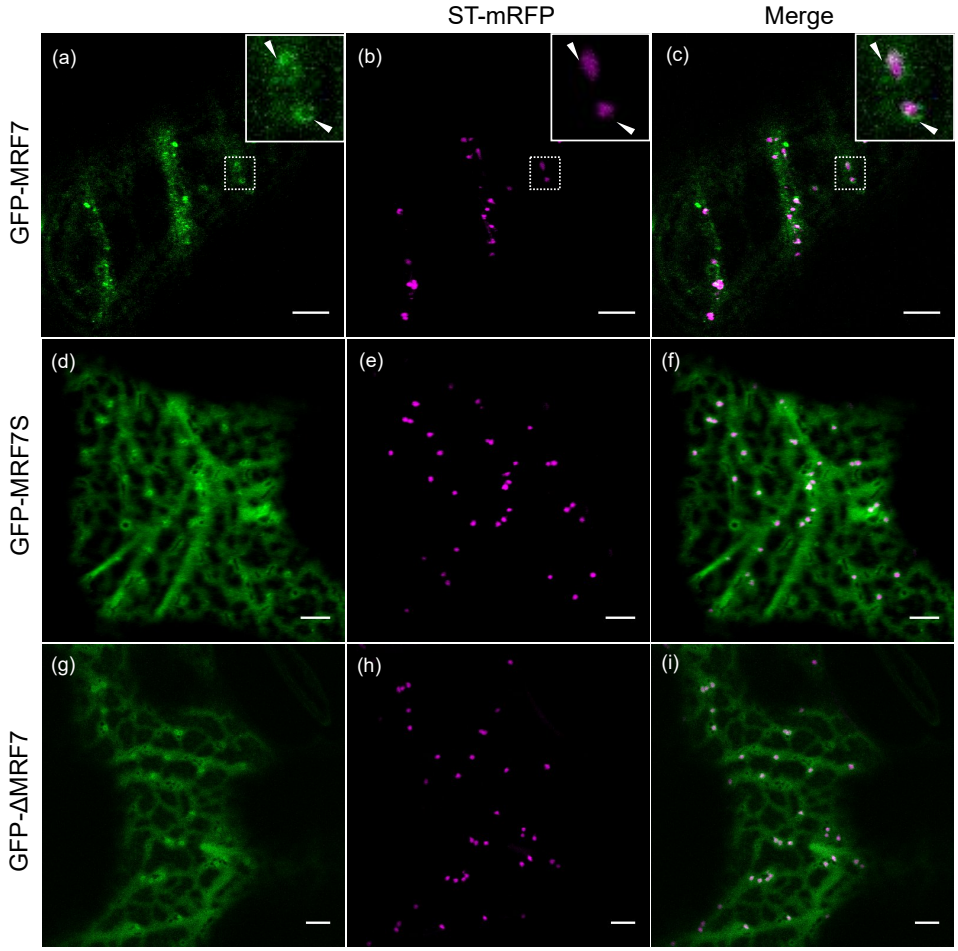

Figure 3.5: Subcellular localisation of GFP-MRF7, GFP-MRF7S and GFP-ΔMRF7 in *N. tabacum* leaf epidermal cells. GFP-MRF7 (a), GFP-MRF7S (d) and GFP-ΔMRF7 (g) were transiently transfected into tobacco leaf epidermal cells, in combination with the Golgi marker ST-mRFP (b, e, h) and imaged at 2 DPI. GFP-MRF7 (a, b, c) mainly localises to moving puncta, but is also occasionally present as a faint halo on the Golgi membrane (white arrowheads). GFP-MRF7S (d, e, f) and GFP-ΔMRF7 (g, h, i) also show a dual localisation: like GFP-MRF7 they can localise to the Golgi membrane (f, i), but are unable to form moving puncta, instead showing a more cytoplasmic distribution. Scalebars = 5 µm.

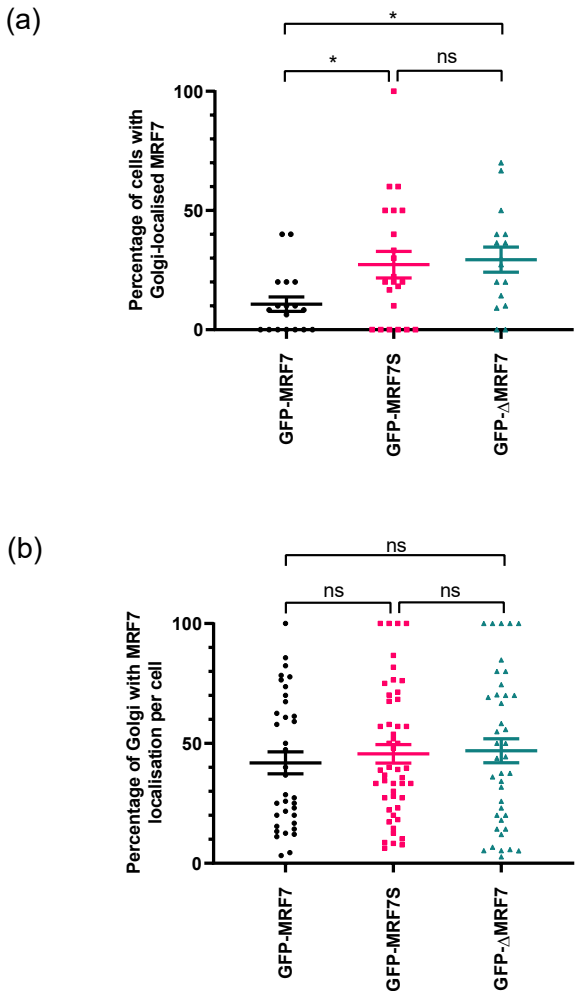

Figure 3.6: Quantification of Golgi localisation of wild-type and N-terminal truncations of GFP-MRF7 in tobacco cells. GFP-MRF7, GFP-MRF7S and GFP-ΔMRF7 were agroinfiltrated with the Golgi marker ST-mRFP in tobacco leaves to allow quantification of the fusions' localisation. Still images of the abaxial leaf epidermal cortex were taken at 2 DPI. Each still image corresponds to one cell. In (a), each data point represents one independent infiltration. The values on the y-axis represent the ratio of cells from that specific infiltration that have at least one Golgi with the indicated GFP fusion on its membrane. One-way ANOVA ($F(2, 53)=4.181$). Asterisks indicate statistically significant differences by post-hoc Tukey's test with $P<0.05$. In (b), data points represent each cell from (a) in which the wild-type or truncated MRF7 fusions were detected on Golgi. Values on the y-axis represent the number of Golgi in imaged area of one cell with the indicated MRF7 fusion on the Golgi, as a percentage of the total number of Golgi counted in the image. One-way ANOVA ($F(2, 122)=0.317$). The study was performed on a minimum of 140 images across 16 independent infiltrations. Where possible, 10 still images for each infiltration were taken. Horizontal bars represent the sample mean ± SEM.

3.2.4 Localisation of MRF7 fusions in *A.thaliana* transgenic plants

Transient expression of GFP-MRF7 and its N-terminal truncations in *N.tabacum* has shed light on the localisation of the receptor and the role of the DUF593 domain in Golgi targeting. To test that the results observed thus far in the heterologous expression system are consistent in the native plant species, stable *A.thaliana* trasformants over-expressing GFP-MRF7, GFP-MRF7S and GFP-ΔMRF7 were generated. The lines obtained were then crossed with *A.thaliana* plants over-expressing the Golgi marker ST-mRFP, and protein localisation in the progeny was observed on a confocal microscope.

Representative images for such observations are reported in Fig.3.7; all MRF7 fusions are reported in green, whereas ST-mRFP is in magenta. Similar to tobacco, GFP-MRF7 shows a dual localisation: it can label the Golgi membrane (Fig.3.7a-c) or move in punctate structures in the cytoplasm (Fig.3.7d-f). The puncta appear to be very similar to those observed for other MyoB receptors (Peremyslov et al., 2013; Peremyslov et al., 2015; Kurth et al., 2017).

As in tobacco, not all the Golgi in the observed cells had GFP-MRF7 association: in panels (a) to (c) most Golgi have associated GFP-MRF7, excluding a couple of them in the top part of the image, where the cell in focus neigbours a guard cell. GFP-MRF7 appears to be more concentrated on certain domains of the Golgi. Although this could be an effect of the Golgi orientation within the cytoplasm, certain areas seem to be brighter than others. This characteristic has been observed previously for the GNOM and GNL1 (Naramoto et al., 2014): both proteins co-localise with ST-mRFP in *A.thaliana*, but Super-resolution Confocal Live Imaging Microscopy (SCLIM) analysis highlighted a distinct localisation of the two proteins at the periphery of the Golgi cisternae, suggesting that they occupy different subdomains.

GFP-MRF7S (Fig.3.7g-i) and GFP-ΔMRF7 (Fig.3.7j-l), show the same localisation observed in tobacco: by truncating or removing the myosin-

binding domain, the punctate structures typical of GFP-MRF7 are absent, instead showing a dual Golgi/cytoplasmic localisation. Like GFP-MRF7, GFP-MRF7S and GFP-ΔMRF7 appear to be brighter on certain regions of the Golgi membrane.

Three independent lines over-expressing GFP-MRF7S x ST-mRFP and GFP-ΔMRF7 x ST-mRFP, and two for GFP-MRF7 x ST-mRFP were generated. Expression between different seedlings from the GFP-ΔMRF7 x ST-mRFP and GFP-MRF7 x ST-mRFP lines proved to be quite variable, requiring imaging at different laser powers and acquisition settings. This variability prevented comparison between seedlings and independent lines. Instead, it was possible to use the same imaging parameters for GFP-MRF7S x ST-mRFP lines; two of the independent lines only displayed a cytoplasmic localisation for GFP-MRF7S, while the Golgi localisation quantification was possible for the third line. Results of the quantification are shown in Fig.3.8. The quantification compares the results obtained in tobacco (see also Fig.3.6b for reference) with those observed at 10 and 14 days after germination (DAG) in *A.thaliana* seedlings. Young seedlings were monitored due to a drop in fluorescence in 3-4 weeks old plants (data not shown). Seedlings were grown on agar plates and GFP-MRF7S Golgi localisation quantified.

In Fig.3.8, each data point represents a cell where at least one Golgi was co-localising with GFP-MRF7S: the values on the y-axis indicate the percentage of Golgi within that cell that displayed GFP-MRF7S. There is consistency between the results obtained in tobacco and in *Arabidopsis* (Fig.3.8), suggesting that the ratio of Golgi localisation could be tightly regulated in the cell (One-way ANOVA; $F(2, 73)=0.4301$, $P=0.6521$).

3.2.5 The Golgi targeting information is contained within the C-terminus of MRF7

Results obtained in sections 3.2.3 and 3.2.4 suggest that the myosin binding domain at the N-terminus of MRF7 is responsible for the puncta formation/localisation for GFP-MRF7, but is not essential for its Golgi targeting. To confirm that the myosin binding region (DUF593) is not

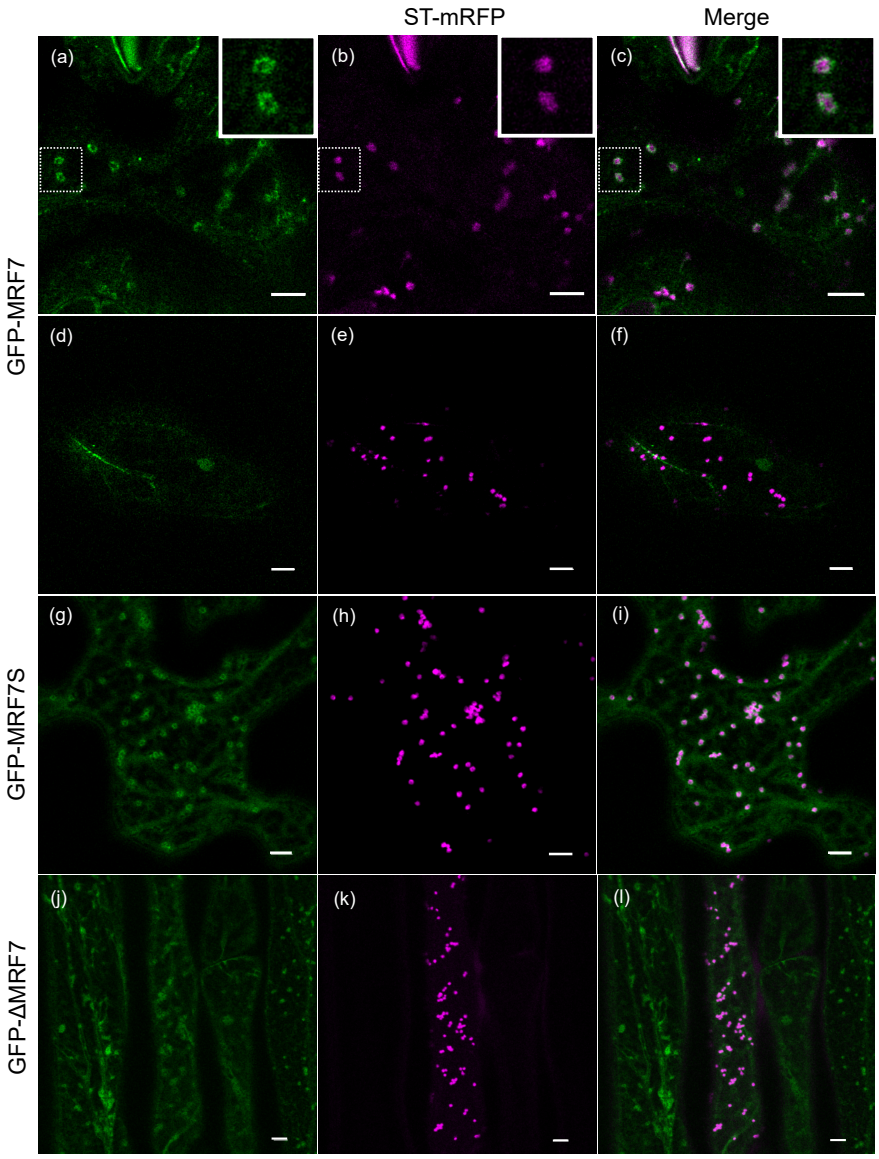

Figure 3.7: Representative images of the localisation of MRF7, MRF7S and ΔMRF7 in *A.thaliana* plants, 14 days after germination. *A.thaliana* lines stably over-expressing GFP-MRF7, GFP-MRF7S and GFP-ΔMRF7 were generated by floral dipping of wild-type Col-0 plants. Stable lines from the T4 generation were then crossed to an ST-mRFP Golgi marker line and progeny were imaged 14 days post-germination on a confocal microscope. Two representative images are shown for the GFP-MRF7 x ST-mRFP line. In (a) to (c), GFP-MRF7 localises to the Golgi. GFP-MRF7 seems to be sometimes more concentrated on certain regions of the membrane, as highlighted by some brighter spots on the organelle surface. In (d) to (f), GFP-MRF7 is localised on puncta in a straight line. Localisation of GFP-MRF7S, panels (g) to (i), and GFP-ΔMRF7, panels (j) to (l), in the crosses reflects what was observed in tobacco (Fig.3.5), with a dual Golgi and cytoplasmic localisation. Quantification of the Golgi localisation for one of the GFP-MRF7S lines is provided in Fig.3.8.

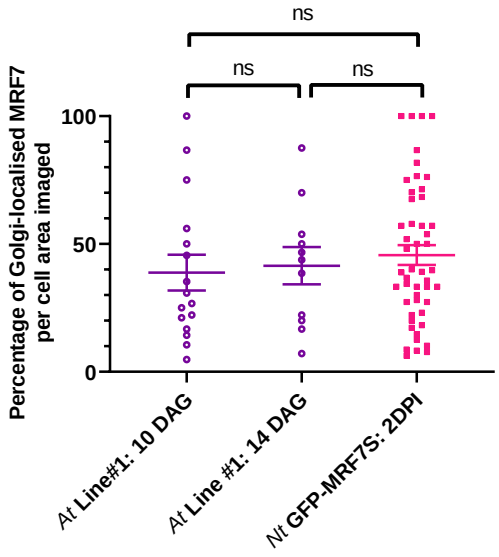

Figure 3.8: Quantification of GFP-MRF7S localisation in *A.thaliana* and *N. tabacum* leaf epidermal cells. GFP-MRF7S localisation in *A.thaliana* cells was quantified in a GFP-MRF7S x ST-mRFP line, 10 and 14 days after germination (DAG). 30 cells from 3 seedlings were imaged for each timepoint. Each data point in the graph represents a cell where GFP-MRF7S showed some extent of Golgi localisation. Numbers on the y-axis indicates the ratio of Golgi displaying GFP-MRF7S in the specific cell area imaged. On the far right of the graph, GFP-MRF7S localisation data from Fig. 3.6b are reported for comparison between the two plant species. One-way ANOVA ($F(2, 73)=0.4301$, $P=0.6521$). Bars represent the mean ± SEM.

responsible for the Golgi localisation, GFP-DUF593 was generated and over-expressed in tobacco leaves with the Golgi marker ST-mRFP (Fig.3.9a-c).

Observations from 3 independent infiltrations indicate the myosin binding domain is cytoplasmic and therefore unable to target MRF7 to Golgi. This domain is also unable to form or be targeted to puncta when expressed by itself.

Expression of C-terminal fusions of GFP with MRF7S (Fig.3.9d-f) and ΔMRF7 (Fig.3.9g-i), show an exclusively cytoplasmic localisation, contrary to that observed for the N-terminal GFP-MRF7S and GFP-ΔMRF7 (see Fig.3.5 and Fig.3.8 for reference). The cytoplasmic localisation of MRF7S-GFP and ΔMRF7-GFP suggests that the Golgi targeting information could be situated at the C-terminus of the protein, potentially "masked" by the GFP tag in the fully folded chimeras. To test this hypothesis, the last 54 amino acids at the C-terminus of MRF7S and ΔMRF7 were removed to obtain the GFP-MRF7SΔC and GFP-ΔMRF7ΔC constructs (see Fig. 3.3 for reference). The quantification in Fig.3.6a shows that cells, on average, display MRF7S or ΔMRF7 on Golgi more frequently then MRF7. For this reason it was decided to only check the effects of C-terminal truncations on Golgi localisation for MRF7S and ΔMRF7. The truncated constructs were agroinfiltrated into tobacco leaves with the Golgi marker ST-mRFP (Fig.3.10a-c and Fig.3.10d-f respectively). For control comparison, plants were also infiltrated with GFP-MRF7S and GFP-ΔMRF7.

Unlike GFP-MRF7S and GFP-ΔMRF7, the C-terminal truncations did not collocate to Golgi and were only present in the cytosol (Fig.3.10, One-way ANOVA; $F(3, 180)=13.63$, $P<0.0001$). The carboxy terminus is therefore essential for MRF7 Golgi localisation.

3.2.6 Effects of actin depolymerisation on GFP-MRF7, GFP-MRF7S and GFP-ΔMRF7 localisation

All MyoB receptors studied so far move in straight trajectories within the cytoplasm; for GFP-MRF7, it was shown that such trajectories correspond to actin tracks (see 3.2.2). MyoB1-YFP was shown to switch

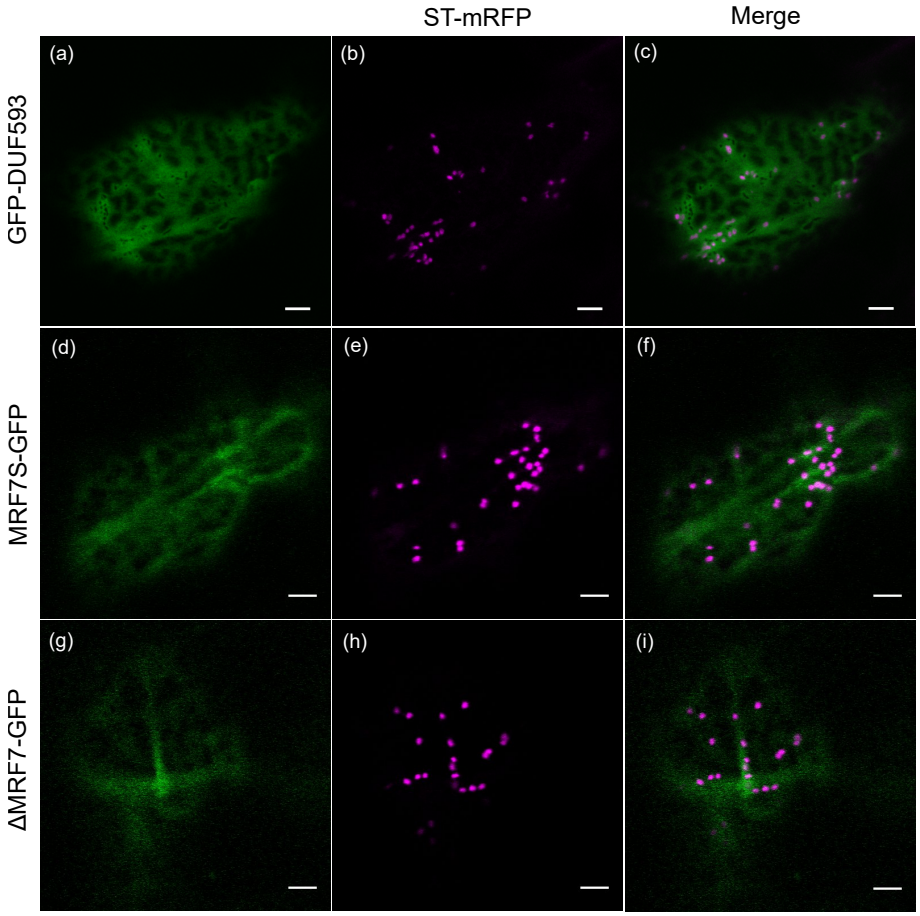

Figure 3.9: Cytoplasmic localisation of GFP-DUF593 domain, MRF7S-GFP and ΔMRF7-GFP. The panels report representative images from qualitative observations of the localisation of GFP-DUF593 (a, b, c), MRF7S-GFP (d, e, f) and ΔMRF7-GFP (g, h, i) in tobacco cells. The constructs were co-infiltrated with the Golgi marker ST-mRFP. Unlike the N-terminus GFP fusions shown in Fig.3.5, MRF7S-GFP, ΔMRF7-GFP are exclusively located in the cell cytoplasm (panels d to f, and g to i respectively). Similarly, GFP-DUF593 shows a diffuse cytoplasmic fluorescence. These observations suggest that the potential myosin binding domain is not responsible for Golgi localisation but that the targeting information could be contained within the C terminus of MRF7. All images were acquired at 2 DPI. Scalebars = 5 µm.

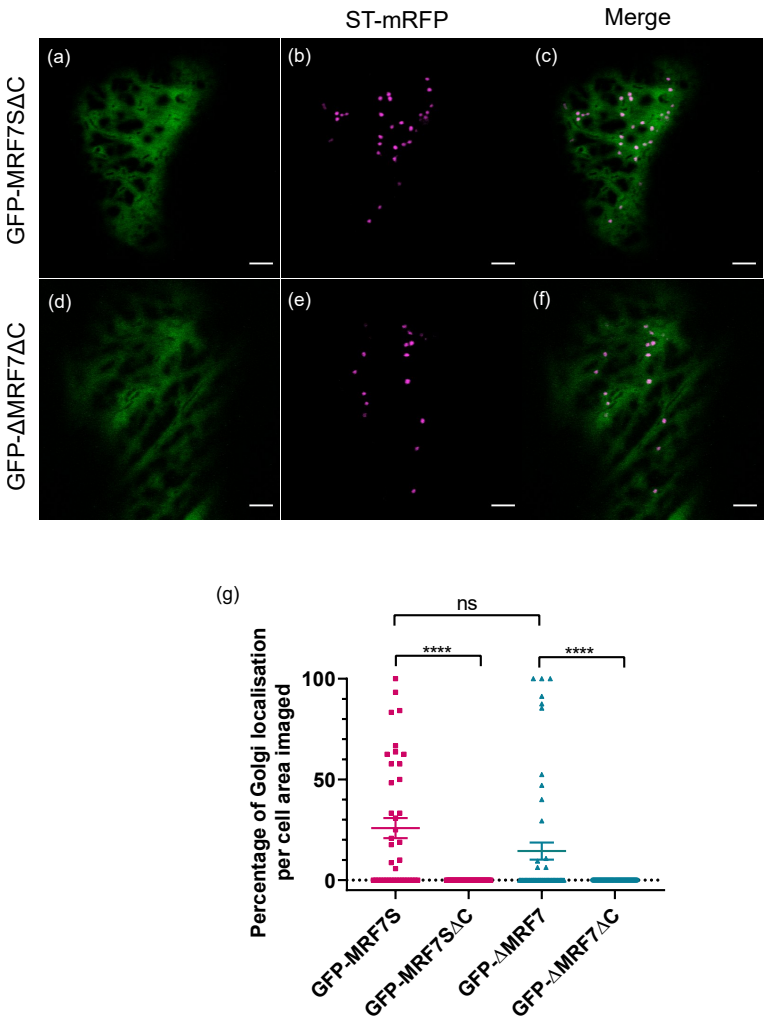

Figure 3.10: C-terminal truncations of GFP-MRF7S and GFP-ΔMRF7 localise to the cytoplasm in tobacco leaf epidermal cells. The GFP-MRF7SΔC and GFP-ΔMRF7ΔC lack 54 C-terminal amino acids. To assess the effects of the truncation on the protein targeting, GFP-MRF7S, GFP-MRF7SΔC (panels a to c), GFP-ΔMRF7 and GFP-ΔMRF7ΔC (panels d to f) were co-expressed with the Golgi marker ST-mRFP in tobacco leaf epidermal cells, and imaged at 2 DPI. Unlike fusions with the intact C-terminus, the constructs harbouring the truncation appear to be completely cytoplasmic. The effect of the truncation mimicks the localisation pattern reported in Fig.3.9, supporting the hypothesis that the Golgi targeting information is contained within the C-terminus of MRF7. The study was performed on a minimum of 40 cells across at least 4 independent infiltrations. The cortex of 10 leaf epidermal cells for each independent infiltration was imaged on a confocal microscope. In (g), each data point represents one cell. Values on the y-axis indicate the percentage of Golgi in that specific cell which displayed the indicated MRF7 fusion on Golgi. Scalebars = 5 µm. One-way ANOVA ($F(3, 180)=13.63$, $P<0.0001$). Asterisks indicate statistically significant differences by post-hoc Tukey's test with $P<0.0001$. Bars represent mean ± SEM.

from its more traditional beads-on-a-string pattern to a more diffuse cytoplasmic localisation upon expression in triple knock-out *xi-k xi-1 xi-2 A.thaliana* genetic background (Peremyslov et al., 2013). The triple mutant also exhibit a misarranged actin network (Cai et al., 2014), perhaps suggesting that MyoB1-YFP cytoplasmic diffusion could be attributed to an altered cytoskeletal organisation. To test this hypothesis the localisation of GFP-MRF7, GFP-MRF7S and GFP-ΔMRF7 was assessed following treatments with the actin depolymerising agent Latrunculin B (LatB).

Observations of the fusions' localisation following LatB treatment is also important concerning FRET-FLIM experiments to test MRF7 interaction with potential binding partners (Chapter 5). Given the high speeds of the GFP-MRF7 puncta (Fig.3.4) and of Golgi bodies in general, reliable FLIM data collection requires the structures labelled by the fusion proteins to be still, condition achieved by depolymerising the actin cytoskeleton. Quantification of GFP-MRF7, GFP-MRF7S and GFP-ΔMRF7 localisation following actin disassembly will give an indication of what the best strategy will be for FRET-FLIM measurements.

GFP-MRF7 is able to localise to Golgi before and after LatB treatments (Tab.3.1). Although more cells appear to display GFP-MRF7 on Golgi in the LatB treated sample, the differences are not statistically significant (Fisher's exact test, P=0.1020). Moreover, LatB alters the diameter of the GFP-MRF7 puncta: although the diameter remains generally smaller than that of spheroid organelles, LatB seems to cause a slight increase in the puncta diameter (Fig.3.11a, P=0.0150). A more general diffuse cytoplasmic fluorescence was also observed in cells treated with LatB, much like what seen for MyoB1-YFP in *xi-k xi-1 xi-2 A.thaliana* plants (Peremyslov et al., 2013). The second noticeable effects of LatB on GFP-MRF7 is a substantial decrease in their number when compared to the DMSO control (Fig.3.11b).

GFP-MRF7S and GFP-ΔMRF7 maintain their dual Golgi/cytoplasmic localisation, suggesting that LatB doesn't affect their Golgi targeting. It does not affect the percentage of cells with the construct on Golgi (Fig.3.12a; one-way ANOVA, $F(3, 180)=13.63$,

P<0.0001), nor does it appear to have an effect on the average percentage of Golgi localisation (Fig.3.12b; one-way ANOVA, $F(3, 42)=0.5161$, $P=0.6735$).

	N cells	Co-loc cells	N Golgi	Co-loc Golgi
GFP-MRF7 ctrl	29	1	692	5
GFP-MRF7 LatB	28	5	496	19

Table 3.1: 25 µM Latrunculin B effects on GFP-MRF7 Golgi localisation. Differences in Golgi localisation are non-significant. Fisher's exact test (P=0.1020).

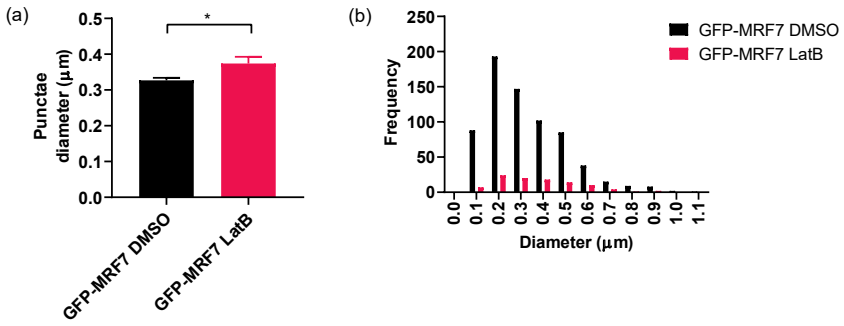

Figure 3.11: Effects of 25 µM Latrunculin B on GFP-MRF7 localisation. GFP-MRF7 was agroinfiltrated in tobacco leaves. The cell cortex of the abaxial epidermis from 30 cells across 3 independent experiments was imaged on a confocal microscope 2DPI. The number and diameters of the GFP-MRF7 puncta in each cell was automatically detected with the "Analyze particles" tool of ImageJ.
Actin depolymerisation appears to cause a significant enlargement of the GFP-MRF7 puncta (a) (Student's t-test (P=0.0150)). Bars represent mean ± SEM.
Latrunculin B treatments also cause a decrease in the number of GFP-MRF7 puncta detected in the imaged area in each cell (b).

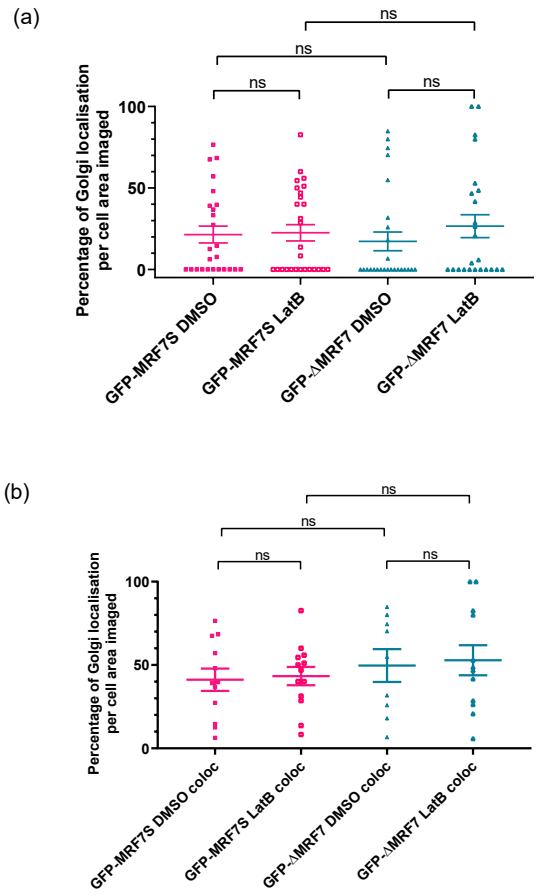

Figure 3.12: Effects of 25 µM Latrunculin B on GFP-MRF7S and GFP-ΔMRF7 localisation. GFP-MRF7S and GFP-ΔMRF7 were agroinfiltrated into tobacco leaves. The cell cortex of the abaxial epidermis from 30 cells across 3 independent infiltrations was imaged on a confocal microscope 2DPI. In (a), each data point represents one cell: numbers on the y-axis indicate the percentage of Golgi displaying either GFP-MRF7S or GFP-ΔMRF7, in presence and absence of Latrunculin B, including cells with a completely cytoplasmic localisation (0% co-localisation). Actin depolymerisation does not seem to influence the percentage of cells with or without GFP-MRF7S or GFP-ΔMRF7 on Golgi. One-way ANOVA ($F(3, 98)=0.4448$, $P=0.7215$).
Dataset presented in panel (b) is the same as in panel (a), but excluding zero values. In cells where GFP-MRF7S or GFP-ΔMRF7 localise to the Golgi, the average percentage of co-localisation doesn't seem to change between the treated and control samples, both for GFP-MRF7S and GFP-ΔMRF7. One-way ANOVA ($F(3, 42)=0.5161$, $P=0.6735$).
Bars represent mean ± SEM.

3.3 Discussion

3.3.1 MRF7 puncta move at high speeds on the actin cytoskeleton

Similarly to other *A.thaliana* MyoB receptors described so far in the literature, GFP-MRF7 localises to unknown punctate structures moving in straight trajectories in the cytoplasm (Peremyslov et al., 2013; Peremyslov et al., 2015; Kurth et al., 2017). Although MyoB1-GFP was observed to partially co-localise with the full-length myosin XI-K (Peremyslov et al., 2013), and XI-K was previously shown to move on actin (Peremyslov et al., 2012), a direct demonstration of the MyoB receptors localisation on the actin cytoskeleton has not been documented. Co-expression of GFP-MRF7 with the actin marker LifeAct-RFP in tobacco leaf epidermal cells showed that the puncta indeed move on the actin cytoskeleton, at a range of speeds which span between 1 and 9 µm/s, with an average speed of 4 µm/s (Fig3.4h). The lowest values are similar to the velocities of organelles such as Golgi and peroxisomes, while the average speed reflects that of other MyoB receptors (Peremyslov et al., 2015) and of cytoplasmic streaming in leaf epidermis of *A.thaliana* (Tominaga et al., 2013).

Notably, the highest speeds registered for the GFP-MRF7 puncta are higher than the speed of cytoplasmic streaming. This was previously observed in *in vitro* assays to determine the speed of full-length and motor domains of myosin XIs (Haraguchi et al., 2018): in particular, the velocities registered for some of the "fast" myosins such as XI-C, XI-D and XI-F were 3- to 4-fold higher than that of cytoplasmic streaming. The authors suggest that these discrepancies can be attributed to physical obstruction by cytoplasmic components and competition with slower myosins (Haraguchi et al., 2018). Other works in *A.thaliana* atrichoblasts registered cytoplasmic streaming velocities of up to 7 µm/s (Akkerman et al., 2011). Of course the speed of cytoplasmic streaming could perhaps vary in different cell types and tissues. Mathematical models have shown that cytoplasmic streaming does not depend solely on myosin movement,

as motor proteins alone don't have the characteristics to exert the necessary drag force to create a bulk flow movement of cytoplasm and organelles (Nothnagel and Webb, 1982). It was suggested that cytoplasmic streaming in plants is the result of myosin-directed movement of membranous organelles (Stefano et al., 2014; Tominaga and Ito, 2015). The role of MyoB receptors on cytoplasmic streaming is quite difficult to untangle: given the association with membranous structures (Peremyslov et al., 2013), they were suggested to constitute a completely new compartment that is the main driving force of cytoplasmic streaming (Peremyslov et al., 2013; Peremyslov et al., 2015; Kurth et al., 2017). Another tempting explanation is that MyoB could bind to sub-domains of known organelles, which are then detect as puncta, and recruit a myosin to move specific organelles within the cytoplasm. Mathematical models in *Chara chorallina* suggest that small structures with a diameter of approximately 0.5 µm, thus very similar to the MyoB particles (Kurth et al., 2017) could drive the cytoplasmic streaming but would have to be present as a solid line on the actin cytoskeleton (Nothnagel and Webb, 1982; Peremyslov et al., 2013; Peremyslov et al., 2015). Assuming that all other structures move passively within the cytoplasm, these beads would have to move at twice the speed of the cytoplasmic streaming in order to sustain the passive movement of other organelles. Given that, on average, MyoB move roughly at the same velocity as the cytoplasmic streaming in leaf epidermis, then this model cannot be excluded but perhaps can be implemented to explain the wide range of speeds registered for GFP-MRF7.

The observation that myosin XI-K partially co-localises with the MyoB puncta (Peremyslov et al., 2013), could suggest that the two can perhaps bind and move on actin in a coordinated manner. Moreover, the concept of competition between slower and faster myosins cannot be excluded as it was shown that *A.thaliana* myosin XI can be divided into three main groups based on their tissue specificity and speed (Haraguchi et al., 2018).

Ultimately, it has to be noted that even with the optimised parameters, it was still sometimes challenging for TrackMate to distinguish some of the

puncta from the background, or to keep track of very fast-moving objects between frames. In that sense, although the speed values registered agree with those previously observed for other MyoBs, the possibility that there might have been an under/overestimation in the speed measurement cannot be excluded.

3.3.2 Role of the C-terminus of MRF7 on Golgi targeting

In addition to its punctate localisation, low levels of GFP-MRF7 were detected on the Golgi when over-expressed in tobacco, compared to what observed for GFP-MRF7S and GFP-ΔMRF7 (Fig.3.5a-c, white arrowheads) and *A.thaliana*. This result is perhaps surprising considering that none of the other *A.thaliana* MyoB described so far seem to collocate with a known compartment, but maybe not implausible given the localisation of *Nt*RISAP on the TGN (Stephan et al., 2014) and *Zm*Fl1 on the endoplasmic reticulum (Holding et al., 2007). It is important to point out that other reported *At*MyoBs were expressed in *A.thaliana* cells under the control of their native promoters (Peremyslov et al., 2013; Peremyslov et al., 2015; Kurth et al., 2017), whereas GFP-MRF7 was over-expressed in tobacco leaves. It is possible that the required levels of MyoBs on the organelles membrane are so low that it is only possible to detect them by using an over-expressing system. On the other hand, MyoBs from different subfamilies might behave differently, especially given the variation in domain composition (Peremyslov et al., 2013).

Wild-type GFP-MRF7 localises to the Golgi membrane and on moving puncta, whereas constructs with partially or completely deleted DUF593 display a dual Golgi membrane and cytoplasmic localisation. The localisation appears to be consistent between *A.thaliana* and *N.tabacum*, which perhaps allows to rule out a species-specific localisation. Expression of the DUF593 domain construct indicates that the myosin-binding portion of MRF7 is not essential for the protein's targeting to Golgi. DUF593 also does not appear to have the ability to localise to moving puncta. Could this indicate a coordination between different MRF7 domains to allow the puncta formation? Studies of

non-DUF593 myosin V receptors and adaptors in yeast and mammalian cells suggest that, particularly for proteins that are part of a scaffold, it is fundamental that all domains are present and functional in order to correctly assemble the myosin recruitment complex in a linear way (Yan et al., 2005; Hume et al., 2007).

In addition to the cytoplsmic localisation of DUF593, fusion of GFP at the C-termini of MRF7S and ΔMRF7 suggested that the Golgi targeting information is contained within the C-terminal amino acids and that it is potentially masked in the fully folded chimeras. Altered subcellular localisation following GFP tagging of proteins at either the N- or C-terminus is not uncommon: *At*DHAR3, a chloroplastic dehydroascorbate reductase, localises to chloroplasts when expressed in *A.thaliana* as DHAR3-GFP, but to the cytosol when expressed as GFP-DHAR3 (Rahantaniaina et al., 2017). The observations were consistent with DHAR3 having a predicted N-terminal plastid signal peptide, which the GFP tag was probably masking in the fully folded GFP-DHAR3. In the same way, the protein *At*EMP12 has a Golgi retention signal at the C-terminus and is mislocalised when expressed as EMP12-GFP fusion (Gao et al., 2012).

Truncation of the last 54 amino acids in the N-terminally GFP tagged MRF7S and ΔMRF7, indeed shows that the targeting information is contained within the C-terminus of MRF7. GFP-MRF7SΔC and GFP-ΔMRF7ΔC relocate to the cytoplasm, mimicking observations of the MRF7S-GFP and ΔMRF7-GFP constructs. LocSigDB (University of Nebraska Medical Center) is an online tool that predicts protein localisation by comparing a query amino acidic sequence with those of proteins for which the subcellular localisation and targeting motifs have been characterised (Negi et al., 2015). Analyses of the MRF7 sequence highlighted the presence of two motifs at the C-terminus, which remain intact in the MRF7S and ΔMRF7 protein but are not present in their C-terminally truncated versions MRF7SΔC and ΔMRF7ΔC. The first motif is ^{320}YxxΦ^{324}, situated at the very C-terminus of the protein where Φ represents a bulky amino acid; the second motif is ^{274}KxxxQ^{279}.

The YxxΦ sequence is traditionally associated with sorting of transmembrane proteins to the vacuole or lysosomes and protein internalisation from the plasma membrane through the binding with μ-adaptins of chlatrin coated vesicles (Bonifacino and Traub, 2003). In particular, the *A.thaliana* transmembrane protein EMP12 localises to the Golgi apparatus and its localisation is dependent upon the YxxΦ contribution to the Golgi retention (Gao et al., 2012). Moreover, the YxxΦ motif in the ARF domain of the ARD1 protein in mammalian cells is involved in localisation to Golgi (Vitale et al., 2002). Interestingly, the KxxxQ motif within the GAP domain of ARD1 is responsible for its targeting to lysosomes (Vitale et al., 2002).

Although it seems possible that the ^{320}YxxΦ^{324} could be responsible for the Golgi targeting of MRF7, probably even more so than the ^{274}KxxxQ^{279} motif, I also cannot exclude the possibility that the motifs identified by *in silico* comparison of the MRF7 sequence with the LocSigDB database might not be involved at all in the Golgi localisation. More selective truncations are needed to narrow down the targeting information position within the the C-terminus of MRF7.

3.3.3 Regulation of MRF7 localisation

It appears as if the localisation of GFP-MRF7, GFP-MRF7S and GFP-ΔMRF7 on the Golgi membrane is tightly regulated. As can be observed in Fig.3.5, not all the Golgi within a cell display the MRF7 fusions on their membrane; this is particularly evident in the representative images in panels a-c (GFP-MRF7), but it was also consistently observed for GFP-MRF7S and GFP-ΔMRF7. A quantification of the percentage of Golgi per cell displaying the fusions is provided in Fig.3.6b: the ratio between the number of Golgi with the fusion proteins and the total number of Golgi in that cell was calculated for all the cells in which co-localisation was observed. It appears as if the average percentage of Golgi localisation does not vary between GFP-MRF7 and its N-terminal truncations which could suggest that, regardless of how many cells show a certain degree of colocalisation in that specific experiment (Fig.3.6a), on average 45% of

Golgi in colocalising cells will display the fusions on the membrane. This seemingly tightly regulated localisation of the three fusions could suggest that there are functionally distinct Golgi subpopulations.

Studies from other model organisms, such as *Saccharomyces cerevisiae* (*S.cerevisiae*), suggest that the presence of myosin receptors on the membrane of a specific organelle is tightly regulated to influence the fate or function of the organelle. For example, the proteins *Sc*Inp1p and *Sc*Inp2p act in an antagonistic and coordinated manner to regulate peroxisome inheritance in budding yeast. While Inp1p is responsible for retention of 50% of peroxisomes in the mother cell by anchoring them to the cell cortex (Fagarasanu et al., 2005), Inp2p is a transmembrane peroxisomal protein that interacts with Myo2p and allows the transport of peroxisomes into the forming bud (Fagarasanu et al., 2006). Although it is unclear how peroxisomes are "selected" to migrate to the bud rather than staying in the mother cell, the authors suggest that a "tug-of-war" mechanism is responsible for determining which peroxisomes are retained in the mother cell by Inp1p and which are transported to the bud by Inp2p. In this sense, although we don't know what the role of MRF7 is on Golgi function or positioning, it is tempting to speculate that the appearance of the protein on the Golgi membrane could be imporant to coordinate Golgi functions such as secretion, cell wall deposition and so on.

Considering MRF7 is not necessarily homogeneously distributed on the surface of the Golgi, it is tempting to speculate that localised concentrated patches may reflect a "docked" puncta. Here, puncta could possibly reflect vesicles docking or perhaps budding from the Golgi surface.

On the other hand, the quantification shown in Fig.3.6a could suggest that the partial or complete absence of DUF593 stabilises the fusions on Golgi, as more cells per infiltration appear to display GFP-MRF7S and GFP-ΔMRF7 on Golgi than GFP-MRF7. Despite using an over-expression system, it has to be noted that this discrepancy could be due to differences in expression levels, where higher expression in a particular cell or tissue could signify more frequent Golgi localisation. It

is relatively difficult to estimate expression in infiltrated leaves: although the same OD of infiltration and infiltration procedure were used for all three construct, I cannot exclude "patchy" expression where some cells do get the infiltrated construct and others are more "resistant" to expressing the transgene.

3.3.4 Effects of actin cytoskeleton depolymerisation on MRF7 subcellular localisation

*At*MyoB1-YFP localisation was disrupted in *xi-k xi-1 xi-2 A.thaliana* plants, where it appeared to have a more diffuse cytoplasmic distribution in contrast with the beads-on-a-string configuration from wild-type plants (Peremyslov et al., 2013). Recent works have highlighted that myosins XI-K, XI-1 and XI-2 contribute to maintaining the orientation, organisation and dynamicity of the actin array. Simultaneous knock-out of all the three myosins led to a less dense and more bundled actin array, and also to a significant reduction in actin dynamicity (Peremyslov et al., 2010a; Cai et al., 2014). Thus, the effects seen on MyoB1-YFP localisation upon expression in the triple knock-out suggests that MyoB1 binds to either of those myosins (Peremyslov et al., 2013; Kurth et al., 2017) and indeed the localisation is affected on a severely altered acto-myosin network (Peremyslov et al., 2013). The effects of Latrunculin B-dependent actin depolymerisation on GFP-MRF7, GFP-MRF7S and GFP-ΔMRF7 localisation were analysed.

While actin depolymerisation does not appear to have any significant effects on the localisation of GFP-MRF7S and GFP-ΔMRF7 compared to non-treated leaf samples, it has instead a peculiar effect on GFP-MRF7 localisation. Consistent with that observed for MyoB1-YFP (Peremyslov et al., 2013), GFP-MRF7 has a more diffuse cytoplasmic localisation in LatB treated samples; the diffusion coincided with a lower number of puncta detected in the cytoplasm. In addition, polymerisation of actin affected myosin XI-K and XI-E puncta localisation (Sparkes et al., 2008), suggesting that the receptors:myosin:actin association could be tightly regulated and dependent on F-actin presence.

Average diameter of the GFP-MRF7 puncta in DMSO control sample was of approximately 0.3 µm, very similar to that observed for MyoB12 and MyoB13 (Kurth et al., 2017). The LatB treatment appears to cause an enlargement of the puncta; it is unclear how actin depolymerisation could cause such an effect. MyoB1-YFP expressed in *xi-k A.thaliana* plants appear to behave in a similar way (Peremyslov et al., 2013): although the authors did not provide a quantification, it appears as if the deletion of myosin XI-K leads to a less beads-on-a-string configuration for MyoB1. This suggests that an intact actin array and fully functional myosin motors are needed for the maintainance of the MyoB structures. Nevertheless it is so far unclear why the puncta size would increase following LatB treatment.

Chapter 4

Control of organelle dynamics

Localisation of the potential myosin receptor MRF7 and its N-terminal truncations to the Golgi represents a novel finding within the *Arabidopsis thaliana* MyoB family. To test a potential link between MRF7 localisation and function, the effects of over-expression of different MRF7 constructs were tested on Golgi and peroxisomes dynamics.

4.1 Introduction

4.1.1 Effects of dominant negative mutants *At*MyoB receptors on organelle movement

The *A.thaliana* MyoB receptors described so far in the literature do not appear to localise to known organelles, but they rather move in straight lines as punctate structures (Peremyslov et al., 2013; Kurth et al., 2017). The effects of *At*MyoB receptors on organelle dynamics have been assessed through transient over-expression of their DUF593 domain in *N.benthamiana* leaf epidermal cells (Peremyslov et al., 2015). Over-expression of DUF593 from *At*MyoB1 and *At*MyoB2 caused a significant reduction of the mean velocity of several organelles, such as Golgi, peroxisomes and mitochondria (Peremyslov et al., 2015). This effect mimics, although not to the same extent, the effects of over-expression of myosin XI tails (Avisar et al., 2009; Peremyslov et al., 2015), thus suggesting that DUF593 has a dominant negative effect on the movement of organelles.

DUF593 from MyoB2 appeared to influence organelle movement more than DUF593 from MyoB1, effect which the authors attribute to a potential higher myosin-binding affinity of MyoB2 DUF593 (Peremyslov et al., 2015). In both cases, despite differences in absolute velocities for different compartments, the relative decrease in movement upon expression of DUF593 is consistent between organelles. The decrease in velocity was quantified as ∼45% and ∼65% following over-expression of DUF593 from MyoB1 and MyoB2, respectively (Peremyslov et al., 2015).

Interestingly, movement of full-length MyoB1-GFP puncta and of the inert cytoplasmic tracer mCherry-µNS, a non-structural protein from a mammalian orthoreovirus (Miller et al., 2007), was also affected by dominant negative MyoBs. µNS cytoplasmic inclusions with a similar size to that of Golgi, peroxisomes and mitochondria were shown to move at similar speeds as the organelles, and to be subject to the same decrease in movement upon DUF593 expression (Peremyslov et al., 2015). Moreover, cytoplasmic velocity was shown to decrease in quadruple *myob1-4*

knock-out plants (Peremyslov et al., 2015). In light of these considerations, the authors challenged the more traditional mechanism for acto/myosin-based organelle movement (Fig.4.1). It was proposed that the myosins and the MyoB compartment could function as the main drivers of cytoplasmic streaming, with all the organelles following passively in the stream (Peremyslov et al., 2015). Although these considerations cannot be fully excluded, mathematical models appear to suggest that movement of such small structures might not be sufficient to drive cytoplasmic streaming (Nothnagel and Webb, 1982).

4.1.2 Effects of full-length MyoB receptors on organelle movement

As mentioned in section 4.1.1, effects of MyoB receptors in *A.thaliana* were only studied through transient over-expression of the DUF593 domain (Peremyslov et al., 2015). Although the effects of full-length *At*MyoBs could perhaps be inferred from dominant negative constructs expression, a study of the effects of full-length MyoB on organelle dynamics has not been carried out yet.

Unlike MyoBs from *A.thaliana*, the *N.tabacum* MyoB protein RISAP specifically localises to the Trans-Golgi Network (TGN) in the subapical region of tobacco pollen tubes and interacts with the tail of MYOXIpt in an actin-dependent way (Stephan et al., 2014). RISAP remains associated with vesicles following their budding from the TGN, and facilitate their transport towards the plasma membrane on the tip of pollen tubes. Once the plasma membrane is reached, the bond between RISAP and MYOXIpt is weakened, leading to the release of the vesicles at the tip (Stephan et al., 2014).

Over-expression of RISAP causes the disappearance of the clear zone (CZ), where the secretory vesicles are released, and inhibits pollen tube growth. Moreover, over-expression of RISAP also causes the formation of cytoplasmic structures labelled by both YFP-RISAP and the plasma membrane marker RCI2a: the authors suggest that these are

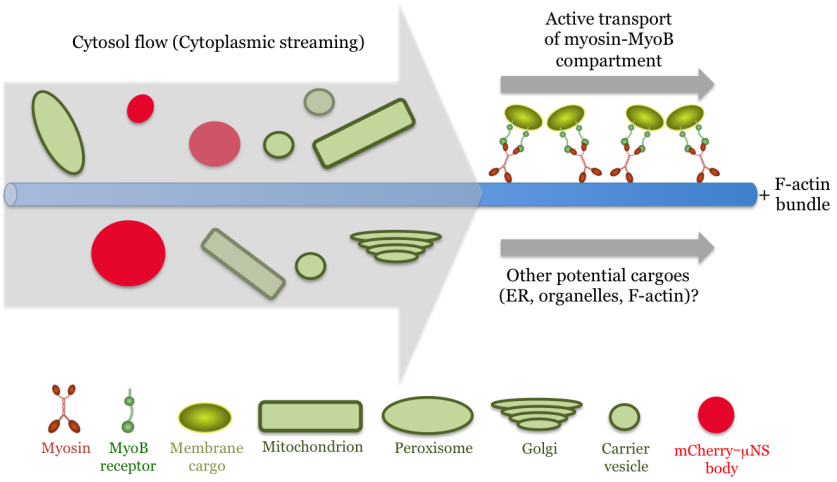

Figure 4.1: Suggested model for the generation of cytoplasmic streaming and organelle movement in plant cells (taken from Peremyslov et al., 2015). Myosins from class XI and the MyoB compartment are depicted as the main drivers of cytoplasmic streaming. Other organelles (in light green) would passively move within the stream.

endomembrane-derived aberrant structures, most likely originating from the TGN itself. Parts of the TGN might be transported from their normal localisation through interaction of excess RISAP molecules with MYOXIpt and the actin cytoskeleton (Stephan et al., 2014).

Another member of the MyoB family that was localised to a specific compartment is *Zm*Fl1. Fl1 was detected on the protein bodies ER membrane during endosperm development by immunogold labelling (Holding et al., 2007). Although Fl1 does not appear to directly interact with a myosin, it was shown to interact with α-zein *via* its C-terminal domain (Holding et al., 2007). *fl1* mutants display protein bodies of normal size and shape, but in which the 22-kD α-zein deposition is altered. While in wild-type plants the 22-kD α-zein localises to a ring area between the outer γ-zein layer and the core of the protein body (Lending and Larkins, 2007), in *fl1* the 22-kD α-zein is dispersed throughout the protein body core (Holding et al., 2007). Kernels of *fl1* mutants have a thicker starchy endosperm compared to kernels from wild-type plants, suggesting that *Fl1* is involved in correct layering of the endosperm and in particular in the positioning of the 22-kD α-zein (Holding et al., 2007).

4.1.3 Effects of myosin receptors on organelle dynamics in yeast and mammals

Although the rate at which organelles move in yeast and mammalian cell is lower than the rate of movement in plant cells, correct assembly and functioning of myosin receptor complexes is fundamental to secure appropriate positioning of the transported compartments within the cell (Yokota et al., 2011; Hammer and Sellers, 2012).

In *S.cerevisiae* cells the acto/myosin-based transport of organelles is particularly important, among other processes, for organelle inheritance (Ishikawa et al., 2003; Tang et al., 2003; Fagarasanu et al., 2006). For example, myosin *Sc*Myo2p regulates peroxisome inheritance by mediating the transport of peroxisomes from the mother cell to the forming bud (Hoepfner et al., 2001). Peroxisomes inheritance was shown to be the result of a tug-of-war between Inp1p, which anchors the peroxisomes to

the mother cell cortex, and Inp2p, an integral membrane protein which works as Myo2p receptor on the peroxisomal membrane (Fagarasanu et al., 2005; Fagarasanu et al., 2006). Tracking of peroxisomes in budding cells reaveled that peroxisomes destined for the bud slowly detach from the cortex of the mother cell and start heading towards the daughter cell (Fagarasanu et al., 2006). Deletion of Inp2p impairs peroxisomes transport to the bud, whereas over-expression of the protein leads to a depletion of peroxisomes from the mother cell (Fagarasanu et al., 2006).

4.1.4 Aims

This chapter explores the effects of MRF7 expression on Golgi and peroxisome dynamics. In particular, by using MRF7 constructs lacking part or all the DUF593 domain I aim to define the role of the myosin-binding region in regulating Golgi and peroxisomes dynamics.

4.2 Results

4.2.1 Triple expression system as a tool to study the effects of MRF7 fusions on multiple compartments

Over-expression of the *At*MyoB1 and *At*MyoB2 DUF593 domains in *N.benthamiana* leaf epidermal cells leads to a significant general decrease in organelle movement (Peremyslov et al., 2015). Despite these observations, the effects of full-length *At*MyoB on organelle dynamics have not been assessed yet (Peremyslov et al., 2013; Peremyslov et al., 2015; Kurth et al., 2017). Localisation of MRF7 and its N-terminal truncations to the Golgi (Fig.3.5) raises the possibility that MRF7 could play a role in regulating Golgi movement. If so, MRF7 could represent the first example of a link between MyoB localisation and role on organelle dynamics in *A.thaliana*.

A triple expression system was used to test the effects of full-length and N-teminally truncated MRF7 on organelle dynamics. The MRF7 constructs were transiently over-expressed in *N.tabacum* leaf epidermal cells with Golgi and peroxisome markers (Fig.4.2 a-d), and movement of these compartments tracked over time. Golgi and peroxisome movement parameters were then compared to those obtained in control cells expressing only the organelle markers.

This strategy allowed to test whether MRF7 exerts an effect on the compartment where it sometimes localises (by monitoring Golgi movement), and whether such effect is specific (by monitoring peroxisomes movement). Peroxisomes were chosen for tracking over other organelle classes, such as mitochondria or chloroplasts. This is due to the possibility for peroxisomes to be tracked with parameters compatible to those used for Golgi. Moreover, with the triple expression system Golgi and peroxisomes within the same cell are theoretically exposed to the same levels of MRF7. Therefore, organelle tracking with this system can help reduce the variability associated with MRF7 expression levels. All movement data collected from *N.tabacum* are from a triple expression system (Sections 4.2.2, 4.2.3, 4.2.4).

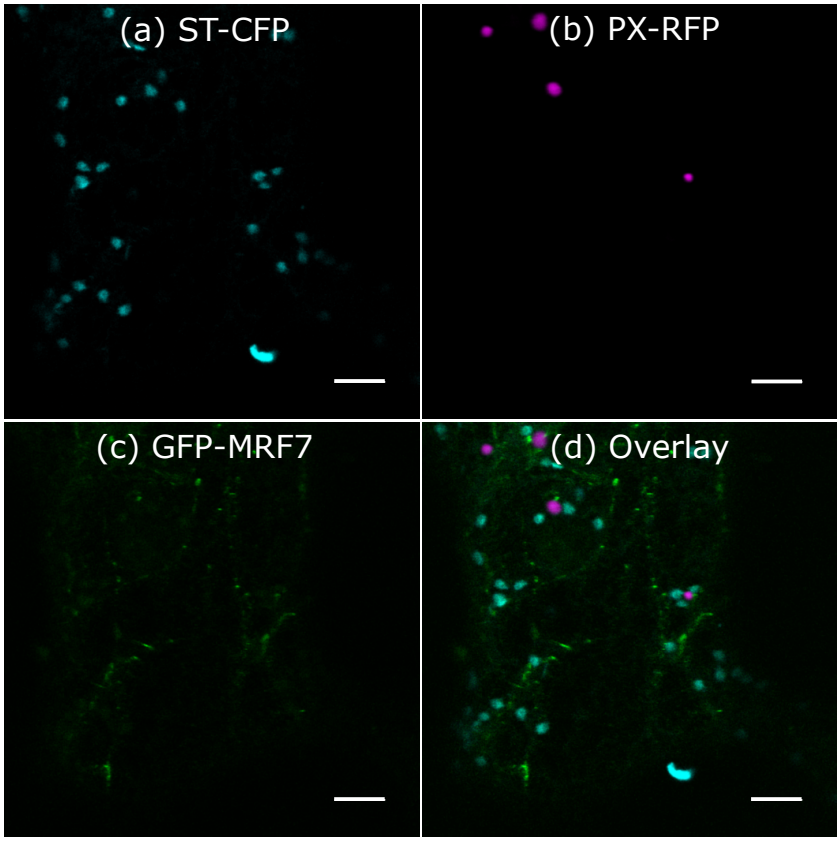

Figure 4.2: Representative image of triple expression of Golgi and peroxisome markers and MRF7 GFP-tagged fusions. Confocal image of a tobacco leaf epidermal cell transiently expressing the Golgi marker ST-CFP (a), the peroxisome marker (b) and the MRF7 fusion of interest (c, GFP-MRF7 in this instance). The overlay (d) allows the visualisation of the three channels at once. All scalebars = 5 µm.

4.2.2 GFP-MRF7 does not influence Golgi and peroxisome speed in *N.tabacum*

Despite influencing organelle dynamics upon over-expression of their DUF593 domain, full-length *At*MyoB receptors have not been localised on any of the affected compartments (Peremyslov et al., 2015). Here, in addition to a more traditional MyoB beads-on-a-string configuration, the *At*MyoB receptor MRF7 was identified on the Golgi (see Fig.3.4 and 3.5). The effects of full-length GFP-MRF7 on Golgi dynamics were tested in tobacco leaf epidermal cells; peroxisome movement was also monitored using the strategy described in 4.2.1.

Data shown in Fig.4.3 indicates that GFP-MRF7 over-expression does not significantly influence Golgi speed (P=0.0735, Fig.4.3a), but increases its displacement rate (P<0.0001, Fig.4.3b) and meandering index (P<0.0001, Fig.4.3c). Interestingly, the same effect was observed for peroxisomes; GFP-MRF7 does not significantly influence peroxisomes speed (P=0.0972, Fig.4.4a), but increases their displacement rate (P=0.0121, Fig.4.4b) and meandering index (P=0.0045, Fig.4.4c).

Overall, these results indicate that although the speed of Golgi and peroxisomes is not influenced by GFP-MRF7, both compartments follow straighter trajectories within the cell upon GFP-MRF7 over-expression.

4.2.3 GFP-MRF7S increases Golgi and peroxisome movement in *N.tabacum* and *A.thaliana*

Effects of GFP-MRF7S in *N.tabacum*

Partial deletion of the DUF593 domain causes the disappearance of the typical MyoB punctate structures, but does not impair the ability of MRF7 to localise to the Golgi (Fig.3.5). Despite retaining its Golgi localisation, MRF7S effectively lacks four of the eight conserved residues within DUF593 (see Fig.3.2 for reference), which could perhaps perturb the ability of MRF7 to bind to a myosin and regulate Golgi movement. Effects of a partial deletion of DUF593 on Golgi and peroxisome dynamics are assessed in this section.

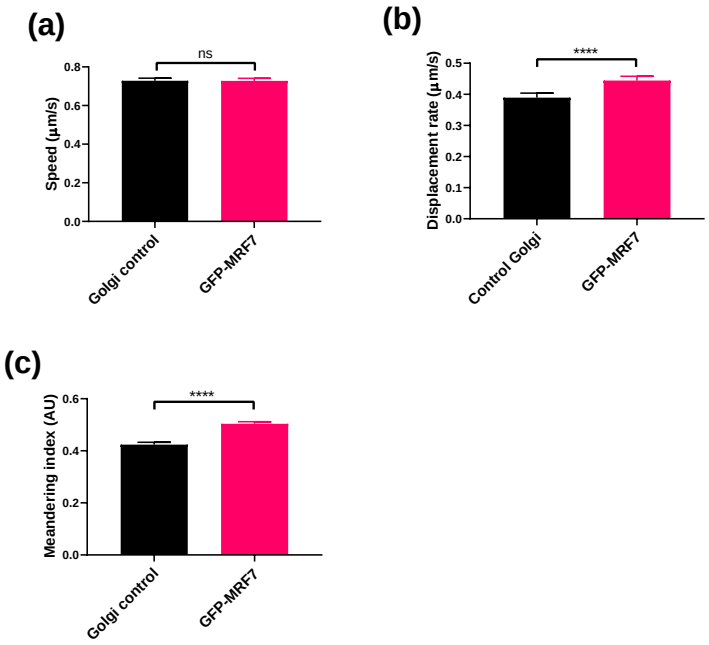

Figure 4.3: Effects of GFP-MRF7 expression on Golgi dynamics. Results of Golgi tracking in control and GFP-MRF7 over-expressing cells. Histograms represent mean absolute values ± SEM for speed (a), displacement rate (b) and meandering index (c) from four independent infiltrations. GFP-MRF7 does not significantly influence Golgi speed (Panel (a), P=0.0735), but increases Golgi displacement rate (Panel (b), P<0.0001) and meandering index (Panel (c), P<0.0001).
Mann-Whitney U test, n_1=1000, n_2=1185, **** P<0.0001, ns = non significant.

	Speed (µm/s)	Displ. Rate (µm/s)	Meand. Index (AU)
Control Golgi	0.73	0.39	0.42
GFP-MRF7 Golgi	0.73	0.44	0.50

Table 4.1: Effects of expression of GFP-MRF7 on Golgi dynamics, absolute values. Absolute mean values of Golgi speed, displacement rate and meandering index before and after GFP-MRF7 over-expression.

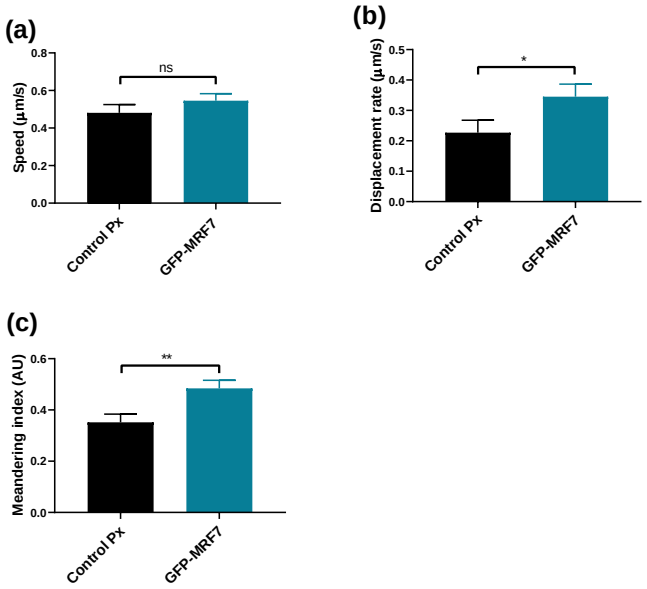

Figure 4.4: Effects of GFP-MRF7 expression on peroxisomes dynamics. Results of peroxisomes tracking in control and GFP-MRF7 over-expressing cells. Histograms represent mean absolute values ± SEM for speed (a), displacement rate (b) and meandering index (c) from four independent infiltrations. GFP-MRF7 does not significantly influence peroxisome speed (Panel (a), P=0.0972) but increases displacement rate (Panel (b), P=0.0121) and meandering index (Panel (c), P=0.0045).
Mann-Whitney U test, n_1=72, n_2=95, * P<0.05, ** P<0.01, ns = non significant.

	Speed (µm/s)	Displ. Rate (µm/s)	Meand. Index (AU)
Control Px	0.48	0.23	0.35
GFP-MRF7 Px	0.55	0.35	0.48

Table 4.2: Effects of expression of GFP-MRF7 on peroxisome dynamics, absolute values. Absolute mean values of peroxisome speed, displacement rate and meandering index before and after GFP-MRF7 over-expression.

Opposite to observations in section 4.2.2, in this instance control peroxisomes have higher average speeds compared to control Golgi (Tab.4.3 and Tab.4.4, respectively). Displacement rate and meandering index average values are similar in control cells for both Golgi and peroxisomes.

GFP-MRF7S significantly increases Golgi speed (Fig.4.5a, $P<0.0001$), displacement rate (Fig.4.5b, $P<0.0001$) and meandering index (Fig.4.5c, $P=0.0003$). GFP-MRF7S also significantly increases peroxisomes speed (Fig.4.6a, $P=0.0002$), displacement rate (Fig.4.6b, $P=0.0037$) and meandering index (Fig.4.6c, $P=0.0003$). The relative increase in speed, displacement rate and meandering index is different between Golgi and peroxisomes (Tab.4.7).

Effects of GFP-MRF7S on Golgi dynamics in *A.thaliana*

Over-expression of GFP-MRF7S in tobacco leaf epidermal cells led to a significant increase in Golgi movement (Fig.4.5). Localisation studies indicated that the percentage of GFP-MRF7S Golgi localisation is consistent between transiently transfected *N.tabacum* and a stably expressing ST-mRFP x GFP-MRF7S *A.thaliana* line (Line#1, Fig.3.8). This result suggests that GFP-MRF7S can behave similarly in the heterologous transiently expressing system and in stably expressing lines. To further rule out a species-specific effect of GFP-MRF7S on Golgi dynamics, Golgi movement was monitored in *A.thaliana* plants 10 and 14 days after germination (DAG). The two timepoints were chosen due to fluorescence decaying after approximately 14 DAG, and because leaves younger than 10 DAG were observed to be easily damaged when cutting them for imaging.

Golgi bodies were tracked 10 and 14 days after germination from three seedlings expressing the ST-mRFP Golgi marker and three seedlings co-expressing ST-mRFP and GFP-MRF7S (Line#1, see section 3.2.4). The average speed of control Golgi bodies at 10 DAG (Fig.4.7a, Tab.4.5) is higher than the average speed at 14 DAG (Fig.4.7b, Tab.4.5), whereas the average displacement rate appears to be consistent between the two

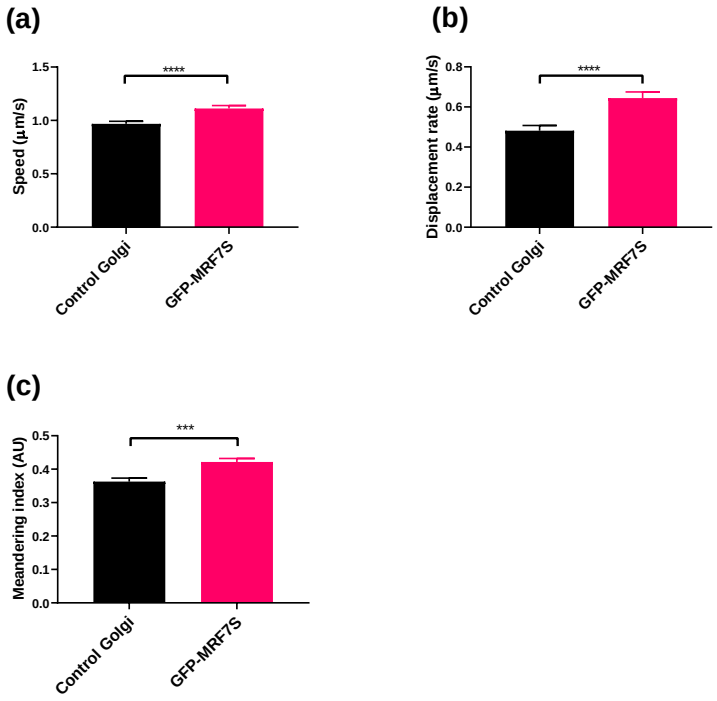

Figure 4.5: Effects of GFP-MRF7S expression on Golgi dynamics. Results of Golgi tracking in control and GFP-MRF7S over-expressing cells. Histograms represent mean ± SEM for speed (a), displacement rate (b) and meandering index (c) from five independent infiltrations. GFP-MRF7S significantly increases Golgi speed (Panel (a), $P<0.0001$), displacement rate (Panel (b), $P<0.0001$) and meandering index (Panel (c), $P=0.0003$).
Mann-Whitney U test, $n_1=789$, $n_2=831$, **** $P<0.0001$, *** $P<0.001$.

	Speed (µm/s)	Displ. Rate (µm/s)	Meand. Index (AU)
Control Golgi	0.97	0.48	0.36
GFP-MRF7S Golgi	1.11	0.64	0.42

Table 4.3: Effects of GFP-MRF7S on Golgi dynamics, absolute values. Absolute mean values of Golgi speed, displacement rate and meandering index before and after GFP-MRF7S over-expression.

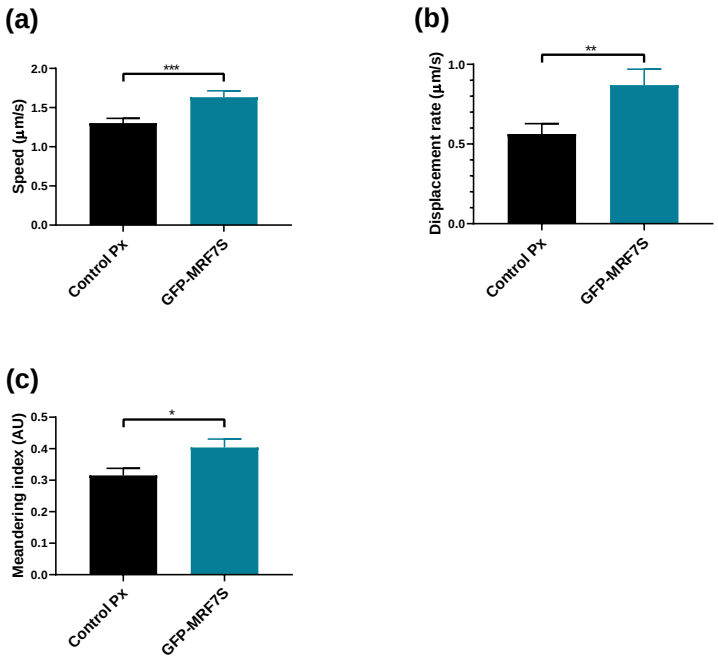

Figure 4.6: Effects of GFP-MRF7S on peroxisome dynamics. Results of peroxisome tracking in control and GFP-MRF7S over-expressing cells. Histograms represent mean ± SEM for speed (a), displacement rate (b) and meandering index (c) from six independent infiltrations. GFP-MRF7S significantly increases peroxisomes speed (P=0.0002), displacement rate (P=0.0037) and meandering index (P=0.0236). Mann-Whitney U test, n_1= 173, n_2= 143, *** P<0.001, ** P<0.01, * P<0.05.

	Speed (µm/s)	Displ. Rate (µm/s)	Meand. Index (AU)
Control Px	1.30	0.56	0.32
GFP-MRF7S Px	1.60	0.87	0.40

Table 4.4: Effects of GFP-MRF7S on peroxisome dynamics. Absolute mean values of peroxisome speed, displacement rate and meandering index before and after GFP-MRF7S over-expression.

timepoints (Tab.4.5).

Expression of GFP-MRF7S exerts opposite effects on Golgi movement in a timely manner. Golgi speed ($P<0.0001$) and displacement rate ($P=0.033$) significantly decrease at 10 DAG (Fig.4.7a, Tab.4.5). On the contrary, Golgi speed ($P=0.00099$), displacement rate ($P=0.0089$) and meandering index ($P=0.0048$) significantly increase 14 DAG in the presence of GFP-MRF7S (Fig.4.7b, Tab.4.5). Interestingly, the relative speed decrease at 10 DAG (ratio=0.84, -16%, Tab.4.6) and the relative speed increase at 14 DAG (ratio=1.18, +18%, Tab.4.6) are quite similar. The same conclusion cannot be drawn for the relative decrease and increase in displacement rate and meandering index.

Despite differences in absolute average values, the ratio of Golgi movement increase is consistent between transiently transfected tobacco leaves (Fig.4.3, Tab.4.7) and 14 DAG *A.thaliana* seedlings (Fig.4.7, Tab.4.6). Overall, Golgi tracking in *A.thaliana* revealed that the effects of GFP-MRF7S on Golgi movement is most likely developmentally regulated. Moreover, the effects observed in transiently transfected tobacco are consistent with those in *A.thaliana* at 14 DAG. These results, together with those obtained in sections 3.2.3 and 3.2.4 rule out a species-specific behaviour of GFP-MRF7S for localisation and effects on Golgi movement.

4.2.4 GFP-ΔMRF7 increases Golgi and peroxisome movement in *N.tabacum*

Like GFP-MRF7S, GFP-ΔMRF7 does not display the traditional MyoB punctate localisation but can still localise to the Golgi (Fig.3.5). Partial deletion of the DUF593 domain of MRF7 consistently increases Golgi movement in tobacco and 14 DAG *A.thaliana* seedlings. Here, the effects of a complete deletion of DUF593 are assessed on Golgi and peroxisome movement using the strategy described in 4.2.1.

GFP-ΔMRF7 significantly increases Golgi speed, displacement rate and meandering index ($P<0.0001$, Fig.4.8a-b-c). It also significantly increases peroxisome speed ($P<0.0001$, Fig.4.9a), displacement rate

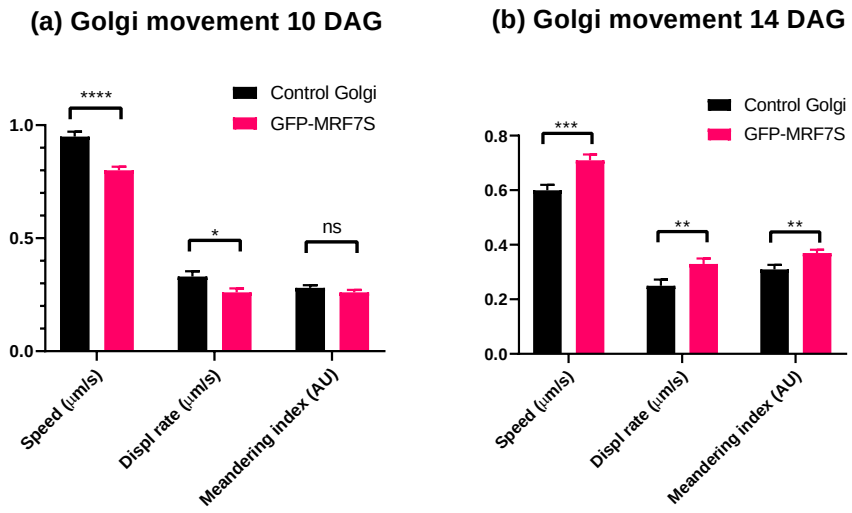

Figure 4.7: Effects of GFP-MRF7S on Golgi dynamics in *A.thaliana*. Golgi movement was tracked at two different timepoints after germination. **(a)** Speed, displacement rate and meandering index of Golgi bodies 10 days after germination (DAG) in control (black) and GFP-MRF7S expressing cells (magenta). Over-expression of GFP-MRF7S at 10 DAG significantly decreases Golgi speed (df=984, P<0.0001) and displacement rate (df=984, P=0.033) compared to control cells. **(b)** Speed, displacement rate and meandering index of Golgi bodies 14 DAG in control (black) and GFP-MRF7S expressing cells (magenta). Over-expression of GFP-MRF7S at 14 DAG significantly increases Golgi speed (df=802, P=0.00099), displacement rate (df=802, P=0.0089) and meandering index (df=802, P=0.0048) compared to control cells.
Histograms represent mean ± SEM. Statistical significance calculated with the Mann Whitney U test. **** indicates P<0.0001, ** indicates P<0.01, * indicates P<0.05, ns indicates non significant results.

	Speed (µm/s)	Displ. Rate (µm/s)	Meand. Index (AU)
Control Golgi - 10 DAG	0.95	0.33	0.28
GFP-MRF7S - 10 DAG	0.80	0.26	0.26

	Speed (µm/s)	Displ. Rate (µm/s)	Meand. Index (AU)
Control Golgi - 14 DAG	0.60	0.25	0.31
GFP-MRF7S - 14 DAG	0.71	0.33	0.37

Table 4.5: Golgi movement 10 and 14 days after-germination, absolute values. Absolute mean values of Golgi speed, displacement rate and meandering index 10 and 14 DAG.

	Speed (ratio)	Displ. Rate (ratio)	Meand. Index (ratio)
Control Golgi	1	1	1
GFP-MRF7S - 10 DAG	0.84	0.79	0.93
GFP-MRF7S - 14 DAG	1.18	1.32	1.19

Table 4.6: Golgi movement 10 and 14 days after-germination, relative values. Relative mean values of Golgi speed, displacement rate and meandering index 10 and 14 DAG expressed as fractions of the control.

(P=0.0001, Fig.4.9b) and meandering index (P<0.01, Fig.4.9c).

Relative values (Tab.4.7) indicate that GFP-ΔMRF7 increases Golgi and peroxisome movement to a larger extent than GFP-MRF7S. It appears as if Golgi and peroxisome movement progressively increase following the shortening of the DUF593 domain.

4.2.5 Summary of movement analyses

The effects of GFP-MRF7 and N-terminal truncations on Golgi movement appear to be of more complex interpretation than anticipated. Overall, the movement analyses suggest that:

1. GFP-MRF7 expression in *N.tabacum* does not influence Golgi and peroxisome speed, but increases their displacement rate.

2. GFP-MRF7S expression in *N.tabacum* increases Golgi and peroxisome movement.

3. GFP-MRF7S expression in *A.thaliana* regulates Golgi movement in a timely manner. The movement increase at 14 DAG with a similar relative increase to that observed in tobacco.

4. GFP-ΔMRF7 expression in *N.tabacum* increases Golgi and peroxisomes movement. Relative increase in both compartments' dynamics is greater than that observed following GFP-MRF7S over-expression.

5. The relative increase in Golgi and peroxisome movement appears to be the consequence of a progressive shortening of the DUF593 domain.

	Speed (ratio)	Displ. Rate (ratio)	Meand. Index (ratio)
Control Golgi	1	1	1
GFP-MRF7	1	1.13	1.19
GFP-MRF7S	1.14	1.33	1.17
GFP-ΔMRF7	1.50	1.95	1.24

	Speed (ratio)	Displ. Rate (ratio)	Meand. Index (ratio)
Control Px	1	1	1
GFP-MRF7	1.15	1.52	1.37
GFP-MRF7S	1.23	1.55	1.25
GFP-ΔMRF7	1.37	1.79	1.34

Table 4.7: Summary of GFP-MRF7, GFP-MRF7S and GFP-ΔMRF7 effect on Golgi and peroxisomes, relative mean values.

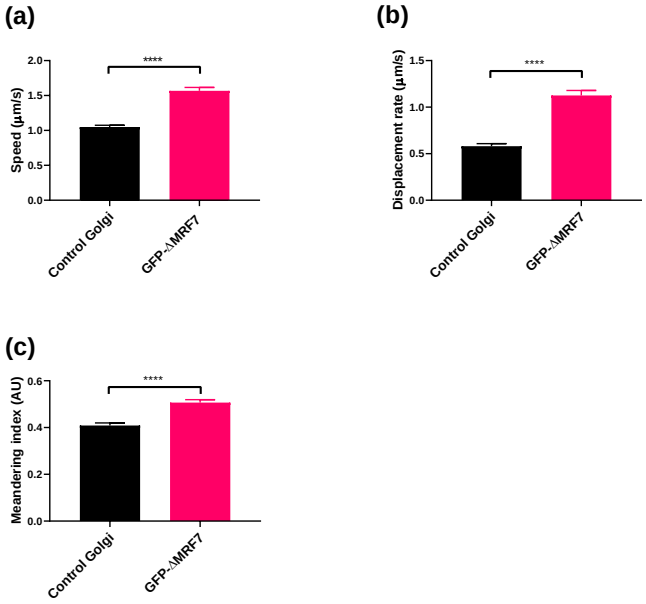

Figure 4.8: Effects of GFP-ΔMRF7 on Golgi dynamics. Results of Golgi tracking in control and GFP-ΔMRF7 over-expressing cells. Histograms represent mean ± SEM for speed (a), displacement rate (b) and meandering index (c) from five independent infiltrations. GFP-ΔMRF7 significantly increases Golgi speed (Panel (a), P<0.0001), displacement rate (Panel (b), P<0.0001) and meandering index (Panel (c), P<0.0001). Mann-Whitney U test, n_1=855, n_2=717, **** P<0.0001.

	Speed (µm/s)	Displ. Rate (µm/s)	Meand. Index (AU)
Control Golgi	1.05	0.58	0.41
GFP-ΔMRF7 Golgi	1.57	1.13	0.51

Table 4.8: Effects of GFP-ΔMRF7 on Golgi dynamics. Absolute mean values of Golgi speed, displacement rate and meandering index before and after GFP-ΔMRF7.

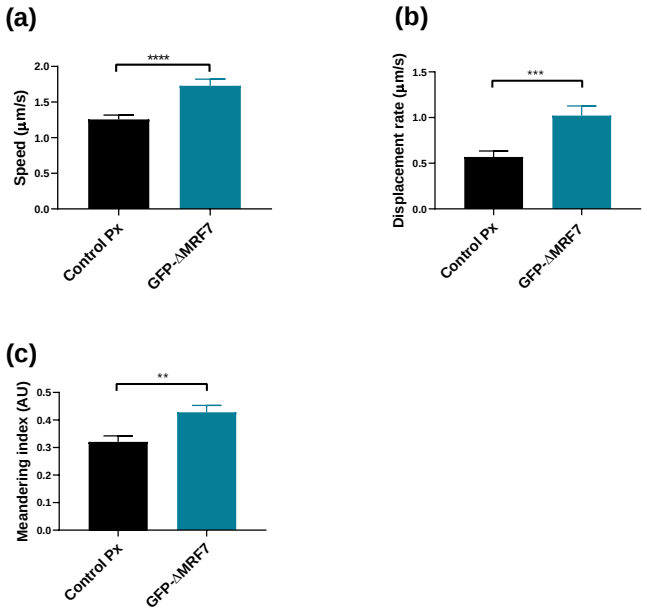

Figure 4.9: Effects of GFP-ΔMRF7 on peroxisomes dynamics. Results of peroxisomes tracking in control and GFP-ΔMRF7 over-expressing cells. Histograms represent mean ± SEM for speed (a), displacement rate (b) and meandering index (c) from six independent infiltrations. GFP-ΔMRF7 significantly increases peroxisomes speed (Panel (a), P<0.0001), displacement rate (Panel (b), P=0.0001) and meandering index (Panel (c), P=0.0021).
Mann-Whitney U test, n_1=188, n_2=181, **** P<0.0001, *** P=0.001, ** P<0.01.

	Speed (µm/s)	Displ. Rate (µm/s)	Meand. Index (AU)
Control Px	1.26	0.57	0.32
GFP-ΔMRF7 Px	1.73	1.02	0.43

Table 4.9: Effects of GFP-ΔMRF7 on peroxisomes dynamics. Absolute mean values of peroxisomes speed, displacement rate and meandering index before and after GFP-ΔMRF7.

4.3 Discussion

4.3.1 Partial or complete deletion of DUF593 increases Golgi and peroxisome speed

MRF7 represents a novelty within the *A.thaliana* MyoB family as it localises to a specific compartment (Peremyslov et al., 2013; Peremyslov et al., 2015; Kurth et al., 2017). The current chapter explored the relationship between MRF7 localisation and function through movement analysis of Golgi and peroxisomes.

Effects of MRF7 fusions on Golgi movement

The MRF7 fusions have differential effects on Golgi movement. GFP-MRF7 does not influence Golgi speed, but significantly increases its displacement rate and meadering index. Because displacement rate is defined mathematically as the shortest path from the initial to the final position of an organelle over time (Section 2.6), it provides information about the directionality of movement (Sparkes et al., 2008; Avisar et al., 2009). Speed instead takes into account the whole length of the track followed by an organelle from the initial to the final position (Sparkes et al., 2008; Avisar et al., 2009). In this sense, GFP-MRF7 could perhaps not directly alter the speed of Golgi when compared to control cells, but it appears to make the movement more directional.

There could be multiple explanations as to why Golgi tracks are straighter following GFP-MRF7 over-expression. The GFP-MRF7 puncta move in mostly straight trajectories on the actin cytoskeleton (Fig.3.4); expression of the fusion protein could perhaps alter the actin configuration to induce GFP-MRF7 puncta formation from Golgi bodies. This effect could cause the Golgi to move roughly at the same speed but in a more directional way, thus explaining the increase in displacement rate and meandering index. Another option is that GFP-MRF7 can perhaps increase the number of Golgi moving within the stream; organelles moving within a stream tend to follow straighter trajectories compared to organelles moving out of the stream (Nebenführ et al., 1999;

Stefano et al., 2014). Further experiments are needed to verify either of these scenarios.

Perhaps counterintuitively, partial or complete deletion of the DUF593 domain induces an increase in Golgi movement. How to reconcile the effects observed for full-length MRF7 with those observed following GFP-MRF7S and GFP-ΔMRF7 over-expression? The overall redundancy of the MyoB (Peremyslov et al., 2013; Peremyslov et al., 2015; Kurth et al., 2017) and myosin XI (Sparkes et al., 2008; Avisar et al., 2009) *A.thaliana* families suggests that it could be possible for more than one MyoB receptor or myosin XI to be associated to an organelle. In mammalian cells, both myosin Vb and myosin Vc are targeted to the transferrin receptor recycling vesicles (Yan et al., 2005; Rodriguez and Cheney, 2002); targeting of myosin Vb can happen *via* the Hrs/Actinin-4/BERP (Yan et al., 2005) or the Rab11a/FIP2 complexes (Lapierre et al., 2001), whereas myosin Vc targeting is suggested to happen *via* Rab8 (Rodriguez and Cheney, 2002).

Therefore, perhaps in plants there could be multiple different MyoB-myosin associated complexes controlling Golgi movement. As depicted in Fig.4.10, Golgi bodies could preferentially move following MRF7 binding to a certain myosin (brown, Fig.4.10a). MRF7 is depicted as an adaptor linking the myosin to a protein stably residing on the Golgi membrane. Other myosins could be able to bind to the Golgi via another MyoB receptor, but may be kept in an inactive form when the preferred myosin is bound to MRF7 (blue, Fig.4.10a). Inactivation of myosins in this instance is represented as a folded myosin for simplicity, which is enzymatically and mechanically switched off. Regulation of myosin activity can also occur upon fluctuations of calcium (Ca^{2+}) levels (Tominaga and Nakano, 2012). Following deletion of the DUF593 domain, MRF7 is no longer able to bind the preferred myosin (Fig.4.10b), thus potentially encouraging the Golgi to use a different, perhaps faster, MyoB-myosin complex.

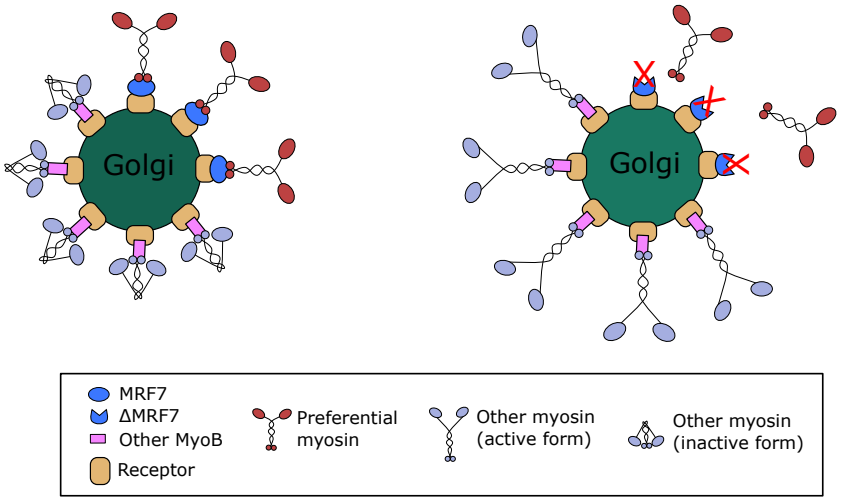

Figure 4.10: Suggested model for MRF7 role on Golgi movement. (a) Golgi movement is preferentially directed by MRF7 binding to a certain myosin (brown). Other MyoB receptors could be associated to the Golgi and bind to a myosin (blue), but kept in an inactive form if the MRF7 binding is intact. (b) Deletion of the DUF593 domain impairs the binding of MRF7 to a myosin; in this scenario the alternative receptor associated with Golgi could recruit another myosin.

Effects of MRF7 fusions on peroxisomes movement

The effects of the MRF7 fusions on peroxisome movement are slightly more difficult to interpret. Similarly to its effects on Golgi, GFP-MRF7 does not increase peroxisome speed but increases the displacement rate and meandering index, while GFP-MRF7S and GFP-ΔMRF7 cause an overall increase in peroxisome dynamics. This result might appear surprising considering MRF7 does not localise to peroxisomes (Chapter 3). The models in Fig.4.11 (Perico and Sparkes, 2018) represents possible explanations for MRF7 effects on peroxisome dynamics.

In scenario 4.11a two organelle classes, Golgi (organelle A) and peroxisomes (organelle B) in this instance, move independently using different myosin motors. MRF7 could perhaps be somehow part of the movement machinery associated with both Golgi and peroxisomes, although localisation data appear to exclude this possibility. In scenario 4.11b an organelle is transported actively throughout the cytoplasm and drags a tethered organelle. This "piggybacking" mechanism was previously decribed in the fungal model *U.maydis* (Guimaraes et al., 2015). Scenario 4.11c represents a mixed situation between (a) and (b), where both organelle classes recruit their specific movement machinery, but their physical tethering and actin polarity influence the speed at which they move.

Regarding scenarios (b) and (c), there are no indications of a physical interaction between peroxisomes and Golgi. Whilst several compartments have been shown to physically interact in plant cells (Sparkes et al., 2009; Gao et al., 2016; Osterrieder et al., 2017; Wang et al., 2017), no evidence is currently available that indicates a physical or biochemical connection between Golgi and peroxisomes. Fig.4.11d explores the possibility that changes in Golgi movement could be "transferred" indirectly to peroxisomes through a third compartment, the ER in this instance. Physical connection was shown between the ER and Golgi (Sparkes et al., 2009; Osterrieder et al., 2017); although tethering between the ER and peroxisomes has not been proven in plants yet, evidence from mammalian cells strongly suggest a physical connection between the two compartment

(Costello et al., 2017; Hua et al., 2017). In this scenario, differences in Golgi movement could induce an ER re-organisation and, in turn, this could affect peroxisome movement as a consequence. Thus far, the model depicted in Fig.4.11d appears to be the most likely. Over-expression of several *At*DUF593 domains result in the same relative decrease in the movement of several organelles (Peremyslov et al., 2015). Instead, expression of MRF7 and its N-terminal truncations have differential effects on Golgi and peroxisomes, perhaps indicating that a certain level of specificity exists.

4.3.2 Effects of GFP-MRF7S on Golgi dynamics are consistent in *N.tabacum* and *A.thaliana*

Heterologous expression of proteins can sometimes lead to slightly different effects at the subcellular level depending on the expression system used. Over-expression of myosin XI tails in *N.tabacum* and IQ-tails in *N.benthamiana* leaf epidermal cells showed that the two constructs from the same myosin have overall similar effects on Golgi movement (Avisar et al., 2009). Nevertheless, expression of IQ-tails from myosins XI-B, XI-F, XI-G, XI-H, ATM1 and ATM2 had slightly different effects when expressed in *N.tabacum* or *N.benthamiana*. Differences observed on Golgi movement were attributed to the variability associated with the two systems (Avisar et al., 2009).

In this sense, the effects of the MRF7 fusions on Golgi and peroxisome dynamics could derive from a species-specific effect of heterologous expression of *A.thaliana* genes in tobacco. The consistent effect of GFP-MRF7S on Golgi movement in *N.tabacum* and 14 DAG *A.thaliana* plants appears to exclude this possibility. These observations fit with those from localisation studies in section 3.2.4: the *A.thaliana* ST-mRFP x GFP-MRF7S stable line used for movement analysis showed not only an identical effect of GFP-MRF7S on Golgi movement, but also a similar percentage of GFP-MRF7S Golgi localisation as experiments in tobacco. Analysis of movement and localisation from more independent lines will confirm observations from Line#1.

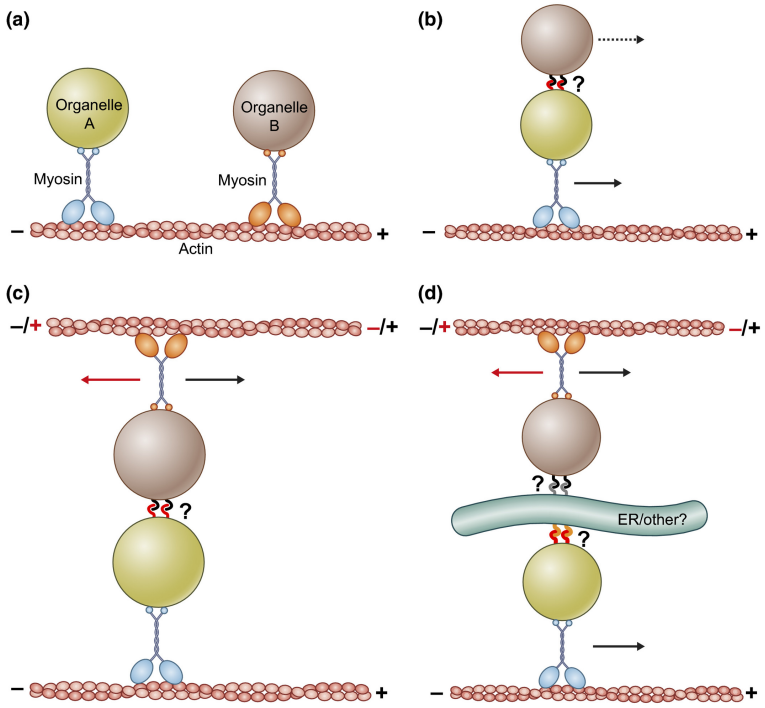

Figure 4.11: Model for MRF7 role on peroxisome movement (Perico and Sparkes, 2018). (a) Organelle A and organelle B are not physically tethered and move independently using different myosin motors. (b) Organelle A and organelle B are tethered (black and red hooks) but only one organelle moves actively on the actin and drags the second along. (c) Organelles A and B are tethered and they both move actively using different myosin motors. Movement is subject to resulting forces due to actin polarity, myosin speed and strength of the tethering. (d) Organelle tethering can involve multiple compartments. In this model the ER could act as a bridge between organelle A and organelle B; any differences in movement of one organelle could be reflected onto another compartment through the ER "bridge".

Comparison of Golgi movement in control cells at 10 and 14 DAG revealed that, perhaps unexpectedly, Golgi bodies move faster in younger seedlings. Studies in *A.thaliana* cotyledons suggest that ER streaming and maximal organelle velocities increase during cell expansion (Stefano et al., 2014). Observations of Golgi movement in *A.thaliana* fully-elongated or actively elongating hypocotyls cells appears to confirm that organelle movement is correlated with cell expansion and global actin configuration (Breuer et al., 2017). Although just a speculation, it is possible that Golgi could perhaps behave differently in epidermal cells from true leaves compared with cotyledons or hypocotyl cells.

4.3.3 Comment on the relationship between MRF7 localisation and function

As observed in Chapter 3, there is a certain degree of variability related to the MRF7 association with Golgi (Fig.3.6); this variability was observed between independent experiments, but also between cells within the same experiment.

It is possible that the MRF7 fusions could exert differential effects on Golgi and peroxisome movement depending on their localisation; in this scenario, the effects observed on Golgi and peroxisomes in this chapter could effectively represent an average of this heterogeneous pattern. *Sc*Inp2p, which regulates peroxisomes inheritance in yeast, recruits Myo2p only on peroxisomes destined to the forming bud. A mislocalisation of *Sc*Inp2p impairs peroxisomes inheritance (Fagarasanu et al., 2006). In a similar, but perhaps not identical way, MRF7 could cycle between an "active - myosin binding" or "non active - myosin free" state based on its localisation on Golgi or in the cytoplasm.

A full understanding of the relationship between the MRF7 role on Golgi and peroxisome movement and its subcellular localisation would require to test whether there is a correlation between the effects on a specific Golgi body and the state of MRF7 association with the same organelle. An attempt at answering this question was carried out as explained further below, but for which results are not reported in this dissertation.

The strategy used consisted in simultaneous imaging of the GFP channel (to visualise the localisation of the MRF7 fusions) and the organelle marker channels (Golgi and/or peroxisomes); this method would have theoretically allowed a correlation between movement parameters for a specific organelle and visualisation of the MRF7 localisation state on that same organelle. Unfortunately, while the MRF7 association to Golgi is easily identifiable from still images (Chapter 3), gathering the same type of information from movies proved challenging. The generally high cytoplasmic background of the GFP fusions (Fig.3.5) made it sometimes impossible to distinguish between cytoplasmic and Golgi-localised MRF7, particularly at the scan rate used to take movies destined for tracking.

Imaging with improved temporal and spatial resolution conditions will be necessary to assess the effect of MRF7 Golgi association on Golgi and peroxisomes movement.

Chapter 5

Myosin recruitment

Localisation of MRF7 on Golgi and its effect on Golgi dynamics suggests a potential role in recruitment of motor proteins to such compartment. In this chapter I aim to identify MRF7 binding partners and to investigate their effect on MRF7 localisation.

5.1 Introduction

5.1.1 Myosin class XI localisation in higher plants

As mentioned in the general introduction, plant myosins from class XI are the main drivers of organelle movement (Peremyslov et al., 2008; Avisar et al., 2008; Sparkes et al., 2008; Avisar et al., 2009; Peremyslov et al., 2010a; Ojangu et al., 2012). One of the main challenges has consisted in linking the effects of myosins on organelle dynamics and plant development with their subcellular localisation; it does not appear to be a simple case of one myosin localising to one organelle and affecting its movement. Several approaches have been employed to address this issue, from over-expression as well as expression at physiological levels of full-length myosins fluorescent fusions, over-expression of specific myosin tails and tail domains and immunohistochemistry.

Early attempts at defining the subcellular localisation of plant myosins were mainly carried out by immunohistochemistry. Animal antibodies were initially employed to detect myosins in the cytoplasm of plant cells, particularly in lily and *Nicotiana alata* pollen tubes (Miller et al., 1995) and rhizoids of *Chara globularis* (Braun, 1996). Despite the similarities between plant myosins XI and myosins V of mammals (Kinkema and Schiefelbein, 1994), the employment of animal antibodies to detect plant myosins inevitably raised the issue of specificity. Later on, an antibody raised specifically against a peptide within the *A.thaliana* myosin MYA-2 tail allowed the detection of such myosin on the actin cytoskeleton and peroxisomes in leaf epidermal cells (Hashimoto et al., 2005).

Expression of fluorescent fusions of full-length myosin XI-K (Peremyslov et al., 2012), one of the main regulators of organelle movement in *A.thaliana*, showed that myosin XI-K moves on the actin cytoskeleton with a beads-on-a-string configuration, much like that observed for some MyoB receptors (Peremyslov et al., 2013; Kurth et al., 2017). Moreover, XI-K was shown to partially co-localise with Golgi, secretory vesicles and the ER. The extent of colocalisation observed for ER and actin cytoskeleton was greater than that observed for Golgi and

secretory vesicles (Peremyslov et al., 2012); the authors suggest that perhaps large endomembrane compartments are the main target of myosins. Interestingly, even in areas of extensive overlap between XI-K and the ER, the myosin maintained its beads-on-a-string configuration, therefore suggesting that the overlap could also be a co-localisation driven by the actin cytoskeleton position rather than a true physical interaction with the ER (Peremyslov et al., 2012).

Another attempt at defining myosins subcellular localisation involved the use of dominant negative myosin mutants (Sparkes et al., 2008; Avisar et al., 2009). Motor-less constructs of myosins from class XI (and VIII) were transiently over-expressed in *N.tabacum* and *N.benthamiana* leaf epidermal cells. Expression of non motile myosins would allow in the first instance to monitor the effects of specific myosins on organelle movement (Golgi and mitochondria in particular) and in second instance to define their subcellular localisation. In this sense, the truncated myosins would recognise their cargo organelle but are not able to detach from it, thus labelling its membrane. The combination of informations on localisation and effects on movement would then allow to reconstruct a network defining which myosins are involved in controlling the movement of a certain organelle. While the effects of myosin tails on Golgi, peroxisomes and mitochondria had been extensively described (Avisar et al., 2009; Sparkes et al., 2008), their localisation remained elusive. Only myosin XI-I clearly labelled the nuclear envelope, whereas other myosin XI tails mostly exhibited a diffuse cytoplasmic or punctate localisation (Avisar et al., 2009).

Similar approaches were attempted by over-expressing only certain subdomains of myosin XI tails. Table 5.1 reports a summary of the localisation of full-length and truncated *A.thaliana* myosins, with references to the respective journal papers and the plant species in which they were expressed. In particular, the DIL and PAL domains, homologous to the yeast Myo2p secretory vesicles binding domain and vacuole and mitochondria inheritance domain respectively (Sattarzadeh et al., 2011; Sattarzadeh et al., 2013) were transiently expressed in

N.benthamiana. Interestingly, DIL and PAL domains from the same myosin were localised on multiple organelles, sometimes even on membrane of organelles whose movement was not shown to be affected by such myosins; for example, the DIL domain of myosin XI-D localised on the Golgi membrane, despite XI-D tail was not shown to affect Golgi movement in *N.tabacum* and *N.benthamiana* (Avisar et al., 2009; Sattarzadeh et al., 2011; Sattarzadeh et al., 2013).

Although these works signified an important step forward in understanding what drives myosin recruitment to certain compartments, expression of myosins or myosin fragments suggests that a higher level of control is necessary to trigger full-length myosin recruitment to specific organelles. The following sections explore myosin recruitment taking into consideration the interaction with potential receptors and adaptor proteins.

5.1.2 Myosin recruitment in plants

Myosin recruitment by MyoB receptors

Members of the MyoB family from *A.thaliana* and *N.tabacum* were shown to bind myosin *At*XI-K (Peremyslov et al., 2013) and *Nt*MYOXIpt (Stephan et al., 2014) through their DUF593 domain. The TGN-localised protein *Nt*RISAP (RAC5 interacting subapical pollen tube protein) interacts with the pollen specific myosin *Nt*MYOXIpt (Stephan et al., 2014). RISAP was initially identified through a yeast-2-hybrid screen as the effector of GTP-bound RAC5, a RHO GTPase responsible for polarity maintainance of F-actin in growing pollen tubes (Klahre and Kost, 2006; Stephan et al., 2014). Binding with MYOXIpt is mediated by DUF593 and is suggested to trigger correct positioning of the TGN at the pollen tube tip and to support the movement of plasma membrane (PM)-directed secretory vesicles; it interacts with RAC5 through its N-terminal hydrophobic region. Release of RAC5 containing vesicles at the PM could be the result of binding of adaptor or co-factor molecules which reduce RISAP affinity for MYOXIpt (Stephan et al., 2014).

Despite influencing multiple organelles dynamics as full-length or

Localisation	Myosin	Domain(s)	Organism and references
P-bodies	XI-K	Full-length	*A.thaliana*; (Steffens et al., 2014)
Peroxisomes	MYA2, XI-K, XI-B, XI-E, XI-G, XI-H, XI-I	DIL domain	*N.benthamiana*; (Sattarzadeh et al., 2009)
	MYA1	GT1, GT2 domain	*A.thaliana*; (Li and Nebenführ, 2007)
	MYA2	GT2 domain	*A.thaliana*; (Li and Nebenführ, 2007)
	MYA1, MYA2, XI-I, XI-K	GT1+GT2 domains	*A.thaliana*; (Li and Nebenführ, 2007)
Nuclear membrane	XI-I	Tail and IQ-tail	*N.benthamiana*, *N.tabecum*, *A.thaliana*; (Avisar et al., 2009; Tamura et al., 2013)
	MYA1, XI-B, XI-C, XI-E, XI-G, XI-K	PAL domain	*N.benthamiana*; (Sattarzadeh et al., 2013)
	XI-C, XI-E, XI-G	DIL domain	*N.benthamiana*; (Sattarzadeh et al., 2009)
Chloroplasts	XI-F	Tail, PAL domain	*N.benthamiana*; (Sattarzadeh et al., 2009; Sattarzadeh et al., 2013)
Golgi	XI-C, XI-G	DIL domain	*N.benthamiana*; (Sattarzadeh et al., 2009)
	MYA1	DIL, PAL, GT2 domain	*A.thaliana*, *N.benthamiana*; (Li and Nebenführ, 2007; Sattarzadeh et al., 2009; Sattarzadeh et al., 2013)
	XI-B, XI-D, XI-G, XI-H, XI-I	PAL domain	*N.benthamiana*; (Sattarzadeh et al., 2013)
	XI-K	Full length, PAL domain	*A.thaliana*, *N.benthamiana*; (Peremyslov et al., 2012; Sattarzadeh et al., 2013)
	MYA2	Tail	*N.benthamiana*; (Reisen and Hanson, 2007)
Plasma membrane	XI-B	PAL domain	*N.benthamiana*; (Sattarzadeh et al., 2013)
	MYA2	DIL, PAL domain	*N.benthamiana*; (Sattarzadeh et al., 2013)
	XI-A, XI-E, XI-I, XI-K	DIL domain	*N.benthamiana*; (Sattarzadeh et al., 2009)
ER	XI-K, XI-G	DIL domain	*N.benthamiana*; (Sattarzadeh et al., 2009)
	XI-K	Full length	*A.thaliana*; (Peremyslov et al., 2012)
Secretory vesicles	XI-K	Full length	*A.thaliana*; (Peremyslov et al., 2012)
Mitochondria	XI-C, XI-E, XI-G, XI-H, XI-I, XI-K	PAL domain	*N.benthamiana*; (Sattarzadeh et al., 2013)

Table 5.1: Subcellular localisation of full-length and truncated *A.thaliana* myosins from class XI.

dominant negative mutants (Peremyslov et al., 2015), members of the *A.thaliana* MyoB family do not appear to colocalise to a known compartment (Peremyslov et al., 2013; Kurth et al., 2017). As single MyoB knock-outs do not cause any growth or developmental defects in *A.thaliana*, these receptors appear to have overlapping functions (Peremyslov et al., 2013; Peremyslov et al., 2015). In order to determine whether this redundancy also reflects their ability to bind myosin motors, yeast-2-hybrid screens were carried out on five myosin XI globular tails using an *A.thaliana* cDNA library in order to build a network of myosin and myosin receptors interaction (Kurth et al., 2017). Figure 5.1 schematically summarises the results of such analysis: aside from some occasional specific interactions, one of which is the previously described WIT2/XI-I dimer (Tamura et al., 2013), most of the MyoB receptors seem to be able to bind multiple myosin tails, and *viceversa*. The overall complexity of the network suggests that other adaptor proteins might be needed to determine any form of specificity between a myosin and a receptor. Moreover, MyoB1-GFP collocates with full length XIK-mCherry but the co-expression does not appear to trigger any specific organelle localisation (Peremyslov et al., 2013). For this reason, the authors suggested that MyoB vesicles define a plant specific compartment driving organelle movement and cytoplasmic streaming (Peremyslov et al., 2013; Peremyslov et al., 2015).

Myosin recruitment by plant non-MyoB receptors

Myosin recruitment in plants is not exclusively mediated by MyoB receptors. One of the first resolved recruitment complexes was the WIT1/WIT2 dimer on the outer nuclear membrane (Tamura et al., 2013). Myosin XI-I tail localises to the outer nuclear membrane in transiently transfected tobacco cells (Avisar et al., 2009) and in stably expressing *A.thaliana* plants (Tamura et al., 2013). In *wit1 wit2 A.thaliana* background, myosin XI-I is unable to localise to the nucleus, indicating that WIT1/WIT2 are directly responsible for its localisation (Tamura et al., 2013). Dark-induced nuclei movement is impaired in *xi-i* or *wit1*

wit2 A.thaliana plants, indicating that the WIT1/WIT2/XI-I complex anchors the nucleus to the actin cytoskeleton. As observed for myosins in other organisms (Li and Nebenführ, 2008), myosin XI-I is not exclusively involved in nuclear relocation (Avisar et al., 2009), although it is specifically recruited to such compartment by WIT1/WIT2.

MadA and MadB are two novel classes of myosin binding proteins identified in *A.thaliana* (Kurth et al., 2017). These two families are composed of four members each and are structurally different from one another and from the MyoB family (Peremyslov et al., 2013; Kurth et al., 2017). Expression of fluorescent fusions of MadA and MadB proteins showed that, similarly to MyoBs, they localise to punctate structures, with the exception of MadA1 which localises to the nucleoplasm (Kurth et al., 2017). Yeast-2-hybrid screen showed that the same MadA-B protein can bind multiple myosins (Kurth et al., 2017), contributing to the redundancy of the myosin-myosin receptors network (Fig.5.1). Given their lack of transmembrane domains (TMDs), the MadA-B families were suggested to act more as adaptor proteins in a myosin-recruiting complex than as receptors, although the composition of the protein scaffold to which they might belong to was not discussed (Kurth et al., 2017).

The decapping protein DCP1 was identified as the P-bodies myosin receptor in *A.thaliana*. P-bodies are highly dynamic cytoplasmic membrane structures responsible for quality control and storage of translationally repressed mRNAs (Sheth and Parker, 2003; Hamada et al., 2012). DCP1 was shown to interact with *A.thaliana* myosin XI-K, MYA1, MYA2 and XI-I tails and to colocalise with full-length myosin XI-K, which appeared to provide the major contribution to P-bodies movement (Steffens et al., 2014).

Lastly, Rab GTPases are also good candidate myosin receptors. Due to their ability to cycle between active and inactive states through binding to GTP or GDP, Rabs can recruit different effectors (Pfeffer, 2017) and have been implicated in MyoV recruitment to melanosomes and recycling vesicles (Li and Nebenführ, 2008). Their ability to switch between different activation states can perhaps suggest a role in regulated

recruitment of myosin adaptors and receptors. Recent work in *P.patens* showed that myosin XIa binds to all five RabE proteins and that such interaction is fundamental for correct polarised growth (Orr et al., 2019). Moreover, *At*RabD1 and *At*RabC2A have been localised to peroxisomes (Hashimoto et al., 2008) and Golgi stacks/trans-Golgi network (Pinheiro et al., 2009) respectively. Both Rabs interact with myosin XI-2 tail (Hashimoto et al., 2008), suggesting a role in myosin targeting to those compartments.

5.1.3 Myosin recruitment in non-plant systems

The mechanisms of myosin recruitment have so far been more extensively characterised in yeast and animals than in plant cells (Li and Nebenführ, 2008). Examples of some protein complexes for motor proteins recruitment are shown in Fig.5.2. Acto-myosin dependent transport of organelles in yeast and animals is mediated by myosins from class V, a family structurally similar to the plant-specific class XI (Thompson and Langford, 2002; Li and Nebenführ, 2007; Sebé-Pedrós et al., 2014). Partially or completely resolved complexes in non-plant organisms suggest that myosin recruitment rarely involves a single protein localised on the cargo organelle (Fagarasanu et al., 2006); instead it is more often organised as a finely tuned scaffold assembly that ultimately allows correct myosin "docking" on the cargo. Specific regulation of single components within the scaffold are responsible for correct organelle positioning.

S.cerevisiae Myo2p is responsible for movement of secretory vesiscles (Wagner et al., 2002), peroxisomes (Fagarasanu et al., 2006), mitochondria (Itoh et al., 2004) and vacuoles (Ishikawa et al., 2003; Tang et al., 2003). Binding of Myo2p to each of these compartments is regulated by different adaptors and receptors which appear to bind to different amino acidic residues within the Myo2p C-terminal region (Pashkova et al., 2005a; Pashkova et al., 2005b). Given that some of these motifs partially overlap, recent work suggest an intrinsic flexibility within the cargo binding domains of Myo2p which could allow accommodation of structurally different receptors and adaptors (Taylor Eves et al., 2012;

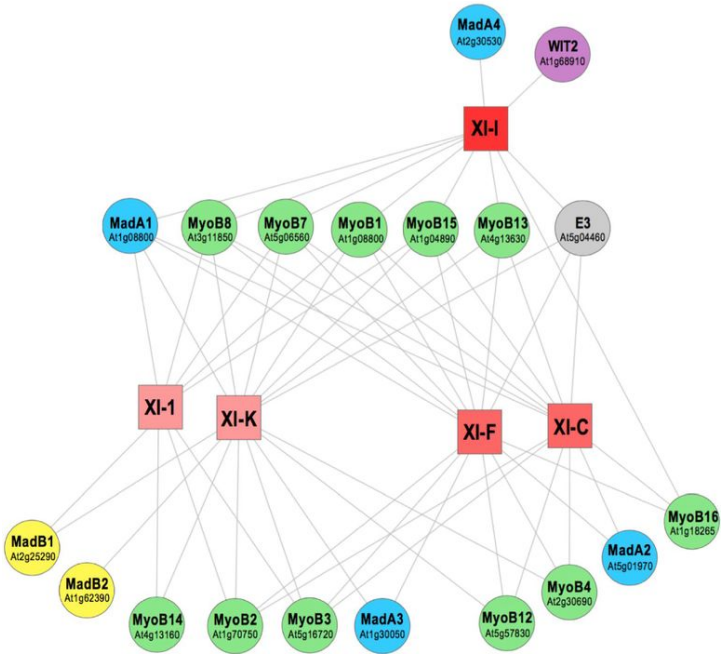

Figure 5.1: Schematic representation of interaction network of myosin and myosin receptors from *A.thaliana* (Kurth et al., 2017). Squares indicate the five tails used as baits for yeast-2-hybrid analyses, circles indicate receptors or adaptor proteins (MyoB, MadA-B, WIT2 and E3). Lines connecting squares and circles indicate interacting pairs.

Tang et al., 2019). These observations could also imply that competition of cargoes for myosin binding could play an important role in organelle movement and inheritance.

Myosin recruitment complexes in mammalian cells also suggest a role for Rab GTPases in specific organelle targeting (Li and Nebenführ, 2008). Rab27a is localised on melanosomes membrane in mouse melanocytes and binds to myosin Va *via* the adaptor protein melanophilin (Mlph) in a GTP-dependent manner (Wu et al., 2002; Ohbayashi et al., 2010). Inhibition of Rab27a and Mlph interaction by the flavonoid hesperidin causes clustering of melanosomes around the nucleus (Kim et al., 2013a).

Regulation of receptors and adaptors activity and localisation mainly relies on the regulation of mRNA levels or selective degradation of the receptor/adaptor upon correct cargo delivery. The *S.cerevisiae* proteins Vac17p, Mmr1p and Inp2p were shown to recruit Myo2p and orchestrate delivery of vacuoles (Ishikawa et al., 2003; Tang et al., 2003), mithocondria (Itoh et al., 2004) and peroxisomes (Fagarasanu et al., 2006) during bud formation. mRNA levels of the three genes were shown to fluctuate in a cell cycle-dependent manner, consistent with their role in organelle inheritance (Spellman et al., 1998). Post-translational modifications and targeted degradation also play a role in correct organelle positioning; for example, removal of a PEST sequence from the myosin adaptor Vac17p causes a backward movement of the vacuole from the bud to the mother cell, effectively impairing vacuole inheritance in yeast (Tang et al., 2003).

Overall, the mechanisms regulating myosin recruitment and organelle positoning in yeast and mammals appear to be the result of a finely tuned coordination between specificity of binding sites, receptors/adaptors and myosin activity regulation and correct assembly of the myosin recruitment complexes.

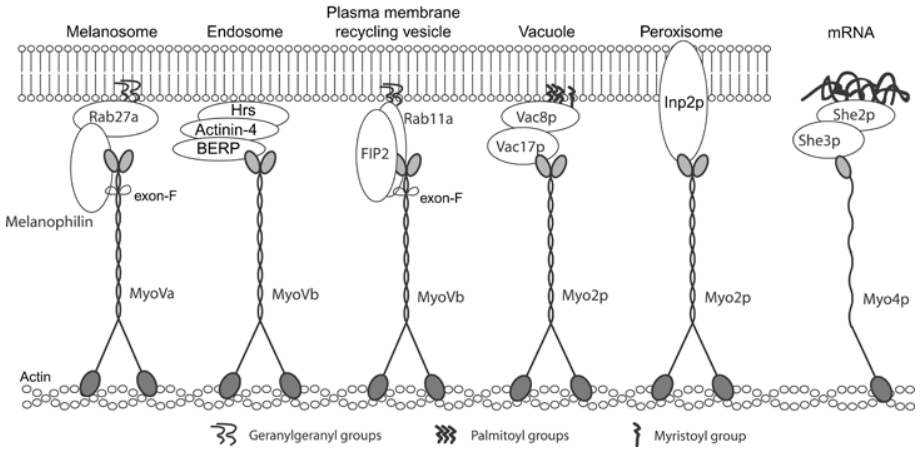

Figure 5.2: Examples of myosin V/Myo2p recruitment complexes from yeast and mammalian cells (Li and Nebenführ, 2008). Schematic representation of recruitment complexes for *S.cerevisiae* Myo2p and mammalian MyoVa and MyoVb. Myosins are represented in grey and the target compartments are specified at the top of the schematic.

5.1.4 Expression profiles of MyoB receptors and class VIII and XI myosins

Expression of myosins and MyoB receptors vary between tissues and plant developmental stages. Figure 5.3 represents the expression data mined from public RNA-seq microarray data with the analysis tool GENEVESTIGATOR®. Myosins such as XI-K, MYA1 (XI-1) and MYA2 (XI-2) appear to be ubiquitously expressed in all tissues. Others are more specifically expressed in certain tissues, consistent with observations from expression studies with GUS staining (Haraguchi et al., 2018). Similar considerations can be drawn for the MyoB receptors. Expression pattern of the MyoB receptor used in this study, MRF7, is highlighted in red (Fig.5.3).

5.1.5 Aims

This chapter aims at indentifying the MRF7 binding partners and, in particular, the role of MRF7 on myosins XI recruitment to the Golgi.

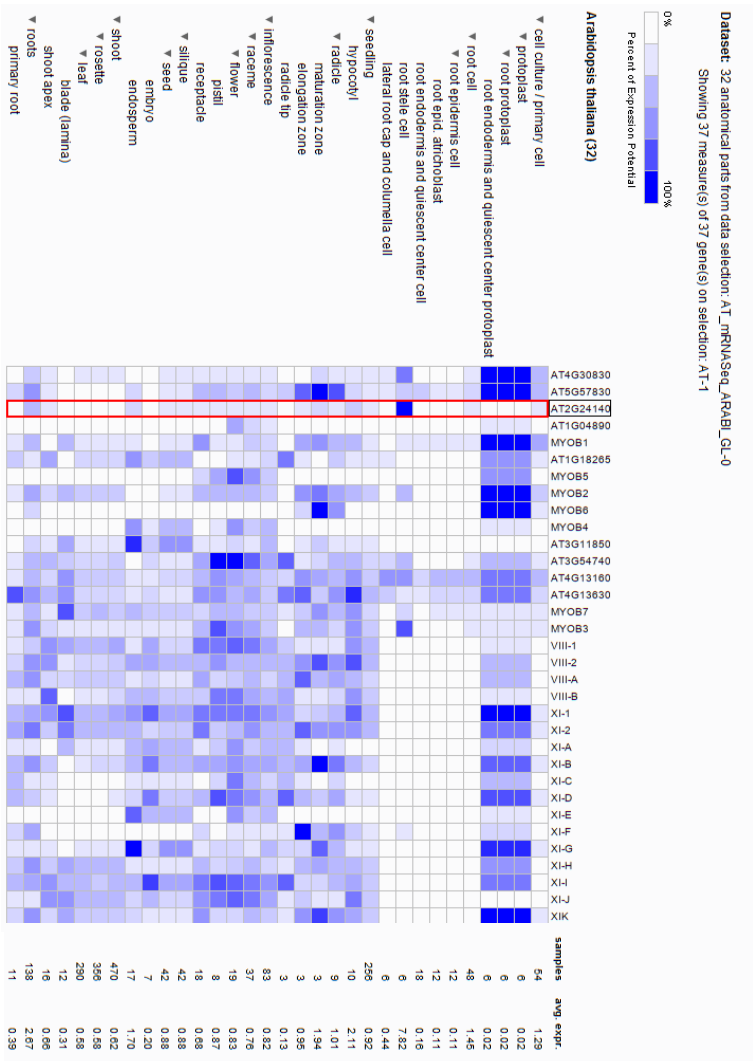

Figure 5.3: Expression profile of *At*MyoB receptors and myosins class VIII and XI. Development and tissue specific expression profiles of *A.thaliana* MyoB receptors and myosins class VIII and XI. The expression heatmap was generated with the GENEVESTIGATOR® analysis tool. The first 16 columns report the expression data for all the MyoB receptors, with MRF7 highlighted in red. Following columns contain data for class VIII and XI myosins.

5.2 Results

5.2.1 Identification of MRF7 interactors

A co-immunoprecipitation (co-IP) using the GFP-Trap® bead technology was carried out to identify MRF7 interactors from crude protein extracts of *A.thaliana* lines over-expressing GFP-MRF7, GFP-MRF7S and GFP-ΔMRF7, respectively. Liquid chromatography mass spectrometry (LCMS) of the resulting pull down was used to identify resulting MRF7 interactors. The rationale for testing all three construct was to try and isolate proteins which interact with MRF7, and to determine which regions within MRF7 are critical for the interaction.

First, expression of the constructs in the crude extracts and purified samples was checked by SDS-PAGE followed by Western blot. GFP-MRF7, GFP-MRF7S and GFP-ΔMRF7 have a predicted molecular weight of 65 kDa, 59 kDa and 54 kDa respectively. For the blot shown in Figure 5.4, 10 µg of total protein extract ("T") and 20 µL of beads-purified sample ("B") were loaded on the gel. The Ponceau staining in Fig.5.4a shows equal total protein loading: the band corresponding to the RuBisCo large subunit is visible between the 46 kDa and 58 kDa ladder bands. Fig. 5.4b and 5.4c are images of the same blot developed with two different ECL solutions and at different exposure times. Two methods were used for protein detection due to sensitivity of detecting lower ("T", total) and higher ("B", beads) abundance levels of GFP-MRF7, GFP-MRF7S and GFP-ΔMRF7.

The position of the bands corresponding to GFP-MRF7 (65 kDa), GFP-MRF7S (59 kDa) and GFP-ΔMRF7 (54 kDa) are indicated for the purified samples ("B", Fig.5.4b, asterisks) and the total protein extracts ("T", Fig.5.4c, black squares). As expected, the GFP-fusions are present in all the samples except for the wild-type Col-0 crude extracts and purified fraction. In addition to the expected bands corresponding to the three GFP fusions, bands of lower molecular weight were also observed, which could perhaps constitute degradation products.

Smeared bands of high molecular weight ($\simeq$175 kDa) are also present in all "B" samples except for the wild-type Col-0. Given the absence of

such bands in the wild-type, non-specific detection can perhaps be excluded; furthermore, these bands have slightly increasing molecular weights going from left to right from the GFP-ΔMRF7 to the GFP-MRF7 wells. It is currently unknow whether MRF7 or other MyoB receptors are able to dimerise or oligomerise (Holding et al., 2007; Peremyslov et al., 2013; Stephan et al., 2014). Although β-mercaptoethanol was added and the samples were boiled before SDS-PAGE gel loading, it cannot be excluded that MRF7 monomers might associate in a more complex quaternary structure. The higher molecular weight bands appear to be quite large to correspond to dimers (MW>130 kDa), suggesting perhaps a higher degree quaternary structure (possibly a trimer). Future tests could confirm complex formation by running a native gel.

The α-GFP antibody also appears to be recognising some non-specific bands: 1) two closely migrating bands between 30 and 46 kDa (Fig.5.4c, black arrowheads); 2) a single band with a molecular weight <30 kDa, present in all the samples (Fig.5.4b-c).

Following expression check, purified samples were sent for LC-mass spectrometry analyses (Proteomics Facility, University of Bristol). Three independent protein extractions and mass-spectrometry analyses were carried out and results indicated an interaction of GFP-MRF7 and GFP-MRF7S with myosin XI-K. On the contrary, GFP-ΔMRF7 appears to be unable to bind to myosin XI-K, suggesting that DUF593 region is responsible for myosin binding.

5.2.2 Assessment of the effects of MRF7 and ΔMRF7 expression on myosin XI-K localisation

Results obtained from co-immunoprecipitations and mass spectrometry experiments indicate myosin XI-K as a candidate interactor of MRF7. The interaction is suggested to happen *via* the myosin binding domain DUF593, consistent with that observed for other MyoB receptors (Peremyslov et al., 2013; Stephan et al., 2014). Indication of *in vivo* interaction can sometimes be inferred from the relocation of proteins from a subcellular compartment to another following co-expression. For this

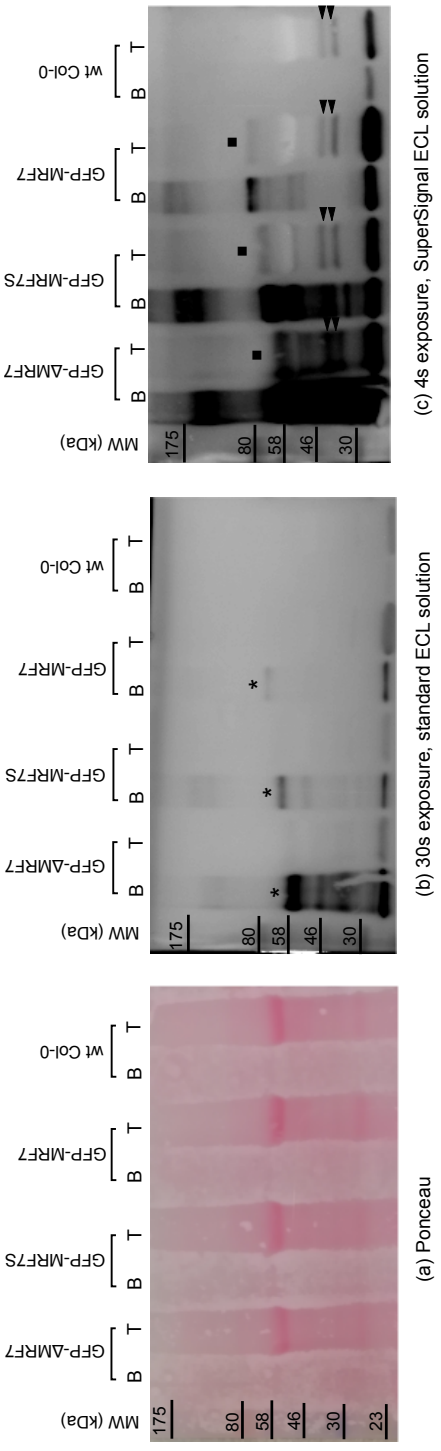

Figure 5.4: Expression of GFP-MRF7, GFP-MRF7S and GFP-ΔMRF7 in crude extracts and antibody-purified samples from *A.thaliana* transgenic plants. SDS-PAGE gel was loaded with 10 µg of total protein extract ("T") and 20 µL of purified samples ("B") from GFP-MRF7, GFP-MRF7S, GFP-ΔMRF7 and wild-type Col-0 plants. **(a)** Ponceau staining of the PVDF membrane: bands corresponding to the RuBisCo large subunit are visible between the 46 and 58 kDa marker bands. **(b)** The same membrane from (a) was developed with a standard ECL solution for 30s: asterisks indicate the bands corresponding to GFP-ΔMRF7, GFP-MRF7S and GFP-MRF7 in the purified samples ("B"). A non-specific band was detected in the lower part of the blot (<30 kDa). **(c)** Membrane was washed and developed with the SuperSignal ECL solution for 4s. Bands corresponding to the fusion proteins can now be seen also in the total protein extract samples ("T", black squares). Arrowheads indicate non-specific bands detected by the α-GFP antibody in the total protein extract samples.

reason, myosin XI-K localisation was monitored in the presence and absence of MRF7 and ΔMRF7 in tobacco leaf epidermal cells. A motor-less construct of myosin XI-K (XI-K tail) was used in this study (Avisar et al., 2009).

Consistent with that described in the literature (Avisar et al., 2009), RFP-XIK tail was observed to be cytoplasmic or occasionally localised to unidentified puncta in the absence of either GFP-MRF7 or GFP-ΔMRF7. GFP-MRF7 and GFP-ΔMRF7 maintained the localisation described in sections 3.2.3 and 3.2.4. Upon co-expression with GFP-MRF7, myosin XI-K tail collocates with the receptor and clearly labels circular Golgi-like structures (Fig.5.5a-c); this effect is not obtained through co-expression with GFP-ΔMRF7 (Fig.5.5d-f), suggesting that the lack of DUF593 domain on the receptor influences the binding and successive relocation of the XI-K tail.

By using the triple expression system, quantification of the percentage of Golgi localisation across 30 cells from 3 independent experiments was carried out and results are shown in Fig.5.6e. Triple expression of GFP-MRF7 and RFP-XIK tail with the Golgi marker ST-CFP shows that the round structures labelled by both proteins are indeed Golgi bodies (Fig5.6a-d). Statistical analysis indicates that co-expression of GFP-MRF7 and RFP-XIK tail mutually influence each other's localisation. While initially RFP-XIK is completely cytoplasmic, upon co-expression with GFP-MRF7 an average of 36% of Golgi per cell displayed XI-K tail (Fig.5.6e, n=30, $P<0.0001$). Moreover, the expression of RFP-XIK significantly stabilises GFP-MRF7 on Golgi, as the percentage of Golgi per cell displaying GFP-MRF7 on the membrane increases from 26% to 62% (Fig5.6e, n=30, $P=0.0005$).

Co-expression of GFP-MRF7 with RFP-XIK tail results in three Golgi subpopulations: 1) no RFP-XIK or GFP-MRF7, 2) only GFP-MRF7 localised and 3) both GFP-MRF7 and RFP-XIK localised to the Golgi. Intriguingly, the increase in subpopulation (2) upon co-expression of RFP-XIK tail (+36%, Tab.5.3, first row) matches the increase of RFP-XIK tail on the Golgi (+36%, Tab.5.4, first row). The potential

matched increase could infer that interaction of MRF7 with XI-K tail directly stabilises MRF7 on the Golgi surface and prevents it from cycling on and off the Golgi.

5.2.3 Validation of *in vivo* interaction between MRF7 and XIK tail by FRET-FLIM

Both pull down (Section 5.2.1) and co-expression studies (Section 5.2.2) indicate that MRF7 interacts with myosin XI-K and that interaction is dependent on the DUF593 domain within MRF7. To further test and validate the interaction *in vivo*, FRET-FLIM was carried out.

FRET-FLIM is a technique that allows to test interactions between proteins *in vivo* (Section 2.5.2). FRET (Förster Resonance Energy Transfer) is a photophysical phenomenon in which energy is non-radiatively transferred from an excited donor to a non-excited quencher (acceptor) within a maximum distance of approximately 10 nm (Förster, 1948). FRET can be quantified with several methods, one of which is FLIM (Fluorescence Lifetime IMaging); upon occurrence of FRET, a reduction of the excited state lifetime (τ) of the donor molecule is observed, so the donor molecule will remain in an excited state for a shorter period of time. Measuring the donor's lifetime in the presence and absence of the acceptor (quencher) molecule can give an indication of whether the two are interacting. As FRET is a function of distance between the donor and the acceptor (Section 2.5.2), it is possible to estimate the distance between the two molecules (r, Eq.2.2) by calculating the efficiency of the energy transfer (FRET efficiency, E_{FRET}, Eq.2.1) for that particular combination of proteins.

Before FRET-FLIM analysis, confocal images were acquired to confirm GFP and RFP expression (Fig.5.7a-c). The imaged cells then underwent lifetime (τ) measurements with FLIM (Fig.5.7d). GFP-MRF7 and GFP-ΔMRF7 were used as donors, while RFP-XIK tail was used as the acceptor (or quencher). By comparing the GFP lifetime between control samples expressing only GFP-MRF7 or GFP-ΔMRF7, and samples co-expressing each of those proteins with RFP-XIK tail, it was

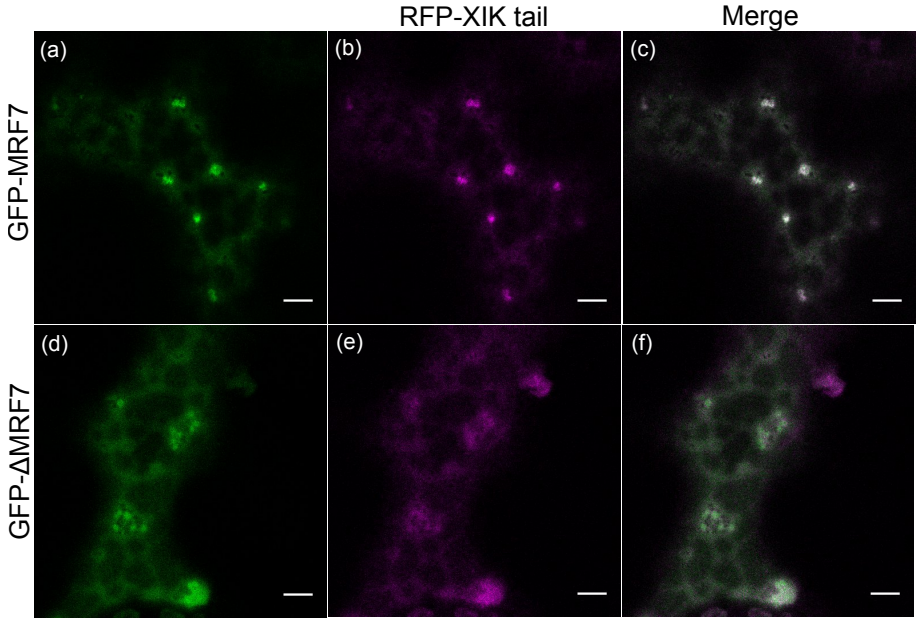

Figure 5.5: Qualitative observations of myosin XI-K tail localisation following co-expression with GFP-MRF7 and GFP-ΔMRF7. Representative images of RFP-XIK tail co-expression with either GFP-MRF7 or GFP-ΔMRF7 in tobacco leaf epidermal cells. Panels (a) to (c) show strong co-localisation of GFP-MRF7 with XI-K tail. Co-localisation was not observed between GFP-ΔMRF7 and RFP-XIK tail: in panel (d), GFP-ΔMRF7 is localising on round subcellular structures, presumably Golgi, but RFP-XIK tail does not migrate to the membrane of such compartment together with GFP-ΔMRF7. All scalebars = 5 µm.

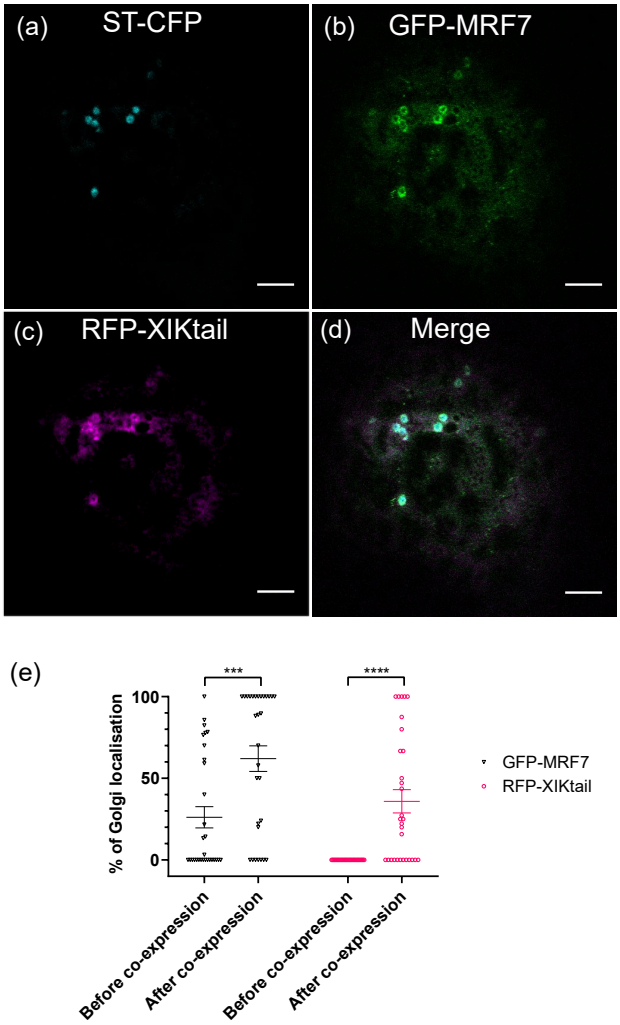

Figure 5.6: GFP-MRF7 and RFP-XIK tail co-localisation study in transiently transfected tobacco leaf epidermal cells. Panels (a) to (d) show a representative image of the localisation of GFP-MRF7 and RFP-XIK tail upon co-expression. ST-CFP is the Golgi marker. All scalebars = 5µm.
Panel (e) is a quantification of the constructs localisation before and after co-expression. Data shown are the results of three independent experiments (n=30). Effects of co-expression were tested by Mann-Whitney U test. *** indicates P<0.001, **** indicates P<0.0001. Each data point represents one cell; values from individual cells are represented as a scatterplot. Error bars indicate mean ± *SEM*.

possible to test for interaction and to validate the observations from mass spectrometry and co-localisation experiments. The fusion proteins locate to both cytoplasm and Golgi bodies. FLIM measurements were carried out on both pools of proteins to determine if interaction occurs either or both sites.

Lifetime was not measured for the GFP-MRF7 puncta for two main reasons: 1) whether observing puncta or Golgi bodies, LatB treatments of leaf samples were necessary prior to lifetime measurements due to the high motility of both structures; moreover, as mentioned in chapter 3.2.6, cells will display very few GFP-MRF7 puncta following a LatB treatment, thus making the GFP lifetime measurements on puncta even more challenging. 2) Collecting enough photon counts for lifetime measurements from small punctate structures proved to be quite challenging: long collection times (>1 min) were required and during those long exposures the sample on the stage would subtly drift in z, making the measurements difficult.

A negative and positive control were initially tested to verify that the system was correctly detecting an interaction or a non-interaction. The Golgi-localised proteins GRIP-GFP and RFP-ARL1 were used as positive control as they were previously described to strongly interact ($\Delta\tau = 0.4$ ns) on the Golgi membrane (Osterrieder et al., 2009). Although the lifetime drop was not as marked here ($\Delta\tau = 0.2$ ns), results show an interaction between the two proteins (Fig.5.8a, t(19.27), df=236, P<0.001). The Golgi marker derived from the transmembrane domain of rat sialyltransferase (C. Hawes lab, Oxford Brookes University) fused to GFP and RFP were used as a negative control. Negative controls traditionally require two proteins localised to the same structure (Golgi in this instance) but which do not physically interact. No interaction was detected for the negative control (Fig.5.8a, t(0), df=307, P>0.999).

GFP-MRF7 lifetime in control cells was consistently determined to be 2.4±0.1 ns on Golgi (Fig.5.8a) and in the cytoplasm (Fig.5.8b). Upon co-expression with RFP-XIK tail, GFP lifetime drops to 2.3±0.1 ns both on Golgi (t(9.413), df=199, P<0.001, Fig.5.8a) and in the cytoplasm (t(3.916), df=29, P=0.0005, Fig.5.8b), suggesting that the proteins are

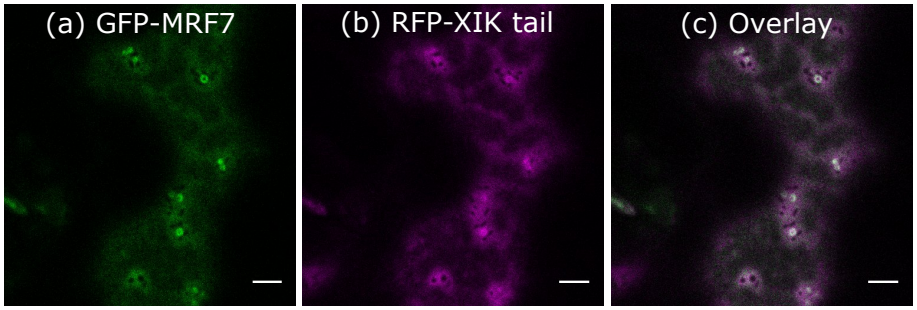

(d) Fluorescence Lifetime IMaging

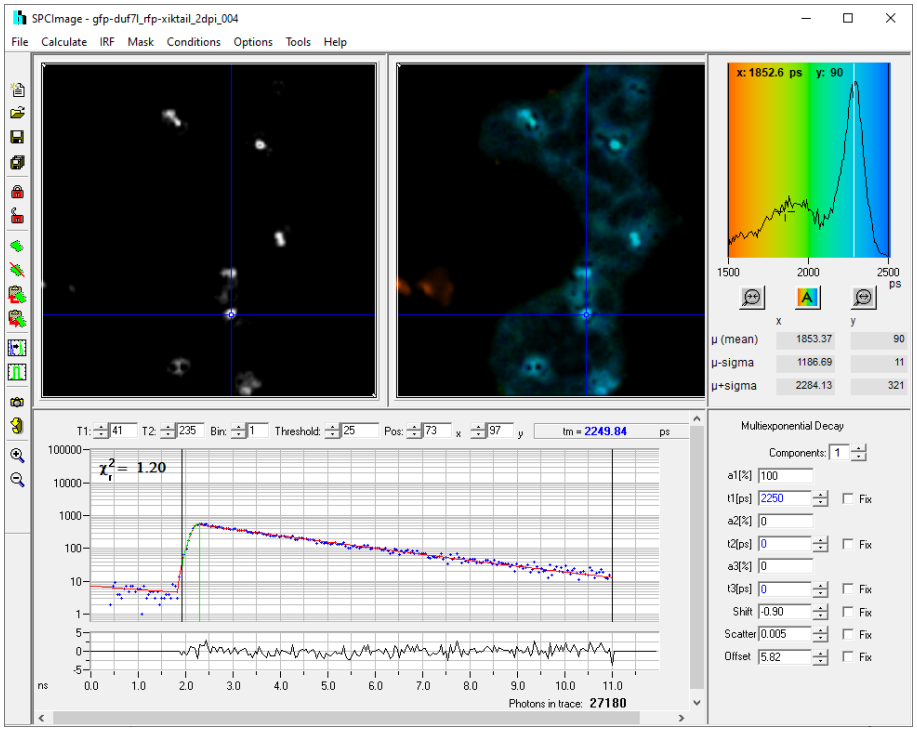

Figure 5.7: Representative confocal images and FRET-FLIM analysis for the GFP-MRF7 and RFP-XIK tail co-expression. Prior to FRET-FLIM analysis, the co-localisation between GFP-MRF7 and RFP-XIK tail was assessed by taking a confocal still image as represented in panels (a) to (c). All scalebars = 5µm.
The same cell then underwent FLIM analysis; the result is shown in panel (d). The greyscale image on the left-hand side displays the raw FLIM data. The pseudo-coloured lifetime heatmap shown on the right-hand side of the panel indicates the distribution of lifetimes within the imaged area. Red corresponds to lower lifetimes, whereas blue pixels correspond to higher lifetime values.

interacting and that the interaction could begin/happen in the cytoplasm. On the contrary, no lifetime reduction was registered between control cells expressing GFP-ΔMRF7 (τ=2.4±0.1 ns) and cells co-expressing GFP-ΔMRF7 and RFP-XIK tail (τ=2.4±0.1 ns, Fig.5.8a-b). GFP-ΔMRF7 does not appear to interact with RFP-XIK tail on Golgi (t(0), df=171, P>0.999, Fig.5.8a), nor in the cytoplasm (t(0), df=23, P>0.999, Fig.5.8b).

FRET efficiencies reported in Table 5.2 indicate that a $\Delta\tau$ = 0.2 ns corresponds to a FRET efficiency of 8.7% for the GRIP-GFP + RFP-ARL1 pair, while a $\Delta\tau$ = 0.1 ns corresponds to a 4.2% efficiency for GFP-MRF7 + RFP-XIK tail. This could indicate a greater distance in the interaction between GFP-MRF7 and RFP-XIK tail than in GRIP-GFP and RFP-ARL1; the estimated distances in Table 5.2 appear to confirm this consideration.

Altogether, these results confirm that the predicted myosin binding domain DUF593 mediates the interaction between MRF7 and myosin XI-K tail. Moreover, the interaction between MRF7 and XI-K can occur in the cytoplasm, resulting in XI-K recruitment to the Golgi. Results do not exclude the possibility that the complex may shuttle on and off the Golgi.

FRET pair	τ_{DA}**(ns)**	τ_{D}**(ns)**	E_{FRET} **(%)**	r**(nm)**
GFP-MRF7 + RFP-XIK tail	2.3±0.1	2.4±0.1	4.2	9.1
GRIP-GFP + RFP-ARL1	2.1±0.1	2.3±0.1	8.7	7.9

Table 5.2: FRET efficiencies and intermolecular distances determined by FLIM. τ_{DA} indicates the lifetime of the donor in presence of the acceptor ±*SD*, whilst τ_{D} indicates the lifetime of the donor in absence of the acceptor ±*SD*. FRET efficiencies (E_{FRET}) and distance between donor and acceptor (r) for interacting protein pairs were calculated according to the equations provided in Section2.5.2.

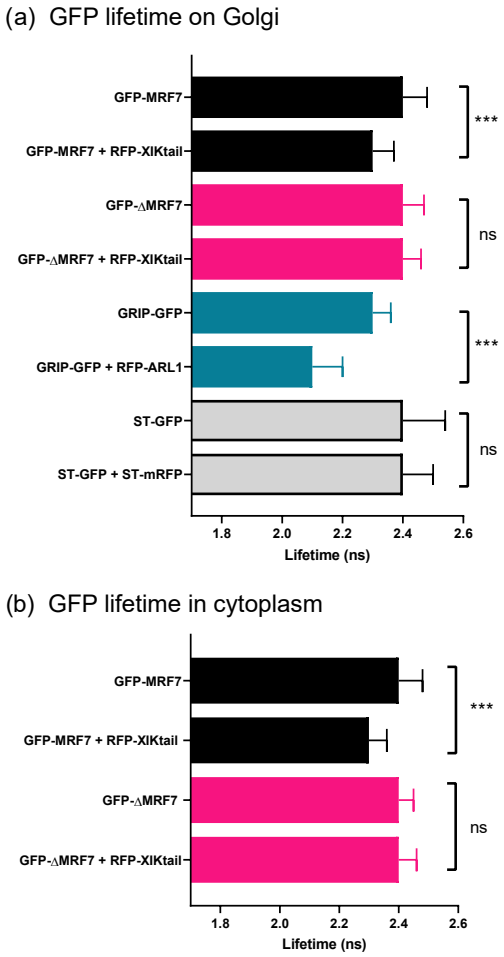

Figure 5.8: FRET-FLIM analysis of RFP-XIK tail interaction with full-length and truncated MRF7. Panel **(a)** compares GFP lifetime values measured on the Golgi membrane between control and co-expressing samples. ST-GFP and ST-mRFP constitute a Golgi-specific negative control. Interaction of the Golgi-localised GRIP-GFP and RFP-ARL1 proteins was previously decribed in literature (Osterrieder et al., 2009). Two-tailed Student's t-test indicates interaction between GFP-MRF7 and RFP-XIK tail (t(9.413), df=199, P<0.001) and between GRIP-GFP and RFP-ARL1 (t(19.27), df=236, P<0.001). No interaction was detected between GFP-ΔMRF7 and RFP-XIK tail (t(0), df=171, P>0.999) and between ST-GFP and ST-mRFP (t(0), df=307, P>0.999). Panel **(b)** compares GFP lifetime values measured in the cytoplasm. Interaction was detected between GFP-MRF7 and RFP-XIK tail (t(3.916), df=29, P=0.0005) but not between GFP-ΔMRF7 and RFP-XIK tail (t(0), df=23, P>0.999). *** indicates P values <0.001. ns indicates non-significant differences. Means ± *SD* are reported in the histograms.

5.2.4 Effects of MRF7 expression on MYA1 and XI-A tail subcellular localisation

FRET-FLIM confirmed the DUF593-dependent interaction between MRF7 and XI-K tail. Although other myosins were not detected in mass spectrometry analysis as potential MRF7 interactors, it is known that some class XI myosins other than XI-K can influence Golgi movement (Prokhnevsky et al., 2008; Peremyslov et al., 2008; Sparkes et al., 2008; Avisar et al., 2009) and that the myosins and myosin receptors network is highly redundant (Kurth et al., 2017). To test whether the MRF7-dependent relocation of myosin XI-K to Golgi is specific to just myosin XI-K, MRF7 was co-expressed with myosin MYA1 and XI-A tails (Avisar et al., 2009) and Golgi localisation was quantified. The choice of MYA1 and XI-A tails was based on the fact that the former was implicated in Golgi movement and that the GT2 domain within its tail was shown to localise to Golgi (Li and Nebenführ, 2007; Avisar et al., 2009), whereas the latter does not appear to have any detectable effects on Golgi dynamics (Avisar et al., 2009).

In the absence of MRF7, MYA1 and XI-A tails are distributed in the cytoplasm and, occasionally, on puncta (Avisar et al., 2009). Co-expression of GFP-MRF7 with RFP-MYA1 tail leads to a partial significant redistribution of RFP-MYA1 tail from the cytoplasm to the Golgi (Fig.5.9a, P=0.0083, n=20, Fig.5.9a). Although not significant, the presence of RFP-MYA1 tail appears to begin to stabilise GFP-MRF7 on Golgi: 18% of Golgi display GFP-MRF7 in the absence of RFP-MYA1 tail, percentage which increases to 44% in the presence of MYA1 (Fig.5.9a, P=0.11, n=20).

No significant differences in GFP-MRF7 or myosin XI-A tail localisation were detected upon co-expression of the two proteins; the average percentage of MRF7 on Golgi does not appear to change before and after co-expression with myosin XI-A (Fig.5.9b, n=20, P=0.7832) and myosin XI-A tail remains cytoplasmic despite co-expression with GFP-MRF7 (Fig.5.9b, n=20, P>0.9999).

Interestingly, the fold increase of GFP-MRF7 localisation on Golgi is identical upon co-expression with myosins XI-K and MYA1 (2.4, Tab.5.3). Altogether, these data suggest that myosins and myosin receptors can have a mutual effect in influencing each other's localisation. In particular, GFP-MRF7 appears to cause a relocalisation of myosins involved in regulation of Golgi dynamics (XI-K and MYA1 in this instance). *Viceversa*, the presence of myosin tails involved in regulation of Golgi movement, in this case significant after expression of XI-K, appears to stabilise MRF7 localisation to the Golgi. No such effect was observed upon co-expression of GFP-MRF7 and RFP-XIA tail, a myosin not involved in regulating Golgi movement (Avisar et al., 2009).

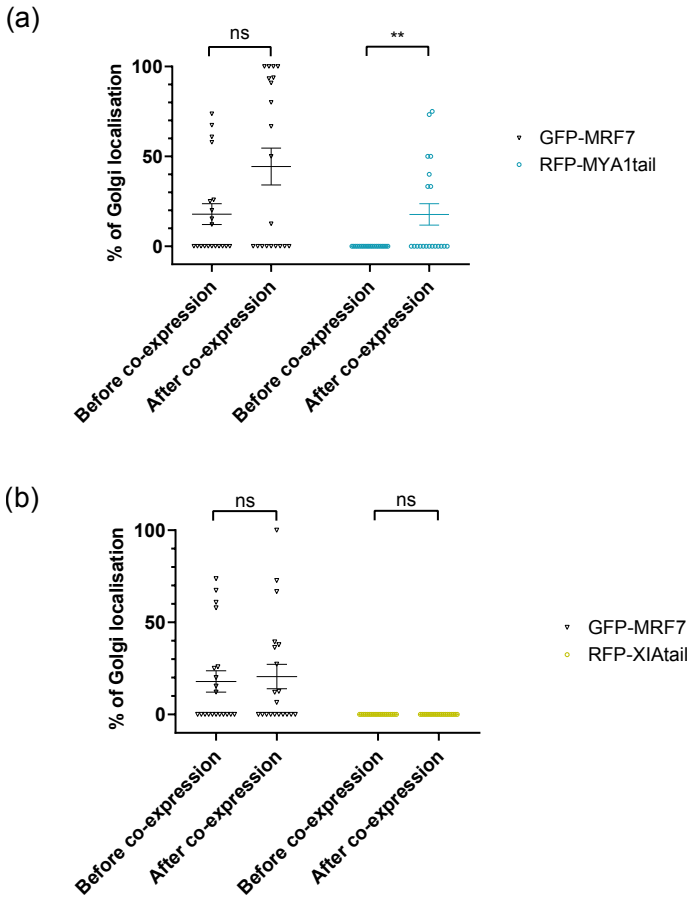

Figure 5.9: Co-localisation study of GFP-MRF7, RFP-MYA1 tail and RFP-XIA tail in transiently transfected tobacco leaf epidermis. Quantification of the co-localisation between GFP-MRF7 and RFP-MYA1tail (panel (a)) and GFP-MRF7 and RFP-XIAtail (panel(b)) before and after co-expression in tobacco leaves. Data shown are the results of two independent experiments (n=20). Effects of co-expression were tested by Mann-Whitney U test. ** indicates $P<0.01$, ns indicates non-significant differences. Each data point represents one cell; values from individual cells are represented as a scatterplot. Error bars indicate mean ± *SEM*.

	% MRF7 localisation on Golgi		
	- Myosin	**+ Myosin**	**fold increase**
XI-K	26%	62%	2.4
MYA1	18%	44%	2.4
XI-A	18%	21%	1.1

Table 5.3: Percentage of MRF7 localisation to the Golgi in the presence and absence of myosin XI-K, MYA1 and XI-A. Average percentage of Golgi per cell displaying GFP-MRF7 before and after co-expression with myosin tails. Fold increase was calculated as the ratio between the "+ Myosin" and "- Myosin" values.

	% myosin localisation on Golgi	
	- GFP-MRF7	**+ GFP-MRF7**
XI-K	0%	36%
MYA1	0%	18%
XI-A	0%	0%

Table 5.4: Percentage of myosin XI-K, MYA1 and XI-A Golgi localisation in the presence and absence of MRF7. Average percentage of Golgi per cell displaying a myosin tail before and after co-expression with GFP-MRF7.

5.3 Discussion

5.3.1 Myosin XI-K tail collocates to Golgi in presence of full-length MRF7

Mass spectrometry data indicated that MRF7 can interact with myosin XI-K *via* its DUF593 domain. Re-localisation of myosin XI-K tail in presence of MRF7 but not of ΔMRF7 appeared to confirm proteomics data. Subcellular re-localisation of a protein in presence or absence of an interactor is not uncommon and is often used to regulate its function by spatially confining it to a specific compartment. An example are the abscissic acid (ABA) responsive transcription factors *At*BLH1 and *At*KNAT3 (Hackbusch et al., 2005; Kim et al., 2013b). At low ABA levels, BLH1 localises to the nucleus and promotes transcription of low levels of the *At*ABI3 gene, while KNAT3 is continuously exported from the nucleus to the cytoplasm by exportins. At higher ABA levels more BLH1 protein is produced, promoting KNAT3 nuclear localisation by masking its nuclear export signal (NES) upon heterodimerisation (Kim et al., 2013b). The KNAT3-BLH1 heterodimer has higher affinity for the ABI3 gene promoter than BLH1 alone and stimulates ABI3 transcription (Staneloni et al., 2009; Kim et al., 2013b).

Use of the Golgi marker ST-CFP confirmed that expression of full-length GFP-MRF7 triggers RFP-XIK tail re-localisation to the Golgi surface (Fig.5.6). One of the major struggles associated with studying myosins and myosin receptors consists in being able to link their role on organelle dynamics with their localisation. Therefore this finding represents an important starting point to untangle myosin and myosin receptors localisation to cargo organelles. Full-length myosin XIK-YFP was occasionally detected on Golgi upon expression at physiological levels in *A.thaliana* midveins (Peremyslov et al., 2012). However, XIK-YFP was mainly found to overlay with actin or the ER rather than with spheroid organelles such as Golgi or peroxisomes (Peremyslov et al., 2012). Moreover, despite being shown to interact *in vitro* (Kurth et al., 2017), MyoB1-GFP only shows a partial co-localisation with full-length myosin

XI-K puncta but doesn't appear to target the myosin to any known structure (Peremyslov et al., 2013). This could indicate that the co-localisation (and perhaps interaction) of myosins with myosin receptors on organelles could happen extremely fast and perhaps at levels non detectable with standard confocal microscopy.

Aside from the clear effect that GFP-MRF7 produces on XI-K tail localisation, RFP-XIK tail also appears to stabilise MRF7 on Golgi. Moreover, over-expression of RFP-XIK tail leads to a gradual disappearance of the typical MyoB/MRF7 puncta from the cytoplasm (Results section, Fig.5.5a-c and Fig.5.6a-d). This phenomenon could be due to a number of reasons. On one hand, it could be a consequence of the effects of non functional XI-K tail on the actin cytoskeleton. In Chapter 3, GFP-MRF7 was shown to move at high speeds (4 µm/s, Fig.3.4) on the actin and that depolymerisation of actin tracks by Latrunculin B led to a more diffuse GFP-MRF7 cytoplasmic localisation. Previous works have also shown that the integrity of the actin cytoskeleton relies on the presence of functional myosins (Murrell and Gardel, 2012; Vogel et al., 2013; Cai et al., 2014). In this sense the expression of a dominant negative mutant of myosin XI-K could cause a mislocalisation of the MRF7 puncta moving on the actin, but not of the GFP-MRF7 fraction already on Golgi, by interfering with the dynamics of the actin tracks (Cai et al., 2014).

Another possibility could be related to the GFP-MRF7 puncta origin; although the nature of the MyoB puncta is so far unclear, previous works have described their membranous nature (Peremyslov et al., 2013). The presence of the ^{320}YxxΦ^{324} motif within the MRF7 sequence could suggest a myosin-dependent formation and budding of the MyoB compartment from the Golgi. Over-expression of a non motile myosin such as RFP-XIK tail could impair this process and prevent the MyoB/MRF7 compartment from "detaching" from Golgi. This could also explain why the puncta are not seen when expressing GFP-ΔMRF7.

In this study, I demonstrated that the use of dominant negative tail constructs is a powerful tool in defining their target compartment, under

the conditions that such constructs are co-expressed with their receptor or adaptor protein.

5.3.2 The DUF593 domain mediates the interaction between MRF7 and XI-K tail

FRET-FLIM has previously been employed to detect *in vivo* protein-protein interactions on Golgi in plant cells (Osterrieder et al., 2009; Schoberer et al., 2013). Results in this study confirm a DUF593-dependent *in vivo* interaction between GFP-MRF7 and RFP-XIK tail; this is consistent with observations that DUF593 mediates the interaction between *At*MyoB2-GFP and myosin XI-K (Peremyslov et al., 2013) and between *Nt*RISAP and *Nt*MYOXIpt (Stephan et al., 2014). The conservation of DUF593 in all land plants (Holding et al., 2007; Peremyslov et al., 2013; Stephan et al., 2014) suggests a generalised myosin-binding role for DUF593 in plant cells.

A consistent, although relatively small, GFP lifetime reduction was registered upon co-expression of GFP-MRF7 with RFP-XIK tail ($\Delta\tau$ = 0.1 ns). It is not unusual to sometimes register such a small reduction of the donor's lifetime: this could depend on a number of factors, one of which is the spatial separation between the donor and the acceptor (Osterrieder et al., 2009; Schoberer et al., 2013; Kriechbaumer et al., 2015; Ahmed et al., 2019). FRET efficiencies calculated from the GFP lifetime values in the presence and absence of the quencher can help draw some conclusions regarding the spatial separation between two fluorophores. Efficiency of the energy transfer is calculated by applying the equation in 2.5.2; for non interacting pairs, such as the negative control or the ΔMRF7 and XI-K tail combination, the efficiency equals to zero given that τ_D=τ_{DA}. Efficiency is a function of the distance between the donor and the quencher (Förster, 1948; Willem Borst and Visser, 2010). Hence, as reported in Table 5.2, a smaller $\Delta\tau$ appears to correspond to a lower energy transfer efficiency and to a larger spatial separtion. The estimated distance values calculated in Tab.5.2 indicate that the GFP-MRF7 and RFP-XIK pair are slightly farther apart than the GRIP-GFP and RFP-ARL1 pair. A

similar effect was observed for the FRET pair GMII-GFP and MNS1-RFP, two *A.thaliana* Golgi-localised enzymes responsible for glycan processing (Schoberer et al., 2013): a $\Delta\tau = 0.1$ ns in the donor lifetime corresponded to a $\sim 5\%$ efficiency.

Comparison of GFP-MRF7 lifetime measurements in the presence and absence of RFP-XIK tail on Golgi and in the cytoplasm suggests that the interaction simultaneously takes place in both compartments. Given that MRF7 is a predicted soluble protein and that not all of the Golgi in a cell display GFP-MRF7 and RFP-XIK tail (see section 5.2.2), it is tempting to speculate that the two proteins could perhaps interact in the cytoplasm, resulting in XI-K recruitment to Golgi *via* the MRF7 Golgi targeting region. It is unclear how certain Golgi bodies appear to be selected by MRF7 and XI-K tail.

GRIP-GFP and RFP-ARL1, and ST-GFP and ST-mRFP have been previously tested for FRET-FLIM experiments on Golgi-localised proteins (Osterrieder et al., 2009). Although the system could correctly detect an interaction, the GRIP-GFP control lifetime ($\tau_{\mathrm{D}} = 2.3$ ns) and lifetime reduction upon RFP-ARL1 co-expression ($\Delta\tau = 0.2$ ns) slightly differs from that reported in the literature ($\tau_{\mathrm{D}} = 2.5$ ns; $\Delta\tau = 0.4$ ns). Unlike this study, previous FRET-FLIM measurements (Osterrieder et al., 2009) have been carried out on a 2-photon system and data analysis performed with a different version of the same software. Moreover, the χ^2 values (goodness of fit to the experimental data points) considered satisfactory to take into account the measured lifetime values are slightly different to the ones used in this study. It is possible that a combination of differences in the system set up and user biases during data analysis could influence the average lifetime. The same conclusions can be drawn for the negative control. Nevertheless, although the registered raw values are different from those reported in the literature (Osterrieder et al., 2009), the system appears to be correctly detecting an interaction or non-interaction between protein pairs.

Lastly, mass spectrometry data also indicated that myosin XI-K can interact with MRF7 and MRF7S, but not with ΔMRF7: this could

suggest that the presence of the first conserved motif (ExxxERxA, Fig.3.2) within DUF593 is not essential for myosin interaction, but that binding to XI-K tail depends on the presence of the second conserved motif (LxxxKxxxxExxQ, Fig.3.2). Future FRET-FLIM analysis will help shed light on the role of the conserved motifs within DUF593.

Collectively, these results indicate that MRF7 interacts with myosin XI-K tail through its DUF593 domain and that the interaction can take place both in the cytoplasm and on the Golgi membrane. Moreover, FRET-FLIM has confirmed to be an excellent technique to validate and complement proteomics data (Kriechbaumer et al., 2015).

5.3.3 Effects of MRF7 on other myosin XI tails localisation

The finding that XI-K tail can be targeted to Golgi in the presence of its receptor represents an important step forward in understanding how myosins localise to target organelles. Although no myosins other than XI-K were detected in mass spectrometry analysis, the specificity of the MRF7 effect on XI-K tail localisation was tested by expressing other myosin tails in the presence and absence of the receptor.

No significant effect was observed upon co-expression of MRF7 with XI-A tail: the percentage of MRF7 on Golgi remains constant before and after co-expression and XI-A tail is solely cytoplasmic. These results are consistent with the observation that myosin XI-A tail is not involved in regulation of Golgi movement in tobacco leaves (Avisar et al., 2009).

The effects of the co-expression of MRF7 and MYA1 tail appear to be more complex. MRF7 triggers a significant re-localisation of MYA1 tail from the cytoplasm to Golgi. Such effect is consistent with the role that MYA1 tail exerts on Golgi movement (Prokhnevsky et al., 2008; Avisar et al., 2009; Peremyslov et al., 2010a) and with the finding that the GT2 domain in MYA1 tail localises to Golgi (Li and Nebenführ, 2007). Unlike XI-K, MYA1 tail expression does not lead to a significant increase of MRF7 localisation to the Golgi. This could be due to the different sample size of the two co-expression datasets, MRF7 with XI-K (n=30, total from three experiments) and MRF7 with MYA1 (n=20, total from two

experiments). One further experiment is required to confirm whether MYA1 and XI-K have similar effects on MRF7 Golgi localisation. This is intriguing considering that XI-K and MYA1 result in a 2.4 fold increase in MRF7 Golgi localisation.

Taken together, these results suggest that MRF7 triggers the localisation to Golgi of myosins involved in the regulation of Golgi movement (XI-K and MYA1). MRF7 Golgi localisation only increases significantly upon XI-K co-expression. Further experiments with other myosins involved in Golgi dynamics (such as XI-2, XI-C, XI-E and XI-I) could help shed more light regarding the specificity of MRF7 interaction.

Chapter 6

General discussion

6.1 General discussion

6.1.1 Summary

Work described in this dissertation aimed at generating the molecular tools to specifically control plant organelle movement and positioning. Here MRF7, a Golgi-localised myosin receptor from the *A.thaliana* MyoB family (Holding et al., 2007; Peremyslov et al., 2013) was used as a case study to characterise myosin recruitment in plant cells.

Chapter 3 investigated the mechanisms of MRF7 association to the Golgi. Like other MyoB receptors, wild-type MRF7 localises to puncta moving in straight lines in the cell cytoplasm; unlike other MyoB receptors though, MRF7 was observed to collocate to the Golgi. Thus, MRF7 is effectively the first *A.thaliana* MyoB receptor to localise to a specific compartment. Due to lack of predicted transmembrane domains or signals for lipid post-translational modifications, MRF7 appears to be a soluble protein. In addition, its heterogeneous localisation suggests that it could perhaps cycle on and off the Golgi, although this aspect has not been addressed in this dissertation. Truncation of the last 54 C-terminal amino acids indicated that this region is responsible for MRF7 localisation to the Golgi.

Localisation of MRF7 to Golgi suggests that it could be involved in regulating its dynamics. In Chapter 4, Golgi movement was analysed in the presence and absence of three MRF7 constructs: GFP-MRF7, GFP-MRF7S and GFP-ΔMRF7. To investigate whether the effects of these fusions are specific for Golgi, peroxisomes were also tracked. Results indicated that GFP-MRF7 does not influence Golgi and peroxisome speed, whereas both GFP-MRF7S and GFP-ΔMRF7 increase Golgi and peroxisome movement. The extent of the relative increase in movement upon expression of GFP-MRF7S or GFP-ΔMRF7 appears to correlate with the progressive shortening of the DUF593 domain; movement in the absence of DUF593 (GFP-ΔMRF7) is higher than with the partially truncated DUF593 domain (GFP-MRF7S).

The effects of the MRF7 DUF593 N-terminal truncations on Golgi

and peroxisome movement suggest that the protein could be involved in recruiting a myosin. Chapter 5 investigated the ability of MRF7 to bind and recruit a myosin to the Golgi. Co-immunoprecipitation followed by mass spectrometry was carried out on protein extracts from *A.thaliana* plants over-expressing GFP-MRF7, GFP-MRF7S and GFP-ΔMRF7 respectively. Comparison of the mass spectrometry results from the three constructs highlighted that full-length GFP-MRF7 binds to myosin XI-K, whereas GFP-ΔMRF7 does not appear to interact with myosin XI-K. This result suggested that the DUF593 domain is responsible for myosin binding, as observed for other MyoB receptors (Peremyslov et al., 2013). Myosin XI-K tail relocates from the cytoplasm to the Golgi in the presence of GFP-MRF7, linking for the first time a myosin to a specific compartment. The interaction between myosin XI-K tail and MRF7 was also verified *in vivo* through FRET-FLIM experiments in tobacco leaf epidermal cells.

6.1.2 Proposed model for the effects of MRF7 on organelle movement

Different MRF7 fusions were shown to lead to differential effects on Golgi and peroxisome dynamics. GFP-MRF7 does not influence Golgi and peroxisome speed, whereas GFP-MRF7S and GFP-ΔMRF7 progressively increase both compartments' movement (Chapter 4). Expression of full-length MRF7 triggers the relocation of myosin XI-K from the cytoplasm to the Golgi and FRET-FLIM results have also highlighted that MRF7 binds to myosin XI-K tail *in vivo*; this confirms the role of MyoBs as myosin receptors/adaptors, and that myosin binding is dependent on the presence of the DUF593 domain. In the light of these results, the model presented in Fig.4.10 can be implemented as follows (Fig.6.1).

As in the previous model, MRF7 is represented as an adaptor protein rather than as a receptor (Fig.6.1a). MRF7 might preferentially bind to myosin XI-K to regulate Golgi dynamics; other MyoBs/other myosin receptors are present on the Golgi and bind to different myosins, but

those motors could be kept in an inactive form if the MRF7/XI-K binding is intact. Note that the interaction between MRF7 and XI-K is represented on the Golgi for simplicity, but FRET-FLIM data indicated that MRF7 and XI-K can also interact in the cytoplasm (Section 5.2.3). It is possible that MRF7 interacts with the cytoplasmic pool of XI-K resulting in recruitment to the Golgi.

Deletion of DUF593 (Fig.6.1b) prevents MRF7 from binding to myosin XI-K; this could "encourage" the Golgi to rely on a different MyoB receptor to direct its movements. The increase in Golgi speed could be the result of two possible mechanisms. The first would involve recruitment of XI-K by another MyoB receptor on the Golgi; although the alternative MyoB is represented in the figure as binding to a different myosin for simplicity (light blue, Fig.6.1b), this mechanism is not implausible given that XI-K was shown to bind to multiple MyoB proteins (Kurth et al., 2017). If the levels of the second MyoB receptor on the Golgi are higher than those of MRF7, then more XI-K motors could be recruited to the organelle, triggering a faster movement of Golgi. A study on the relationship between motor copy number and movement of organelles was carried out on lipid droplets of *D.melanogaster* (Shubeita et al., 2008; Arora et al., 2016). Kinesin-1 moves *D.melanogaster* lipid droplets towards the plus end of microtubules; whilst *in vitro* analysis indicated that more motors recruited corresponds to faster lipid droplets, results *in vivo* suggested that the speed is independent on the number of Kinesin-1 copies (Shubeita et al., 2008). Further works have identified a cofactor, "Halo", which binds to Kinesin-1 and activates it (Arora et al., 2016); Halo is transiently expressed and when levels exceed a certain threshold, lipid droplets start moving towards the plus-end of microtubules. Halo was shown not to interfere with the number of Kinesin-1 motors present on the lipid droplets (Arora et al., 2016). Although this process might work differently for plants and especially for myosin motors, it sets the precedent that the number of myosin molecules on the surface of an organelle could differentially regulate speed.

Golgi movement increases upon GFP-MRF7S and GFP-ΔMRF7 expression and the relative increase is larger following the progressive

shortening of the DUF593 domain. Given the presence of four of the eight conserved residues within the DUF593 domain, GFP-MRF7S could perhaps still bind to myosin XI-K, although in a less efficient manner (Fig.3.2). In this scenario, a co-existence of the mechanims depicted in Fig.6.1a-b is possible upon GFP-MRF7S expression. Complete absence of DUF593 could instead determine a full switch to the model in Fig.6.1b. Interestingly, MRF7 affected MYA1 Golgi localisation. Perhaps MRF7 affinity for XI-K and MYA1 is controlled through specific residues in DUF593; removal of the first four conserved residues prefers MYA1 over XI-K binding.

A second scenario would imply that other MyoBs present on the Golgi membrane are not recruiting XI-K, but other myosins (light blue, Fig.6.1b). A recent study linked myosin tissue expression and velocity (Haraguchi et al., 2018). It suggested that myosins could be grouped into three main speed categories: high, medium and low speed, which were shown to correspond to pollen specific, ubiquitous and other types of localisation respectively (Haraguchi et al., 2018). Transient expression of myosin tails in tobacco cells showed that Golgi movement is best inhibited by myosin XI-1, XI-2, XI-E, XI-C, XI-I and XI-K tails over-expression (Avisar et al., 2009). These six myosins are distributed within the three speed categories, and therefore it is not implausible that an alternative MyoB receptor on Golgi could recruit a myosin faster than XI-K. Good candidates are myosin XI-2 (MYA2) and XI-1 (MYA1) which, as XI-K, are ubiquitously expressed in all tissues but appear to be faster than XI-K (Haraguchi et al., 2018).

Although the MRF7 fusions influence peroxisome dynamics similarly to the effects they have on Golgi, myosin tails co-expression experiments (Sections 5.2.2 and 5.2.4) did not seem to trigger relocalisation of either myosins or MRF7 to peroxisomes. Further studies are needed to untangle the role of the MRF7 constructs on peroxisome dynamics; thus far it appears as if the effects of MRF7 on peroxisomes are a consequence of its effects on Golgi movement (Fig.4.11). This could be due to indirect control through organelle tethering (Section 1.7); Golgi attached to the

ER may pull the ER which, in turn, affects the movement of other organellles tethered to it. Peroxisome tethering to the ER is implied through close positioning (Barton et al., 2013).

6.1.3 Origin and role of the MRF7 puncta

In light of the published work and the results presented in this dissertation, it is still unclear what role the MRF7/MyoB (or MadA-B) puncta may play. Because of the high average speeds ($\sim$ 4 µm/s) reached by the MyoB compartment compared to average speeds reached by organelles (Peremyslov et al., 2015), it was suggested that perhaps the MyoB compartment could be involved in generating cytoplasmic streaming (Peremyslov et al., 2013; Peremyslov et al., 2015; Kurth et al., 2017). In this scenario (Fig.6.2b), the MyoB vesicles move actively on the actin cytoskeleton generating the stream and triggering passive movement of organelles. Although this model cannot be completely excluded, mathematical predictions based on *C.corallina* cytoplasmic streaming have shown that this model alone can perhaps not explain fully the movement characteristics associated with plant organelles (Nothnagel and Webb, 1982).

Results provided in this dissertation have shown for the first time an *A.thaliana* MyoB protein localising to a specific organelle, in addition to its more traditional punctate localisation (Chapter 3). Two alternative suggestions for MyoB puncta are depicted in Fig.6.2. The MyoB vesicles could be physically attached or at least reside next to an organelle (Fig.6.2a). They could recruit myosins and move actively on the actin cytoskeleton, in turn moving the organelle to which they are attached to. Another explanation is that the MyoB/MadA-B proteins are directly located on the organelle membrane, recruit a myosin and trigger active movement of the organelle along the actin (Fig.6.2c). Here, the detected puncta moving in straight lines in the cytoplasm might simply be a subdomain of the organelle to which the myosin receptors localise to.

It is not implausible that the effects of the MyoB compartment could, in fact, be a combination of the three models proposed in Fig.6.2. MRF7 was

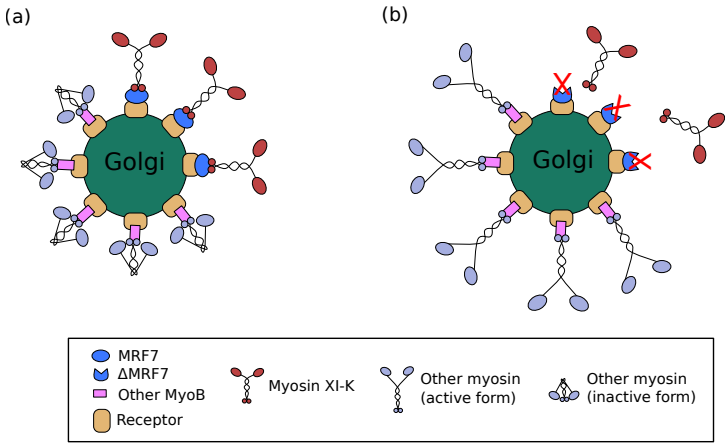

Figure 6.1: Role of MRF7 and ΔMRF7 on Golgi movement.(a) Golgi movement is preferentially directed by binding of MRF7 to myosin XI-K. Other MyoB receptors (pink) could be associated to the Golgi and bind to a myosin (XI-K or other, light blue), which is kept in an inactive form if the MRF7/XI-K binding is intact. (b) Deletion of the DUF593 domain impairs the binding of MRF7 to XI-K; in this scenario the alternative receptor/myosin associated to the Golgi could be responsible for directing Golgi movement.

			Interaction with myosins	
Construct	**On Golgi?**	**Golgi movement?**	**Direct (XI-K)**	**Indirect (MYA1)**
MRF7	✓	x	✓	✓
MRF7S	✓	✓	na	na
ΔMRF7	✓	✓	x	na
MRF7SΔC	x	na	na	na
ΔMRF7ΔC	x	na	na	na

Table 6.1: Summary of localisation, effects on Golgi dynamics and interaction with myosins of the MRF7 constructs used in this study.

shown to localise to both punctate structures and to the Golgi in Chapter 3. The C-terminus of MRF7 contains a YxxΦ motif, traditionally associated with cargoes sorted *via* clathrin coated vesicles (CCVs) (Bonifacino and Traub, 2003). Proteins containing a cytosolic YxxΦ motif bind to the Adaptor Protein-2 (AP-2) complex, specifically to subunit µ2, which links the cargoes to clathrin (Owen et al., 2004). It is tempting to speculate that the motif could be involved in the MRF7 vesicles budding from the Golgi, which are then detected in a beads-on-a-string configuration on the actin cytoskeleton.

Formation of clathrin coated vesicles involves the acto-myosin cytoskeleton (Kaksonen et al., 2006). Depolymerisation of actin with Latrunculin B interfered with, despite not completely abolishing, the number of MRF7 puncta detected (Section 3.2.6), suggesting that LatB could in fact be disturbing puncta budding from Golgi. The role of the puncta thus formed and the mechanisms through which they influence organelle movement is still unclear, and further studies are needed to determine their function. They could be involved in the delivery of Golgi molecules to the cell periphery, driving of cytoplasmic streaming, and so on. Moreover, studies with clathrin inhibitors, such as Pitstop®2 or Concanavalin A (Guo et al., 2015; Nandadasa et al., 2019), could help shed light on whether the MyoB compartment generates from organelle membranes and whether this process is clathrin-dependent.

6.1.4 Interaction with myosin motors

After XI-I, the relocation of myosin XI-K tail from the cytoplasm to the Golgi upon expression of full-length MRF7 (Chapter 5) represents the first example of a myosin XI tail located to a specific compartment (Avisar et al., 2009).

Co-expression experiments with other myosins from class XI, XI-A and MYA-1 respectively, indicated that MRF7 is also able to trigger MYA-1 relocation to the Golgi, although not to the same extent as that observed for XI-K. Localisation of XI-A appeared to be unaffected by the presence of MRF7 (Section 5.2.4). Interestingly, myosins XI-K and

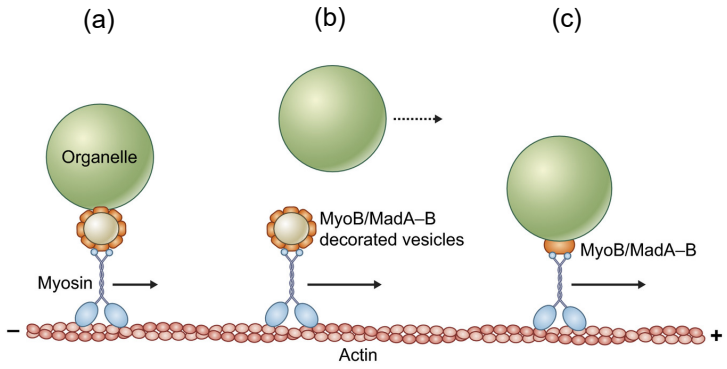

Figure 6.2: Schematic of the possible roles of the MyoB/MadA-B compartment on organelle movement (Perico and Sparkes, 2018). The MyoB/MadA-B compartment moves at higher speeds than that of organelles. Its effect on organelle movement could be explained in three possible ways. (a) The MyoB-decorated vesicles could be located in proximity to, and perhaps physically interact with, subdomains of organelles. Movement of the MyoB vesicles could in turn drag the attached organelle. (b) MyoB/MadA-B compartment is the only compartment actively moving on the actin cytoskeleton and generating the cytoplasmic streaming; this in turn induces passive movement of organelles within the stream (dotted arrow). (c) The MyoB/MadA-B proteins are directly located on the membrane of organelles and recruit myosins directly to induce the organelle's movement. A combination of the three suggested models cannot be excluded.

MYA-1 belong to the same myosin subfamily, whereas XI-A belongs to a different subgroup (Peremyslov et al., 2011). These results fit with the observation that both XI-K and MYA-1 influence Golgi movement when over-expressed in *Nicotiana* species (Avisar et al., 2009), whereas XI-A does not have any apparent effect on the same compartment.

Expression studies of the *A.thaliana* myosin motors have revealed a possible relationship between the speed of certain myosins and their tissue/developmental expression (Haraguchi et al., 2018). The authors divided the myosin motors in fast, medium and low speed. Fast myosins, such as XI-C and XI-E, were shown to mainly be expressed in pollen tubes. This is consistent with the general observation that cytoplasmic streaming reached its highest speeds in tip growing cells (Shimmen, 2007). Myosins such as XI-K and MYA-2 appear to be more ubiquitously expressed in all tissues and developmental stages and are classified as medium speed myosins (Haraguchi et al., 2018).

RNA-seq expression data (Fig.5.3) also suggest a tissue and developmental specificity for MRF7. It is tempting to speculate that MRF7 could perhaps bind to all of the myosins involved in Golgi dynamics; such interaction could be subject to tissue and developmental specificity to determine with which myosin MRF7 will interact with in a certain cell type or tissue.

6.2 Future directions

Work presented in this dissertation identified the molecular mechanisms responsible for MRF7 localisation to the Golgi (Chapter 3), its effects on Golgi and peroxisome dynamics (Chapter 4) and recruitment of myosins to the Golgi (Chapter 5). The following sections discuss possible strategies for further understanding of the MRF7 localisation, function and effects on plant growth and development.

6.2.1 Golgi localisation and targeting information

The MRF7 Golgi targeting information is contained within the last 54 amino acids at the C-terminus (Chapter 3). It could either constitute a Golgi-specific targeting motif, or be a region of interaction with a Golgi-resident protein, which triggers the localisation of MRF7 on that same compartment.

Two predicted conserved motifs have been identified within the MRF7 C-terminal region: ^{320}YxxΦ^{324} and ^{274}KxxxQ^{279}. Although these motifs were in some cases suggested to contribute to the Golgi localisation of certain proteins (Vitale et al., 2002; Gao et al., 2012), further analysis is needed to determine their role on MRF7 localisation. One approach could be substituting critical residues within the motif with amino acids of different steric volumes and net charge (such as alanine) to alter the biophysical properties of the motifs (Gao et al., 2012). Alternatively, the targeting information could be independent from the two conserved motifs: if so, progressive truncations of the C-terminal domain could help narrow down in which region the Golgi-targeting information lies.

Once the exact targeting signal is identified, an interesting application could be to fuse it to a full-length myosin and investigate the effects of directly targeting a myosin to the Golgi and the effects it produces on organelle movement.

6.2.2 Effects of variations of Golgi movement on its subcellular activity

Variations in Golgi (and peroxisome) movement could directly influence its function. The plant Golgi apparatus consitutes the hub for several processes such as secretion, endocytosis, protein glycosylation and synthesis of cell wall polysaccarides. It is not implausible that a direct alteration of Golgi movement could significantly impact on its subcellular roles. For example, correct pausing of Golgi bodies at specific sites on cortical microtubules was shown to be important in delivering cellulose synthase complexes in *A.thaliana* (Crowell et al., 2009).

In the future, monitoring of the effects of different MRF7 fusions on Golgi functions could help shed more light on the relationship between positioning and function. Both biochemical and fluorescence based methods are available to measure secretion in plant cells (Denecke et al., 1990; Zheng et al., 2005; Larson, 2017) and alterations in the cell wall properties could also be investigated, both in terms of physical characteristics and polysaccarides composition.

Similar strategies could be adopted to study how the effects of variations in peroxisome movement could reflect on their functions, such as β-oxidation and phytohormones production.

6.2.3 Effects of organelle movement on plant growth and development

The literature does not lack in studies of the phenotypes derived from knock-outs of myosin and myosin receptor genes (Peremyslov et al., 2010a; Peremyslov et al., 2013; Peremyslov et al., 2015). Nevertheless, it is not clear what the link between movement of certain compartments and plant growth is.

MRF7 was here shown to affect Golgi and peroxisomes movement (Chapter 4). A study of the potential phenotypes associated with knock-out or knock-down of the MRF7 gene could in this sense link the effects of movement with plant growth and development. Previous studies

have highlighted that single knock-outs of MyoB or myosin genes do not, overall, lead to drastic phenotypes (Peremyslov et al., 2010a; Peremyslov et al., 2013; Peremyslov et al., 2015). The only exceptions were knock-out *xi-k*, *xi-2* or *madb1 A.thaliana* lines, which had shorter root hairs (Peremyslov et al., 2013; Peremyslov et al., 2015; Kurth et al., 2017). It is quite likely that given the redundancy of the myosin recruitment network (Kurth et al., 2017), knock-out *mrf7* plants could show none or only a very subtle phenotype. Perhaps a first strategy would consist in looking at the effects on tip growing cells, such as root hair and pollen tubes, as previously carried out for *xi-k* and *xi-2* plants.

More extreme phenotypes on growth and flowering time were observed following multiple knock-outs of myosin genes or myosin receptors. Given that MRF7 was shown to bind to myosin XI-K tail (Chapter 5), it would be interesting to compare the effects of single *xi-k* or *mrf7* knock-outs with a double *xi-k mrf7 A.thaliana* knock-out.

Furthermore, by crossing knock-out *mrf7* lines with *A.thaliana* stable lines expressing a Golgi or peroxisomal marker it will possible to assess the effects on organelle movement and compare those to observations made for over-expressing plants.

6.2.4 Myosin recruitment

MRF7 binding to XI-K through its DUF593 domain is consistent with results obtained from other MyoB receptors (Peremyslov et al., 2013; Stephan et al., 2014). An interesting aspect would be to identify the region within the XI-K tail responsible for binding to MRF7. *A.thaliana* myosin tails contain the DIL and PAL domains, homologous to the *Sc*Myo2p regions responsible for organelle inheritance (Sattarzadeh et al., 2011; Sattarzadeh et al., 2013). Several fluorescent fusions of myosin XI PAL and DIL domains labelled various organelles (Sattarzadeh et al., 2011; Sattarzadeh et al., 2013), perhaps suggesting that such regions could be involved in interaction with myosin receptors on target organelles. Studies of the interaction between MRF7 and XI-K tail PAL and DIL domains could represent a starting point for the identification of

the region of interaction within the myosin.

Another aspect of myosin XI-K recruitment that deserves further characterisation is the composition of the myosin recruitment complex. As previously suggested, MRF7 act like an adaptor protein which link XI-K to a protein stably residing on Golgi. Certainly, examples from yeast and mammals seem to suggest that a scaffold of proteins are necessary to recruit a myosin to a specific organelle (Li and Nebenführ, 2008). Future studies are required to identify other components in the MRF7/XI-K complex.

Ultimately, all the myosin interaction studies in this work were carried out on myosin tails. It would be interesting to see how MRF7 behaves in the presence of a full-length myosin, particularly XI-K.

Appendix A

A.1 Accession numbers

Table A.1 reports the TAIR accession numbers of the *A.thaliana* genes used in this study. For accession numbers of ST Golgi marker (Wee et al., 1998), peroxisome marker (Nelson et al., 2007) and LifeAct (Riedl et al., 2008) refer to the original papers.

Accession number	**Protein encoded**
At2g24140	MRF7
At5g20490	Myosin XI-K
At1g04600	Myosin XI-A
At1g17580	Myosin MYA1
At5g66030	GRIP
At2g24765	ARL1

Table A.1: TAIR accession numbers

A.2 List of Primers

All primers reported in Table A.2 were used for amplification and cloning of full-length and truncated MRF7 fusions from either gDNA or plasmid DNA. Note that cloning of MRF7S and ΔMRF7 was carried out by Dr. Hongbo Gao.

For cloning of myosin XI-K, XI-A and MYA1 tails (Avisar et al., 2009), GRIP-GFP and RFP-ARL1 (Latijnhouwers et al., 2005; Stefano et al., 2006), ST Golgi marker (Wee et al., 1998), peroxisome marker (Nelson et al., 2007) and LifeAct (Riedl et al., 2008) refer to the original papers.

Primer name	**Sequence (5'-3')**
MRF7 Fw	ATGGTAGGAAGAAGCTATAGC
MRF7S Fw	ATGTCTGTGATACTTAGGCTACAA
MRF7S Rv-C	TAGCCAGAAGTAAAGCATTGC
ΔMRF7 Fw	GCTTATAGATGTAAGCTTATGAGTTTG
MRF7 Rv	TCATAGCCAGAAGTAAAGCATT
DUF593 Rv	TCAATGTAAGTCACACTCAAGATTCTTG
MRF7ΔC Rv	TCATCTCTCCTGCTCTAGTCGCTCTACT
attB1(*)	GGGGACAAGTTTGTACAAAAAAGCAGGCTTCCCGCCA
attB2(*)	GGGGACCACTTTGTACAAGAAAGCTGGGTC

Table A.2: List of primers for cloning PCR. Fw: forward primers, Rv: reverse primers for N-terminal fusions, Rv-C: reverse primers for C-terminal fusions. (*) attB1 and attB2 do not indicate primers, but flanking regions on Fw and Rv/Rv-C primers respectively, compatible for Gateway recombination.

A.3 List of Plasmids

Plasmid	Description	Source
pB7RWG2	Gateway® destination vector. C-terminal fusions to RFP.	Ghent University
pB7FWG2	Gateway® destination vector. C-terminal fusions to GFP.	Ghent University
pB7WGR2	Gateway® destination vector. N-terminal fusions to RFP.	Ghent University
pB7WGF2	Gateway® destination vector. N-terminal fusions to GFP.	Ghent University
pDONR207	Gateway® entry clone.	Invitrogen

Table A.3: List of plasmids for Gateway cloning

A.4 Sequences of full-length and truncated MRF7 constructs

A.4.1 DNA sequence of the *A.thaliana* MRF7 gene

The *A.thaliana* MRF7 gene is constituted of two exons and one intron (bold italics font).

ATGGTAGGAAGAAGCTATAGCTTAGAAACGCGTGGATTTGAGT
CCACCACAGATCTTAGAATAGCTCTTTATGAAATGAAAGAAGA
TGTGCAGAGACTTGAGGAAGAGTTGGATGCTGAGAGAGAAGCT
ACTGCTACGTCAGCGAGTGAAGCCATGTCTGTGATACTTAGGC
TACAAGGCGAGAAAGCGTTGCTTGCTATGGAAGCTAGCCAGTA
CAAGAGAATGGTTGAGGAGAGAATGTCTCATGTTGAGTTGTCA
ATGGAGCTTTTGGAGGATTTGAATTACCAGAAAGAAGTTGAAA
TCAAGAATCTTGAGTGTGACTTACATGCTTATAGATGTAAGCT
TATGAGTTTGGGATGGAGTGGACTTGATGATGAGGATTGTATT
AGATTTTGCGATAGATCTCAAACACCGTCTCCAGAACCGAATG
AGACGGTTCTTGTGGAGAAGGGTGTTATAGAGCAGAGCTTGGA
TTCAAGAAGAGATCATGAGAAGAATTTAGATTTGAATTGGGAA
AAGATCAAGAAGGTGGATGAGCAGTTGAAAGAGCTTACAGATT
TTCGAGATTCTGTAAGAGATCAATACAAGATTTTGAAGCAGGA
GACAACTTCTGTTTCTGAAACTAAGAATGGGGAAAAAGGTATG
TGTAAACCTGATTTGTTGGTGAAAAAGATGTCCAAGAAATCAT
TGAAACAGAAAAGAGATAAAAGTATCAAGAGAGATCAAGCACT
AGGAAGTTGTTCTGCAAATGATGCAGAGTATCAAGCCGAGTTA
CAGCGGTTGAGAGAGCGAGTAGAGCGACTAGAGCAGGAGAGA
TGCAACAAAGAGCCAGCTCAAACTAGTGGAGTAAGTCAAGAAA
ATATGAATCTGCAGAGAAAATCAGAAGAAGAGTTAAGTTCTAT
GCAATCTGCAATGTTTAGTTATGACTCAGCTATTGTTTCTGTT
CAAGAG***GTATGGTAAAATTAACTTCTTTCACTAAATTTT***
AGATAGTTCTTAAGTACTAACAAATCTTGGCATGTACA
TTGAAACAGGCAATGCTTTACTTCTGGCTATGA

A.4.2 Amino acidic sequences of full-length and truncated MRF7 constructs

MRF7

MVGRSYSLETRGFESTTDLRIALYEMKEDVQRLEEELDAEREATAT
SASEAMSVILRLQGEKALLAMEASQYKRMVEERMSHVELSMELLED
LNYQKEVEIKNLECDLHAYRCKLMSLGWSGLDDEDCIRFCDRSQT
PSPEPNETVLVEKGVIEQSLDSRRDHEKNLDLNWEKIKKVDEQLKE
LTDFRDSVRDQYKILKQETTSVSETKNGEKGMCKPDLLVKKMSKK
SLKQKRDKSIKRDQALGSCSANDAEYQAELQRLRERVERLEQERCN
KEPAQTSGVSQENMNLQRKSEEELSSMQSAMFSYDSAIVSVQEAML
YFWL

MRF7S

MSVILRLQGEKALLAMEASQYKRMVEERMSHVELSMELLEDLNYQ
KEVEIKNLECDLHAYRCKLMSLGWSGLDDEDCIRFCDRSQTPSPEP
NETVLVEKGVIEQSLDSRRDHEKNLDLNWEKIKKVDEQLKELTDF
RDSVRDQYKILKQETTSVSETKNGEKGMCKPDLLVKKMSKKSLKQ
KRDKSIKRDQALGSCSANDAEYQAELQRLRERVERLEQERCNKEP
AQTSGVSQENMNLQRKSEEELSSMQSAMFSYDSAIVSVQEAMLYF
WL

ΔMRF7

RCKLMSLGWSGLDDEDCIRFCDRSQTPSPEPNETVLVEKGVIEQSL
DSRRDHEKNLDLNWEKIKKVDEQLKELTDFRDSVRDQYKILKQET
TSVSETKNGEKGMCKPDLLVKKMSKKSLKQKRDKSIKRDQALGSC
SANDAEYQAELQRLRERVERLEQERCNKEPAQTSGVSQENMNLQR
KSEEELSSMQSAMFSYDSAIVSVQEAMLYFWL

MRF7ΔC

MVGRSYSLETRGFESTTDLRIALYEMKEDVQRLEEELDAEREATAT
SASEAMSVILRLQGEKALLAMEASQYKRMVEERMSHVELSMELLED
LNYQKEVEIKNLECDLHAYRCKLMSLGWSGLDDEDCIRFCDRSQT

PSPEPNETVLVEKGVIEQSLDSRRDHEKNLDLNWEKIKKVDEQLKE
LTDFRDSVRDQYKILKQETTSVSETKNGEKGMCKPDLLVKKMSKK
SLKQKRDKSIKRDQALGSCSANDAEYQAELQRLRERVERLEQ

MRF7SΔC

MSVILRLQGEKALLAMEASQYKRMVEERMSHVELSMELLEDLNYQ
KEVEIKNLECDLHAYRCKLMSLGWSGLDDEDCIRFCDRSQTPSPEP
NETVLVEKGVIEQSLDSRRDHEKNLDLNWEKIKKVDEQLKELTDF
RDSVRDQYKILKQETTSVSETKNGEKGMCKPDLLVKKMSKKSLKQ
KRDKSIKRDQALGSCSANDAEYQAELQRLRERVERLEQ

ΔMRF7ΔC

CKLMSLGWSGLDDEDCIRFCDRSQTPSPEPNETVLVEKGVIEQSLD
SRRDHEKNLDLNWEKIKKVDEQLKELTDFRDSVRDQYKILKQETT
SVSETKNGEKGMCKPDLLVKKMSKKSLKQKRDKSIKRDQALGSCS
ANDAEYQAELQRLRERVERLEQ

DUF593

MVGRSYSLETRGFESTTDLRIALYEMKEDVQRLEEELDAEREATAT
SASEAMSVILRLQGEKALLAMEASQYKRMVEERMSHVELSMELLED
LNYQKEVEIKNLECDLHAYR

A.5 Constructs diagram

Figure A.1 displays the constructs scheme of the N- and C-terminally GFP tagged fusions used in this study. The position of the 35S CaMV is indicated by pink arrows, whereas the GFP tag is represented as a green box. Constructs represented in (b) and (d) were produced by Dr Hongbo Gao prior to the start of the project.

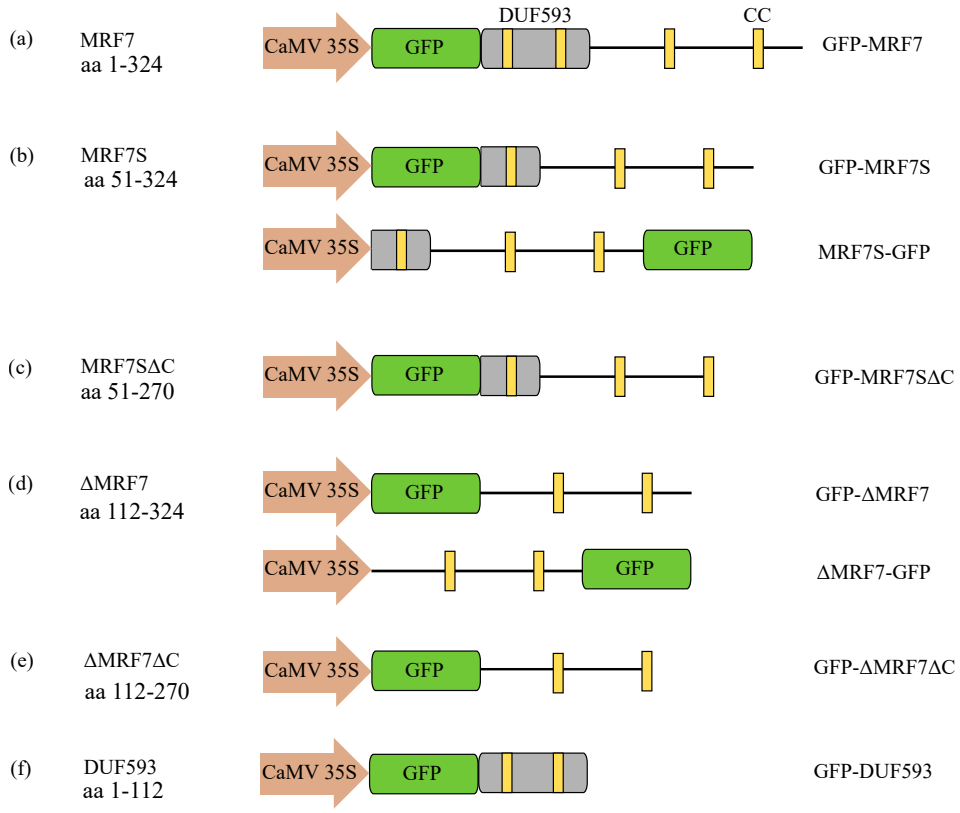

Figure A.1: N- and C-terminally GFP-tagged fusions used in this study. The positions of the CaMV35S promoter and the GFP tag are shown for each construct, represented as a pink arrow and green box respectively. The general domain composition (DUF593 and coiled-coil domains) of the MRF7 constructs is also indicated.

A.6 Mass spectrometry results

Following mass spectrometry analysis, UniProt accession numbers were retrieved for all the highest score hits identified for GFP-MRF7, GFP-MRF7S and GFP-ΔMRF7. Every hit was then classified based on the belonging to a specific protein class with the online tool PANTHER (Protein ANalysis THrough Evolutionary Relationships).
The classifications thus obtained are represented as pie charts in Fig.A.2.

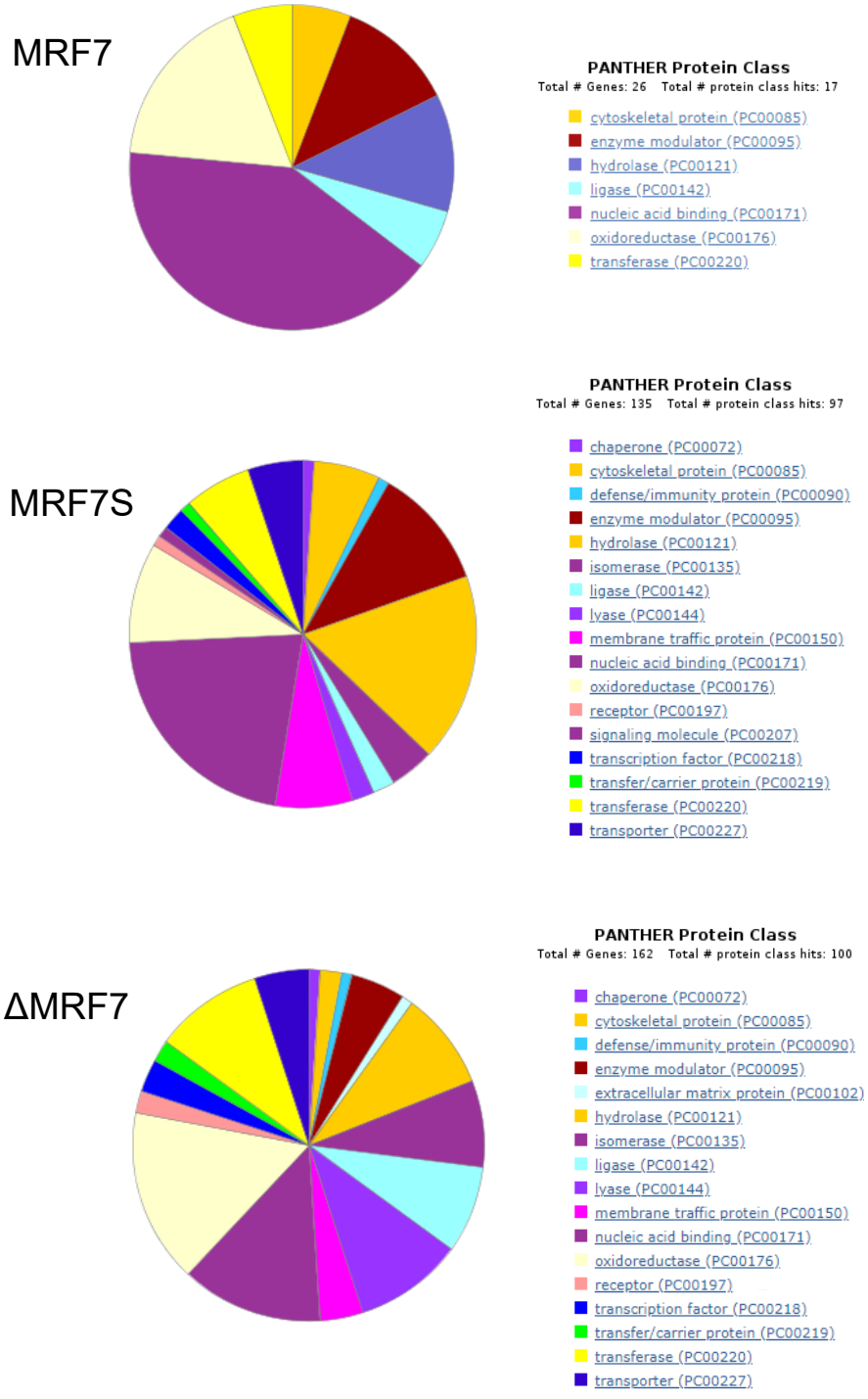

Figure A.2: Pie chart subdivisions of the mass spectrometry top hits for GFP-MRF7, GFP-MRF7S and GFP-ΔMRF7. UniProt accession numbers of potential binding partners of MRF7, MRF7S and ΔMRF7 were retrieved following mass spectrometry analysis. Each hit was then classified into the appropriate protein class using the PANTHER classification system. The total number of genes used to build the charts is reported on the right-hand side of each graph.

Bibliography

Abu-Abied, M., Belausov, E., Hagay, S., Peremyslov, V., Dolja, V., and Sadot, E. (2018). Myosin XI-K is involved in root organogenesis, polar auxin transport, and cell division. *Journal of Experimental Botany*, 69(12):2869–2881.

Ahmed, A. R., Owens, R. J., Stubbs, C. D., Parker, A. W., Hitchman, R., Yadav, R. B., Dumoux, M., Hawes, C., and Botchway, S. W. (2019). Direct imaging of the recruitment and phosphorylation of S6K1 in the mTORC1 pathway in living cells. *Scientific Reports*, 9(1):3408.

Akkerman, M., Overdijk, E. J. R., Schel, J. H. N., Emons, A. M. C., and Ketelaar, T. (2011). Golgi body motility in the plant cell cortex correlates with actin cytoskeleton organization. *Plant and Cell Physiology*, 52(10):1844–1855.

Arora, G. K., Tran, S. L., Rizzo, N., Jain, A., and Welte, M. A. (2016). Temporal control of bidirectional lipid-droplet motion in *Drosophila* depends on the ratio of Kinesin-1 and its co-factor Halo. *Journal of Cell Science*, 129(7):1416–1428.

Avisar, D., Abu-Abied, M., Belausov, E., Sadot, E., Hawes, C., and Sparkes, I. A. (2009). A comparative study of the involvement of 17 *Arabidopsis* myosin family members on the motility of Golgi and other organelles. *Plant Physiology*, 150(2):700–709.

Avisar, D., Prokhnevsky, A. I., Makarova, K. S., Koonin, E. V., and Dolja, V. V. (2008). Myosin XI-K is required for rapid trafficking of Golgi stacks, peroxisomes, and mitochondria in leaf cells of *Nicotiana benthamiana*. *Plant Physiology*, 146(3):1098–1108.

Bajar, B. T., Wang, E. S., Zhang, S., Lin, M. Z., and Chu, J. (2016). A guide to fluorescent protein FRET pairs. *Sensors*, 16(9):1488.

Barton, K., Mathur, N., and Mathur, J. (2013). Simultaneous live-imaging of peroxisomes and the ER in plant cells suggests contiguity but no luminal continuity between the two organelles. *Frontiers in Physiology*, 4(196):1–12.

Boevink, P., Oparka, K., Cruz, S. S., Martin, B., Betteridge, A., and Hawes, C. (1998). Stacks on tracks: The plant Golgi apparatus traffics on an actin/ER network. *Plant Journal*, 15(3):441–447.

Bonifacino, J. S. and Traub, L. M. (2003). Signals for sorting of transmembrane proteins to endosomes and lysosomes. *Annual review of biochemistry*, 72:395–447.

Bradford, M. M. (1976). A rapid and sensitive method for the quantitation of microgram quantities of protein utilizing the principle of protein-dye binding. *Analytical Biochemistry*, 72:248–254.

Braun, M. (1996). Immunolocalization of myosin in rhizoids of *Chara globularis* Thuill. *Protoplasma*, 191(1-2):1–8.

Breuer, D., Nowak, J., Ivakov, A., Somssich, M., Persson, S., and Nikoloski, Z. (2017). System-wide organization of actin cytoskeleton determines organelle transport in hypocotyl plant cells. *Proceedings of the National Academy of Sciences*, 114(32):E5741–E5749.

Cai, C., Henty-Ridilla, J. L., Szymanski, D. B., and Staiger, C. J. (2014). Arabidopsis myosin XI: a motor rules the tracks. *Plant Physiology*, 166(3):1359–1370.

Caplan, J. L., Kumar, A. S., Park, E., Padmanabhan, M. S., Hoban, K., Modla, S., Czymmek, K., and Dinesh-Kumar, S. P. (2015). Chloroplast Stromules Function during Innate Immunity. *Developmental Cell*, 34(1):45–57.

Clough, S. J. and Bent, A. F. (1998). Floral dip: a simplified method for *Agrobacterium*-mediated transformation of *Arabidopsis thaliana*. *Plant Journal*, 16(6):735–743.

Costello, J. L., Castro, I. G., Hacker, C., Schrader, T. A., Metz, J., Zeuschner, D., Azadi, A. S., Godinho, L. F., Costina, V., Findeisen, P., Manner, A., Islinger, M., and Schrader, M. (2017). ACBD5 and VAPB mediate membrane associations between peroxisomes and the ER. *Journal of Cell Biology*, 216(2):331–342.

Crowell, E. F., Bischoff, V., Desprez, T., Rolland, A., Stierhof, Y.-D., Schumacher, K., Gonneau, M., Höfte, H., and Vernhettes, S. (2009). Pausing of Golgi bodies on microtubules regulates secretion of cellulose synthase complexes in *Arabidopsis*. *The Plant Cell*, 21(4):1141–1154.

Deeks, M. J., Fendrych, M., Smertenko, A., Bell, K. S., Oparka, K., Cvrckova, F., Zarsky, V., and Hussey, P. J. (2010). The plant formin *At*FH4 interacts with both actin and microtubules, and contains a newly identified microtubule-binding domain. *Journal of Cell Science*, 123(8):1209–1215.

Denecke, J., Botterman, J., and Deblaere, R. (1990). Protein secretion in plant cells can occur via a default pathway. *Plant Cell*, 2(1):51–59.

Derksen, J., Rutten, T., Lichtscheidl, I. K., de Win, A. H., Pierson, E. S., and Rongen, G. (1995). Quantitative analysis of the distribution of organelles in tobacco pollen tubes: implications for exocytosis and endocytosis. *Protoplasma*, 188(3):267–276.

Ding, X., Jimenez-Gongora, T., Krenz, B., and Lozano-Duran, R. (2019). Chloroplast clustering around the nucleus is a general response to pathogen perception in *Nicotiana benthamiana*. *Molecular Plant Pathology*, 20(9):1298–1306.

Fagarasanu, A., Fagarasanu, M., Eitzen, G. A., Aitchison, J. D., and Rachubinski, R. A. (2006). The peroxisomal membrane protein Inp2p is the peroxisome-specific receptor for the myosin V motor Myo2p of *Saccharomyces cerevisiae*. *Developmental Cell*, 10(5):587–600.

Fagarasanu, M., Fagarasanu, A., Tam, Y. Y. C., Aitchison, J. D., and Rachubinski, R. A. (2005). Inp1p is a peroxisomal membrane protein required for peroxisome inheritance in *Saccharomyces cerevisiae*. *Journal of Cell Biology*, 169(5):765–777.

Förster, T. (1948). Zwischenmolekulare energiewanderung und fluoreszenz. *Annalen der Physik*, 2:55–75.

Foth, B. J., Goedecke, M. C., and Soldati, D. (2006). New insights into myosin evolution and classification. *Proceedings of the National Academy of Sciences*, 103(10):3681–3686.

Gao, C., Yu, C. K. Y., Qu, S., San, M. W. Y., Li, K. Y., Lo, S. W., and Jiang, L. (2012). The Golgi-localized *Arabidopsis* Endomembrane Protein 12 contains both endoplasmic reticulum export and Golgi retention signals at its C terminus. *The Plant Cell*, 24(5):2086–2104.

Gao, H., Metz, J., Teanby, N. A., Ward, A. D., Botchway, S. W., Coles, B., Pollard, M. R., and Sparkes, I. (2016). *In vivo* quantification of peroxisome tethering to chloroplasts in tobacco epidermal cells using optical tweezers. *Plant physiology*, 170(1):263–272.

Goldstein, R. E., Tuval, I., and Van De Meent, J. W. (2008). Microfluidics of cytoplasmic streaming and its implications for intracellular transport. *Proceedings of the National Academy of Sciences of the United States of America*, 105(10):3663–3667.

Golomb, L., Abu-Abied, M., Belausov, E., and Sadot, E. (2008). Different subcellular localizations and functions of *Arabidopsis* myosin VIII. *BMC Plant Biology*, 8(3).

Guimaraes, S. C., Schuster, M., Bielska, E., Dagdas, G., Kilaru, S., Meadows, B. R., Schrader, M., and Steinberg, G. (2015). Peroxisomes, lipid droplets, and endoplasmic reticulum "hitchhike" on motile early endosomes. *Journal of Cell Biology*, 211(5):945–954.

Guo, S., Zhang, X., Zheng, M., Zhang, X., Min, C., Wang, Z., Cheon, S. H., Oak, M. H., Nah, S. Y., and Kim, K. M. (2015). Selectivity

of commonly used inhibitors of clathrin-mediated and caveolae-dependent endocytosis of G protein-coupled receptors. *Biochimica et Biophysica Acta - Biomembranes*, 1848(10):2101–2110.

Hackbusch, J., Richter, K., Muller, J., Salamini, F., and Uhrig, J. F. (2005). A central role of *Arabidopsis thaliana* ovate family proteins in networking and subcellular localization of 3-aa loop extension homeodomain proteins. *Proceedings of the National Academy of Sciences*, 102(13):4908–4912.

Hamada, T., Tominaga, M., Fukaya, T., Nakamura, M., Nakano, A., Watanabe, Y., Hashimoto, T., and Baskin, T. I. (2012). RNA processing bodies, peroxisomes, Golgi bodies, mitochondria, and endoplasmic reticulum tubule junctions frequently pause at cortical microtubules. *Plant and Cell Physiology*, 53(4):699–708.

Hamada, T., Ueda, H., Kawase, T., and Hara-Nishimura, I. (2014). Microtubules contribute to tubule elongation and anchoring of endoplasmic reticulum, resulting in high network complexity in *Arabidopsis*. *Plant Physiology*, 166(4):1869–1876.

Hammer, J. A. and Sellers, J. R. (2012). Walking to work: roles for class V myosins as cargo transporters. *Nature Reviews Molecular Cell Biology*, 13(1):13–26.

Haraguchi, T., Ito, K., Duan, Z., Rula, S., Takahashi, K., Shibuya, Y., Hagino, N., Miyatake, Y., Nakano, A., and Tominaga, M. (2018). Functional diversity of class XI myosins in *Arabidopsis thaliana*. *Plant & cell physiology*, 59(11):2268–2277.

Hashimoto, K., Igarashi, H., Mano, S., Nishimura, M., Shimmen, T., and Yokota, E. (2005). Peroxisomal localization of a myosin XI isoform in *Arabidopsis thaliana*. *Plant and Cell Physiology*, 46(5):782–789.

Hashimoto, K., Igarashi, H., Mano, S., Takenaka, C., Shiina, T., Yamaguchi, M., Demura, T., Nishimura, M., Shimmen, T., and Yokota, E. (2008). An isoform of *Arabidopsis* myosin XI interacts with

small GTPases in its C-terminal tail region. *Journal of Experimental Botany*, 59(13):3523–3531.

Hepler, P. K., Vidali, L., and Cheung, A. Y. (2001). Polarized cell growth in higher plants. *Annual Review of Cell and Developmental Biology*, 17:159–187.

Higa, T., Suetsugu, N., Kong, S. G., and Wada, M. (2014). Actin-dependent plastid movement is required for motive force generation in directional nuclear movement in plants. *Proceedings of the National Academy of Sciences of the United States of America*, 111(11):4327–4331.

Hoepfner, D., Van Den Berg, M., Philippsen, P., Tabak, H. F., and Hettema, E. H. (2001). A role for Vps1p, actin, and the Myo2p motor in peroxisome abundance and inheritance in *Saccharomyces cerevisiae*. *Journal of Cell Biology*, 155(6):979–990.

Holding, D. R., Otegui, M. S., Li, B., Meeley, R. B., Dam, T., Hunter, B. G., Jung, R., and Larkins, B. A. (2007). The maize Floury1 gene encodes a novel endoplasmic reticulum protein involved in zein protein body formation. *The Plant Cell*, 19(8):2569–2582.

Hua, R., Cheng, D., Coyaud, É., Freeman, S., Di Pietro, E., Wang, Y., Vissa, A., Yip, C. M., Fairn, G. D., Braverman, N., Brumell, J. H., Trimble, W. S., Raught, B., and Kim, P. K. (2017). VAPs and ACBD5 tether peroxisomes to the ER for peroxisome maintenance and lipid homeostasis. *Journal of Cell Biology*, 216(2):367–377.

Hume, A. N., Ushakov, D. S., Tarafder, A. K., Ferenczi, M. A., and Seabra, M. C. (2007). Rab27a and MyoVa are the primary Mlph interactors regulating melanosome transport in melanocytes. *Journal of Cell Science*, 120:3111–3122.

Idilli, A. I., Morandini, P., Onelli, E., Rodighiero, S., Caccianiga, M., and Moscatelli, A. (2013). Microtubule depolymerization affects endocytosis and exocytosis in the tip and influences endosome movement in tobacco pollen tubes. *Molecular Plant*, 6(4):1109–1130.

Ishikawa, K., Catlett, N. L., Novak, J. L., Tang, F., Nau, J. J., and Weisman, L. S. (2003). Identification of an organelle-specific myosin V receptor. *Journal of Cell Biology*, 160(6):887–897.

Itoh, T., Toh-E, A., and Matsui, Y. (2004). Mmr1p is a mitochondrial factor for Myo2p-dependent inheritance of mitochondria in the budding yeast. *EMBO Journal*, 23(13):2520–2530.

Iwabuchi, K., Minamino, R., and Takagi, S. (2010). Actin reorganization underlies phototropin-dependent positioning of nuclei in *Arabidopsis* leaf cells. *Plant Physiology*, 152(3):1309–1319.

Jedd, G. and Chua, N. H. (2002). Visualization of peroxisomes in living plant cells reveals acto-myosin-dependent cytoplasmic streaming and peroxisome budding. *Plant and Cell Physiology*, 43(4):384–392.

Kagawa, T., Sakai, T., Suetsugu, N., Oikawa, K., Ishiguro, S., Kato, T., Tabata, S., Okada, K., and Wada, M. (2001). *Arabidopsis* NPL1: a phototropin homolog controlling the chloroplast high-light avoidance response. *Science*, 291(5511):2138–2141.

Kaksonen, M., Toret, C. P., and Drubin, D. G. (2006). Harnessing actin dynamics for clathrin-mediated endocytosis. *Nature Reviews Molecular Cell Biology*, 7(6):404–414.

Kamiya, N. and Kuroda, K. (1956). Velocity distribution of the protoplasmic streaming in *Nitella* cells. *Shokubutsugaku Zasshi*, 69(822):544–554.

Kasahara, M., Kagawa, T., Olkawa, K., Suetsugu, N., Miyao, M., and Wada, M. (2002). Chloroplast avoidance movement reduces photodamage in plants. *Nature*, 420(6917):829–832.

Ketelaar, T., Faivre-Moskalenko, C., Esseling, J. J., de Ruijter, N. C., Grierson, C. S., Dogterom, M., and Emons, A. M. C. (2002). Positioning of nuclei in *Arabidopsis* root hairs: an actin-regulated process of tip growth. *The Plant Cell*, 14(11):2941–2955.

Kim, B., Lee, J. Y., Lee, H. Y., Nam, K. Y., Park, J., Lee, S. M., Kim, J. E., Lee, J. D., and Hwang, J. S. (2013a). Hesperidin suppresses melanosome transport by blocking the interaction of rab27a-melanophilin. *Biomolecules and Therapeutics*, 21(5):343–348.

Kim, D., Cho, Y. H., Ryu, H., Kim, Y., Kim, T. H., and Hwang, I. (2013b). BLH1 and KNAT3 modulate ABA responses during germination and early seedling development in *Arabidopsis*. *Plant Journal*, 75(5):755–766.

King, S. M. (2002). Dyneins motor on in plants. *Traffic*, 3(12):930–931.

Kinkema, M. and Schiefelbein, J. (1994). A myosin from a higher plant has structural similarities to class V myosins. *Journal of Molecular Biology*, 239(4):591–597.

Klahre, U. and Kost, B. (2006). Tobacco RhoGTPase ACTIVATING PROTEIN1 spatially restricts signaling of RAC/Rop to the apex of pollen tubes. *The Plant Cell*, 18(11):3033–3046.

Kollmar, M. and Mühlhausen, S. (2017). Myosin repertoire expansion coincides with eukaryotic diversification in the Mesoproterozoic era. *BMC Evolutionary Biology*, 17:211.

Kriechbaumer, V., Botchway, S. W., Slade, S. E., Knox, K., Frigerio, L., Oparka, K. J., and Hawes, C. (2015). Reticulomics: protein-protein interaction studies with two plasmodesmata-localised reticulon family proteins identify binding partners enriched at plasmodesmata, ER and the plasma membrane. *Plant Physiology*, 169(3):1933–1945.

Kurth, E. G., Peremyslov, V. V., Turner, H. L., Makarova, K. S., Iranzo, J., Mekhedov, S. L., Koonin, E. V., and Dolja, V. V. (2017). Myosin-driven transport network in plants. *Proceedings of the National Academy of Sciences*, 114(8):1385–1394.

Lam, A. J., St-Pierre, F., Gong, Y., Marshall, J. D., Cranfill, P. J., Baird, M. A., McKeown, M. R., Wiedenmann, J., Davidson, M. W., Schnitzer, M. J., Tsien, R. Y., and Lin, M. Z. (2012). Improving FRET

dynamic range with bright green and red fluorescent proteins. *Nature Methods*, 9(10):1005–1012.

Lapierre, L. A., Kumar, R., Hales, C. M., Navarre, J., Bhartur, S. G., Burnette, J. O., Provance, D. W., Mercer, J. A., Bahler, M., and Goldenring, J. R. (2001). Myosin Vb is associated with plasma membrane recycling systems. *Molecular Biology of the Cell*, 12(6):1843–1857.

Larson, E. R. (2017). Measuring plant protein secretion. *Methods in Molecular Biology*, 1662:199–207.

Latijnhouwers, M., Hawes, C., Carvalho, C., Oparka, K., Gillingham, A. K., and Boevink, P. (2005). An Arabidopsis GRIP domain protein locates to the trans-Golgi and binds the small GTPase ARL1. *Plant Journal*, 44(3):459–470.

Lawrence, C. J., Dawe, R. K., Christie, K. R., Cleveland, D. W., Dawson, S. C., Endow, S. A., Goldstein, L. S., Goodson, H. V., Hirokawa, N., Howard, J., Malmberg, R. L., McIntosh, J. R., Miki, H., Mitchison, T. J., Okada, Y., Reddy, A. S., Saxton, W. M., Schliwa, M., Scholey, J. M., Vale, R. D., Walczak, C. E., and Wordeman, L. (2004). A standardized kinesin nomenclature. *Journal of Cell Biology*, 167(1):19–22.

Lawrence, C. J., Morris, N. R., Meagher, R. B., and Dawe, R. K. (2001). Dyneins have run their course in plant lineage. *Traffic*, 2(5):362–363.

Ledbetter, M. C. and Porter, K. R. (1963). A "microtubule" in plant cell fine structure. *Journal of Cell Biology*, 19(1):239–250.

Ledbetter, M. C. and Porter, K. R. (1964). Morphology of microtubules of plant cells. *Science*, 144(3620):872–874.

Lending, C. R. and Larkins, B. A. (2007). Changes in the zein composition of protein bodies during maize endosperm development. *The Plant Cell*, 1(10):1011–1023.

Li, H., Lin, Y., Heath, R. M., Zhu, M. X., and Yang, Z. (1999). Control of pollen tube tip growth by a Rop GTPase-dependent pathway that leads to tip-localized calcium influx. *The Plant cell*, 11(9):1731–1742.

Li, J. F. and Nebenführ, A. (2007). Organelle targeting of myosin XI is mediated by two globular tail subdomains with separate cargo binding sites. *Journal of Biological Chemistry*, 282(28):20593–20602.

Li, J. F. and Nebenführ, A. (2008). The tail that wags the dog: the globular tail domain defines the function of myosin V/XI. *Traffic*, 9(3):290–298.

López, M. P., Huber, F., Grigoriev, I., Steinmetz, M. O., Akhmanova, A., Koenderink, G. H., and Dogterom, M. (2014). Actin-microtubule coordination at growing microtubule ends. *Nature Communications*, 5(4778).

Mathur, J., Mathur, N., and Hülskamp, M. (2002). Simultaneous visualization of peroxisomes and cytoskeletal elements reveals actin and not microtubule-based peroxisome motility in plants. *Plant Physiology*, 128(3):1031–1045.

Miller, C. L., Arnold, M. M., Broering, T. J., Eichwald, C., Kim, J., Dinoso, J. B., and Nibert, M. L. (2007). Virus-derived platforms for visualizing protein associations inside cells. *Molecular & Cellular Proteomics*, 6(6):1027–1038.

Miller, D. D., Scordilis, S. P., and Hepler, P. K. (1995). Identification and localization of three classes of myosins in pollen tubes of *Lilium longiflorum* and *Nicotiana alata*. *Journal of Cell Science*, 108:2549–2653.

Mohri, H. (1968). Amino-acid composition of "tubulin" constituting microtubules of sperm flagella. *Nature*, 217(5133):1053–1054.

Murashige, T. and Skoog, F. (1962). A revised medium for rapid growth and bio assays with tobacco tissue cultures. *Physiologia Plantarum*, 15(3):473–497.

Murrell, M. P. and Gardel, M. L. (2012). F-actin buckling coordinates contractility and severing in a biomimetic actomyosin cortex. *Proceedings of the National Academy of Sciences*, 109(51):20820–20825.

Nandadasa, S., Kraft, C. M., Wang, L. W., O'Donnell, A., Patel, R., Gee, H. Y., Grobe, K., Cox, T. C., Hildebrandt, F., and Apte, S. S. (2019). Secreted metalloproteases ADAMTS9 and ADAMTS20 have a non-canonical role in ciliary vesicle growth during ciliogenesis. *Nature Communications*, 10:953.

Naramoto, S., Otegui, M. S., Kutsuna, N., de Rycke, R., Dainobu, T., Karampelias, M., Fujimoto, M., Feraru, E., Miki, D., Fukuda, H., Nakano, A., and Friml, J. (2014). Insights into the localization and function of the membrane trafficking regulator GNOM ARF-GEF at the Golgi apparatus in *Arabidopsis*. *The Plant Cell*, 26(7):3062–3076.

Nebenführ, A., Gallagher, L. A., Dunahay, T. G., Frohlick, J. A., Mazurkiewicz, A. M., Meehl, J. B., and Staehelin, L. A. (1999). Stop-and-go movements of plant Golgi stacks are mediated by the acto-myosin system. *Plant Physiology*, 121(4):1127–1141.

Negi, S., Pandey, S., Srinivasan, S. M., Mohammed, A., and Guda, C. (2015). LocSigDB: a database of protein localization signals. *Database*, pages 1–7.

Nelson, B. K., Cai, X., and Nebenführ, A. (2007). A multicolored set of in vivo organelle markers for co-localization studies in *Arabidopsis* and other plants. *Plant Journal*, 51(6):1126–1136.

Nothnagel, E. A. and Webb, W. W. (1982). Hydrodynamic models of viscous coupling between motile myosin and endoplasm in characean algae. *Journal of Cell Biology*, 94(2):444–454.

Odronitz, F. and Kollmar, M. (2007). Drawing the tree of eukaryotic life based on the analysis of 2,269 manually annotated myosins from 328 species. *Genome Biology*, 8(9):R196.

Ohbayashi, N., Mamishi, S., Ishibashi, K., Maruta, Y., Pourakbari, B., Tamizifar, B., Mohammadpour, M., Fukuda, M., and Parvaneh, N. (2010). Functional characterization of two RAB27A missense mutations found in Griscelli syndrome type 2. *Pigment Cell and Melanoma Research*, 23(3):365–374.

Ojangu, E. L., Ilau, B., Tanner, K., Talts, K., Ihoma, E., Dolja, V. V., Paves, H., and Truve, E. (2018). Class XI myosins contribute to auxin response and senescence-induced cell death in *Arabidopsis*. *Frontiers in Plant Science*, 9:1570.

Ojangu, E. L., Tanner, K., Pata, P., Järve, K., Holweg, C. L., Truve, E., and Paves, H. (2012). Myosins XI-K, XI-1, and XI-2 are required for development of pavement cells, trichomes, and stigmatic papillae in *Arabidopsis*. *BMC Plant Biology*, 12(81).

Orr, R. G., Furt, F., Warner, E. L., Agar, E. M., Garbarino, J. M., Cabral, S. E., Dubuke, M. L., Butt, A. M., Munson, M., and Vidali, L. (2019). Myosin XI interacting with a RabE GTPase is required for polarized growth. *bioRxiv*.

Osterrieder, A., Carvalho, C. M., Latijnhouwers, M., Johansen, J. N., Stubbs, C., Botchway, S., and Hawes, C. (2009). Fluorescence lifetime imaging of interactions between Golgi tethering factors and Small GTPases in plants. *Traffic*, 10(8):1034–1046.

Osterrieder, A., Sparkes, I. A., Botchway, S. W., Ward, A., Ketelaar, T., de Ruijter, N., and Hawes, C. (2017). Stacks off tracks: a role for the golgin *At*CASP in plant endoplasmic reticulum-Golgi apparatus tethering. *Journal of experimental botany*, 68(13):3339–3350.

Owen, D. J., Collins, B. M., and Evans, P. R. (2004). Adaptors for clathrin coats: structure and function. *Annual Review of Cell and Developmental Biology*, 20:153–191.

Park, Y. G., Mun, B. G., Kang, S. M., Hussain, A., Shahzad, R., Seo, C. W., Kim, A. Y., Lee, S. U., Oh, K. Y., Lee, D. Y., Lee, I. J., and

Yun, B. W. (2017). Bacillus aryabhattai SRB02 tolerates oxidative and nitrosative stress and promotes the growth of soybean by modulating the production of phytohormones. *PLoS ONE*, 12(3):e0173203.

Pashkova, N., Catlett, N. L., Novak, J. L., and Weisman, L. S. (2005a). A point mutation in the cargo-binding domain of myosin V affects its interaction with multiple cargoes. *Eukaryotic Cell*, 4(4):787–798.

Pashkova, N., Catlett, N. L., Novak, J. L., Wu, G., Lu, R., Cohen, R. E., and Weisman, L. S. (2005b). Myosin V attachment to cargo requires the tight association of two functional subdomains. *Journal of Cell Biology*, 168(3):359–364.

Peremyslov, V. V., Cole, R. A., Fowler, J. E., and Dolja, V. V. (2015). Myosin-powered membrane compartment drives cytoplasmic streaming, cell expansion and plant development. *PLoS ONE*, 10(10):e0139331.

Peremyslov, V. V., Klocko, A. L., Fowler, J. E., and Dolja, V. V. (2012). *Arabidopsis* myosin XI-K localizes to the motile endomembrane vesicles associated with F-actin. *Frontiers in Plant Science*, 3(184).

Peremyslov, V. V., Mockler, T. C., Filichkin, S. A., Fox, S. E., Jaiswal, P., Makarova, K. S., Koonin, E. V., and Dolja, V. V. (2011). Expression, splicing, and evolution of the myosin gene family in plants. *Plant Physiology*, (3):1191–1204.

Peremyslov, V. V., Morgun, E. A., Kurth, E. G., Makarova, K. S., Koonin, E. V., and Dolja, V. V. (2013). Identification of myosin XI receptors in *Arabidopsis* defines a distinct class of transport vesicles. *The Plant Cell*, 25(8):3022–38.

Peremyslov, V. V., Prokhnevsky, A. I., Avisar, D., and Dolja, V. V. (2008). Two class XI myosins function in organelle trafficking and root hair development in *Arabidopsis*. *Plant Physiology*, 146(3):1109–1116.

Peremyslov, V. V., Prokhnevsky, A. I., and Dolja, V. V. (2010a). Class

XI myosins are required for development, cell expansion, and F-actin organization in *Arabidopsis*. *The Plant Cell*, 22(6):1883–1897.

Peremyslov, V. V., Prokhnevsky, A. I., and Dolja, V. V. (2010b). Class XI myosins are required for development, cell expansion, and F-actin organization in *Arabidopsis*. *The Plant Cell*, 22:1883–1897.

Perico, C. and Sparkes, I. (2018). Plant organelle dynamics: cytoskeletal control and membrane contact sites. *New Phytologist*, 220(2):381–394.

Pfeffer, S. R. (2017). Rab GTPases: master regulators that establish the secretory and endocytic pathways. *Molecular Biology of the Cell*, 28(6):712–715.

Pinheiro, H., Samalova, M., Geldner, N., Chory, J., Martinez, A., and Moore, I. (2009). Genetic evidence that the higher plant Rab-D1 and Rab-D2 GTPases exhibit distinct but overlapping interactions in the early secretory pathway. *Journal of Cell Science*, 122:3749–3758.

Prokhnevsky, A. I., Peremyslov, V. V., and Dolja, V. V. (2008). Overlapping functions of the four class XI myosins in *Arabidopsis* growth, root hair elongation, and organelle motility. *Proceedings of the National Academy of Sciences*, 105(50):19744–19749.

Rahantaniaina, M.-S., Li, S., Chatel-Innocenti, G., Tuzet, A., Issakidis-Bourguet, E., Mhamdi, A., and Noctor, G. (2017). Cytosolic and chloroplastic DHARs cooperate in oxidative stress-driven activation of the salicylic acid pathway. *Plant Physiology*, 174(2):956–971.

Reddy, A. S. and Day, I. S. (2001). Analysis of the myosins encoded in the recently completed *Arabidopsis thaliana* genome sequence. *Genome biology*, 2(7):0024.1–0024.17.

Reisen, D. and Hanson, M. R. (2007). Association of six YFP-myosin XI-tail fusions with mobile plant cell organelles. *BMC Plant Biology*, 7(6).

Renna, L., Stefano, G., Slabaugh, E., Wormsbaecher, C., Sulpizio, A., Zienkiewicz, K., and Brandizzi, F. (2018). TGNap1 is required for

microtubule-dependent homeostasis of a subpopulation of the plant trans-Golgi network. *Nature Communications*, 9(5313).

Riedl, J., Crevenna, A. H., Kessenbrock, K., Yu, J. H., Neukirchen, D., Bista, M., Bradke, F., Jenne, D., Holak, T. A., Werb, Z., Sixt, M., and Wedlich-Soldner, R. (2008). Lifeact: a versatile marker to visualize F-actin. *Nature Methods*, 5(7):605–607.

Rodriguez, O. C. and Cheney, R. E. (2002). Human myosin-Vc is a novel class V myosin expressed in epithelial cells. *Journal of cell science*, 115:991–1004.

Rodríguez-Serrano, M., Romero-Puertas, M. C., Sanz-Fernández, M., Hu, J., and Sandalio, L. M. (2016). Peroxisomes extend peroxules in a fast response to stress via a reactive oxygen species-mediated induction of the peroxin PEX11a. *Plant Physiology*, 171(3):1665–1674.

Ryan, J. M. and Nebenführ, A. (2018). Update on myosin motors: molecular mechanisms and physiological functions. *Plant Physiology*, 176(1):119–127.

Sampathkumar, A., Lindeboom, J. J., Debolt, S., Gutierrez, R., Ehrhardt, D. W., Ketelaar, T., and Persson, S. (2011). Live cell imaging reveals structural associations between the actin and microtubule cytoskeleton in *Arabidopsis*. *The Plant Cell*, 23(6):2302–2313.

Sandalio, L. M., Rodríguez-Serrano, M., Gupta, D. K., Archilla, A., Romero-Puertas, M. C., and Del Río, L. A. (2012). Reactive oxygen species and nitric oxide in plants under cadmium stress: from toxicity to signaling. In *Environmental Adaptations and Stress Tolerance of Plants in the Era of Climate Change*, pages 199–216.

Sandalio, L. M. and Romero-Puertas, M. C. (2015). Peroxisomes sense and respond to environmental cues by regulating ROS and RNS signalling networks. *Annals of Botany*, 116(4):475–485.

Sattarzadeh, A., Krahmer, J., Germain, A. D., and Hanson, M. R. (2009). A myosin XI tail domain homologous to the yeast myosin vacuole-

binding domain interacts with plastids and stromules in *Nicotiana benthamiana*. *Molecular Plant*, 2(6):1351–1358.

Sattarzadeh, A., Schmelzer, E., and Hanson, M. R. (2011). Analysis of organelle targeting by DIL domains of the *Arabidopsis* myosin XI family. *Frontiers in Plant Science*, 2:72.

Sattarzadeh, A., Schmelzer, E., and Hanson, M. R. (2013). *Arabidopsis* myosin XI sub-domains homologous to the yeast myo2p organelle inheritance sub-domain target subcellular structures in plant cells. *Frontiers in Plant Science*, 4:407.

Schoberer, J., Liebminger, E., Botchway, S. W., Strasser, R., and Hawes, C. (2013). Time-resolved fluorescence imaging reveals differential interactions of N-glycan processing enzymes across the Golgi stack *in planta*. *Plant Physiology*, 161(4):1737–1754.

Sebé-Pedrós, A., Grau-Bové, X., Richards, T. A., and Ruiz-Trillo, I. (2014). Evolution and classification of myosins, a paneukaryotic whole-genome approach. *Genome Biology and Evolution*, 6(2):290–305.

Sheth, U. and Parker, R. (2003). Decapping and decay of messenger RNA occur in cytoplasmic processing bodies. *Science*, 300(5620):805–808.

Shimmen, T. (2007). The sliding theory of cytoplasmic streaming: fifty years of progress. *Journal of Plant Research*, 120(1):31–43.

Shubeita, G. T., Tran, S. L., Xu, J., Vershinin, M., Cermelli, S., Cotton, S. L., Welte, M. A., and Gross, S. P. (2008). Consequences of motor copy number on the intracellular transport of Kinesin-1-driven lipid droplets. *Cell*, 135(6):1098–1107.

Sparkes, I. A., Ketelaar, T., De Ruijter, N. C. A., and Hawes, C. (2009). Grab a golgi: laser trapping of golgi bodies reveals *in vivo* interactions with the endoplasmic reticulum. *Traffic*, 10(5):567–571.

Sparkes, I. A., Runions, J., Kearns, A., and Hawes, C. (2006). Rapid, transient expression of fluorescent fusion proteins in tobacco plants and

generation of stably transformed plants. *Nature Protocols*, 1(4):2019–2025.

Sparkes, I. A., Teanby, N. A., and Hawes, C. (2008). Truncated myosin XI tail fusions inhibit peroxisome, Golgi, and mitochondrial movement in tobacco leaf epidermal cells: a genetic tool for the next generation. *Journal of Experimental Botany*, 59(9):2499–2512.

Spellman, P. T., Sherlock, G., Zhang, M. Q., Iyer, V. R., Anders, K., Eisen, M. B., Brown, P. O., Botstein, D., and Futcher, B. (1998). Comprehensive identification of cell cycle-regulated genes of the yeast *Saccharomyces cerevisiae* by microarray hybridization. *Molecular biology of the cell*, 9(12):3273–3297.

Staneloni, R. J., Rodriguez-Batiller, M. J., Legisa, D., Scarpin, M. R., Agalou, A., Cerdan, P. D., Meijer, A. H., Ouwerkerk, P. B. F., and Casal, J. J. (2009). Bell-like homeodomain selectively regulates the high-irradiance response of phytochrome A. *Proceedings of the National Academy of Sciences*, 106(32):13624–13629.

Stefano, G., Renna, L., and Brandizzi, F. (2014). The endoplasmic reticulum exerts control over organelle streaming during cell expansion. *Journal of cell science*, 127:947–953.

Stefano, G., Renna, L., Hanton, S. L., Chatre, L., Haas, T. A., and Brandizzi, F. (2006). ARL1 plays a role in the binding of the GRIP domain of a peripheral matrix protein to the Golgi apparatus in plant cells. *Plant Molecular Biology*, 61(3):431–449.

Steffens, A., Jaegle, B., Tresch, A., Hulskamp, M., and Jakoby, M. (2014). Processing-body movement in *Arabidopsis* depends on an interaction between myosins and DECAPPING PROTEIN1. *Plant Physiology*, 164(4):1879–1892.

Stephan, O., Cottier, S., Fahlén, S., Montes-Rodriguez, A., Sun, J., Eklund, D. M., Klahre, U., and Kost, B. (2014). RISAP is a TGN-associated RAC5 effector regulating membrane traffic during polar cell growth in tobacco. *The Plant Cell*, 26(11):4426–4447.

Sun, T., Li, S., and Ren, H. (2017). *Os*FH15, a class I formin, interacts with microfilaments and microtubules to regulate grain size via affecting cell expansion in rice. *Scientific Reports*, 7(6538).

Talts, K., Ilau, B., Ojangu, E. L., Tanner, K., Peremyslov, V. V., Dolja, V. V., Truve, E., and Paves, H. (2016). Arabidopsis myosins XI1, XI2, and XIK are crucial for gravity-induced bending of inflorescence stems. *Frontiers in Plant Science*, 7:1932.

Tamura, K., Iwabuchi, K., Fukao, Y., Kondo, M., Okamoto, K., Ueda, H., Nishimura, M., and Hara-Nishimura, I. (2013). Myosin XI-I links the nuclear membrane to the cytoskeleton to control nuclear movement and shape in arabidopsis. *Current Biology*, 23(18):1776–1781.

Tang, F., Kauffman, E. J., Novak, J. L., Nau, J. J., Catlett, N. L., and Weisman, L. S. (2003). Regulated degradation of a class V myosin receptor directs movement of the yeast vacuole. *Nature*, 442:87–92.

Tang, K., Li, Y., Yu, C., and Wei, Z. (2019). Structural mechanism for versatile cargo recognition by the yeast class V myosin Myo2. *Journal of Biological Chemistry*, 294(15):5896–5906.

Taylor Eves, P., Jin, Y., Brunner, M., and Weisman, L. S. (2012). Overlap of cargo binding sites on myosin V coordinates the inheritance of diverse cargoes. *Journal of Cell Biology*, 198(1):69–85.

Thompson, R. F. and Langford, G. M. (2002). Myosin superfamily evolutionary history. *Anatomical Record*, 268(3):276–289.

Tominaga, M. and Ito, K. (2015). The molecular mechanism and physiological role of cytoplasmic streaming. *Current Opinion in Plant Biology*, 27:104–110.

Tominaga, M., Kimura, A., Yokota, E., Haraguchi, T., Shimmen, T., Yamamoto, K., Nakano, A., and Ito, K. (2013). Cytoplasmic streaming velocity as a plant size determinant. *Developmental Cell*, 27(3):345–352.

Tominaga, M., Kojima, H., Yokota, E., Orii, H., Nakamori, R., Katayama, E., Anson, M., Shimmen, T., and Oiwa, K. (2003). Higher plant myosin XI moves processively on actin with 35 nm steps at high velocity. *EMBO Journal*, 22(6):1263–1272.

Tominaga, M. and Nakano, A. (2012). Plant-specific myosin XI, a molecular perspective. *Frontiers in Plant Science*, 3(211).

Ueda, H., Yokota, E., Kutsuna, N., Shimada, T., Tamura, K., Shimmen, T., Hasezawa, S., Dolja, V. V., and Hara-Nishimuraa, I. (2010). Myosin-dependent endoplasmic reticulum motility and F-actin organization in plant cells. *Proceedings of the National Academy of Sciences of the United States of America*, 107:6894–6899.

Van Damme, D., Bouget, F. Y., Van Poucke, K., Inzé, D., and Geelen, D. (2004). Molecular dissection of plant cytokinesis and phragmoplast structure: a survey of GFP-tagged proteins. *Plant Journal*, 40(3):386–398.

Van Gestel, K., Köhler, R. H., and Verbelen, J. P. (2002). Plant mitochondria move on F-actin, but their positioning in the cortical cytoplasm depends on both F-actin and microtubules. *Journal of Experimental Botany*, 53(369):659–667.

Vitale, N., Ferrans, V. J., Moss, J., and Vaughan, M. (2002). Identification of lysosomal and Golgi localization signals in GAP and ARF domains of ARF domain protein 1. *Molecular and Cellular Biology*, 20(19):7342–7352.

Vogel, S. K., Petrasek, Z., Heinemann, F., and Schwille, P. (2013). Myosin motors fragment and compact membrane-bound actin filaments. *eLife*, 2:e00116.

Wagner, W., Bielli, P., Wacha, S., and Ragnini-Wilson, A. (2002). Mlc1p promotes septum closure during cytokinesis via the IQ motifs of the vesicle motor Myo2p. *EMBO Journal*, 21(23):6397–6408.

Wang, J., Zhang, Y., Wu, J., Meng, L., and Ren, H. (2013). *At*FH16, an *Arabidopsis* type II formin, binds and bundles both microfilaments and microtubules, and preferentially binds to microtubules. *Journal of Integrative Plant Biology*, 55(11):1002–1015.

Wang, P., Hawes, C., and Hussey, P. J. (2017). Plant endoplasmic reticulum–plasma membrane contact sites. *Trends in Plant Science*, 22(4):289–297.

Wee, E. G.-T., Sherrier, D. J., Prime, T. A., and Dupree, P. (1998). Targeting of active sialyltransferase to the plant Golgi apparatus. *The Plant Cell*, 10(10):1759–1768.

Willem Borst, J. and Visser, A. J. (2010). Fluorescence lifetime imaging microscopy in life sciences. *Measurement Science and Technology*, 21(10).

Wu, S. Z. and Bezanilla, M. (2014). Myosin VIII associates with microtubule ends and together with actin plays a role in guiding plant cell division. *eLife*, 3:e03498.

Wu, S. Z. and Bezanilla, M. (2018). Actin and microtubule cross talk mediates persistent polarized growth. *The Journal of cell biology*, 217(10):3531–3544.

Wu, X. S., Rao, K., Zhang, H., Wang, F., Sellers, J. R., Matesic, L. E., Copeland, N. G., Jenkins, N. A., and Hammer, J. A. (2002). Identification of an organelle receptor for myosin-Va. *Nature cell biology*, 4(4):271–278.

Yan, Q., Sun, W., Kujala, P., Lotfi, Y., Vida, T. A., and Bean, A. J. (2005). Cart: an hrs/actinin-4/berp/myosin v protein complex required for efficient receptor recycling. *Molecular Biology of the Cell*, 16(5):2470–2482.

Yang, L., Qin, L., Liu, G., Peremyslov, V. V., Dolja, V. V., and Wei, Y. (2014). Myosins XI modulate host cellular responses and penetration

resistance to fungal pathogens. *Proceedings of the National Academy of Sciences of the United States of America*, 111(38):13996–14001.

Yokota, E., Ueda, H., Hashimoto, K., Orii, H., Shimada, T., Hara-Nishimura, I., and Shimmen, T. (2011). Myosin XI-dependent formation of tubular structures from endoplasmic reticulum isolated from tobacco cultured BY-2 cells. *Plant Physiology*, 1:129–143.

Zabala, M. d. T., Littlejohn, G., Jayaraman, S., Studholme, D., Bailey, T., Lawson, T., Tillich, M., Licht, D., Bölter, B., Delfino, L., Truman, W., Mansfield, J., Smirnoff, N., and Grant, M. (2015). Chloroplasts play a central role in plant defence and are targeted by pathogen effectors. *Nature Plants*, 1:15074.

Zheng, H., Camacho, L., Wee, E., Batoko, H., Legen, J., Leaver, C. J., Malhó, R., Hussey, P. J., and Moore, I. (2005). A Rab-E GTPase mutant acts downstream of the Rab-D subclass in biosynthetic membrane traffic to the plasma membrane in tobacco leaf epidermis. *Plant Cell*, 17:2020–2036.